Pattern Recognition and Machine Learning as a Morphology Characterization Tool for Assessment of Placental Health

Anika Mukherjee

A thesis submitted in partial fulfillment of the requirements for the
Master's degree in Interdisciplinary Health Sciences

School of Interdisciplinary Health Sciences
Faculty of Health Sciences
University of Ottawa

Preface

Abstract

Introduction: The placenta is a complex, disk-shaped organ vital to a successful pregnancy and responsible for materno-fetal exchange of vital gases and biochemicals. Instances of compromised placental development or function – collectively termed placenta dysfunction - underlies the most common and devastating pregnancy complications observed in North America, including preeclampsia (PE) and fetal growth restriction (FGR). A comprehensive histopathology examination of the placenta following delivery can help clarify obstetrical disease etiology and progression and offers tremendous potential in the identification of patients at risk of recurrence in subsequent pregnancies, as well as patients at high risk of chronic diseases in later life. However, these types of examinations require a high degree of specialized training and are resource intensive, limiting their availability to tertiary care centers in large city centres. The development of machine learning algorithms tailored to placenta histopathology applications may allow for automation and/or standardization of this important clinical exam – expanding its appropriate usage and impact on the health of mothers and infants. The primary objective of the current project is to develop and pilot the use of machine learning models capable of placental disease classification using digital histopathology images of the placenta.

Methods: 1) A systematic review was conducted to identify the current methods being applied to automate histopathology screening to inform experimental design for later components of the project. Of 230 peer-reviewed articles retrieved in the search, 18 articles met all inclusion criteria and were used to develop guidelines for best practices. 2) To facilitate machine learning model development on placenta histopathology samples, a villi segmentation algorithm was developed to aid with feature extraction by providing objective metrics to automatically quantify microscopic placenta images. The segmentation algorithm applied colour clustering and a tophat transform to delineate the boundaries between neighbouring villi. 3) As a proof-of-concept, 2 machine learning algorithms were tested to evaluated their ability to predict the clinical outcome of preeclampsia (PE) using placental

histopathology specimens collected through the Research Centre for Women's and Infant's Health (RCWIH) BioBank. The sample set included digital images from 50 cases of early onset PE, 29 cases of late onset PE and 69 controls with matching gestational ages. All images were pre-processed using patch extraction, colour normalization, and image transformations. Features of interest were extracted using: a) villi segmentation algorithm; b) SIFT keypoint descriptors (textural features); c) integrated feature extraction (in the context of deep learning model development). Using the different methods of feature extraction, two different machine learning approaches were compared - Support Vector Machine (SVM) and Convolutional Neural Network (CNN, deep learning). To track model improvement during training, cross validation on 20% of the total dataset was used (deep learning algorithm only) and the trained algorithms were evaluated on a test dataset (20% of the original dataset previously unseen by the model).

Results: From the systematic review, 5 key steps were found to be essential for machine learning model development on histopathology images (image acquisition and preparation, image preprocessing, feature extraction, pattern recognition and classification model training, and model testing) and recommendations were provided for the optimal methods for each of the 5 steps. The segmentation algorithm was able to correctly identify individual villi with an F1 score of 80.76% - a significantly better performance than recently published methods. A maximum accuracy of 73% for the machine learning experiments was obtained when using textural features (SIFT keypoint descriptors) in an SVM model, using onset of PE disease (early vs. late) as the output classification of interest.

Conclusion: Three major outcomes came of this project: 1) the range of methods available to develop automated screening tools for histopathology images with machine learning were consolidated and a set of best practices were proposed to guide future projects, 2) a villi segmentation tool was developed that can automatically segment all individual villi from an image and extract biologically relevant features that can be used in machine learning model development, and 3) a prototype machine learning

classification tool for placenta histopathology was developed that was able to achieve moderate classification accuracy when distinguishing cases of early onset PE and late onset PE cases from controls. The collective body of work has made significant contributions to the fields of placenta pathology and computer vision, laying the foundation for significant progress aimed at integrating machine learning tools into the clinical setting of perinatal pathology.

Acknowledgements

I owe the greatest thanks to my two co-supervisors Dr. Shannon Bainbridge-Whiteside and Dr. David Grynspan for their exceptional guidance, patience, and insights. Both brought a unique flavor of mentorship and together, left me with a rounded and enriching experience. Shannon, thank you for providing me with endless support and being truly invested in the project at every step of the way. Thank you for teaching me how to think critically and showing me what it takes to answer a research question with integrity. I now feel closer to being able to wear the title of "scientist". David, thank you for helping me see the importance of the work we do and how this can impact real people in the community. Thank you for teaching me to think abstractly about a problem and how to take novel approaches to solving them. You were always there when I was struggling to see the bigger picture and would always spark inspiration. I cannot reiterate enough how valuable both of your contributions were to this project and to me.

A sincere thank you goes out to my thesis advisory committee members Dr. Adrian Chan, and Dr. Raywat Deonandan for the time and effort they committed to this work. This project was interdisciplinary in the truest sense of the word. It would have been impossible to complete without both the clinical and pathology expertise as well as the computer science and statistical advice. Thank you, Dr. Chan for always steering us in the right direction regarding our decisions for implementing machine learning methods. With the wealth of options available, you helped us tremendously with feeling comfortable in the judgement calls we were making. We look forward to future collaboration with you and your team. Dr. Deonandan, thank you for offering your support with the planning and execution of this project. Knowing we could turn to you for help with interpreting results was immensely helpful. I would also like to thank Dr. Eran Ukwatta for attending our meetings and offering critical assessment of the results and potential avenues for additional investigation.

A huge thank you goes to Sina Salsabilli for his work on the automation of feature extraction from placenta villi. A whole arm of our machine learning experiments would not have been possible without his contribution. As well, I greatly appreciate the help of Michal Leckie and Purvasha Pratnaik for their help collecting data and assessing the risk of bias in the systematic review. Undertaking a review like this was no small task, and it was made much more manageable with their help. I would also like to say thank you to the other members of our lab for their support and for making these past years a lot of fun. Thank you, Dr. Samantha Benton, Jeremiah Gaudet, Philip Marshal, Fahmida Jahan, Sonia Rose Dancey, Erika Mery, Amy Zeglinski-Spinney, Benjamin McLeod, Fadi Gorgi, Peter Pham, and Sapir Fellus.

This work would not have been possible without the mothers at the Mount Sinai hospital in Toronto who kindly consented for their placentas to be used for research into preeclampsia. A very warm thank you goes out to them for making this research possible. They may not realize the magnitude of their contribution or be able to benefit from the ultimate outcomes of the research, but they have indirectly helped many future mothers who will be afflicted with PE.

I would like to give a very heartfelt thanks to my loved ones for their encouragement and support. I appreciate my friends for being patient with me and understanding when I was feeling the stress of writing a thesis. Having a support group of people who would unconditionally listen to my challenges made it a lot easier to work through them. Lastly, I thank my parents and grandparents for encouraging me to work hard and never stop learning. In moving to Canada, they paved a path for me to do more than they could and that motivates me to instill passion in my work.

Authorship Contribution

The following outline lists the contributions of various authors to the manuscripts presented in this thesis.

Manuscript 1: A Systematic Review of Computer Aided Classification of Histopathology Images: Recommendations for Best Practices

Dr. Shannon Bainbridge-Whiteside and Dr. David Grynspan were the principal investigators for the study. Karine Fournier, Dr. Shannon Bainbridge-Whiteside validated the search strategy. Anika Mukherjee, Dr. David Grynspan and Michal Leckie performed full title and abstract screening of 230 articles retrieved from a systematic literature search. Anika Mukherjee and Michal Leckie extracted and compiled data from screened-in articles. Anika Mukherjee and Purvasha Pratnaik assessed the risk of bias in the articles presented. The manuscript was prepared by Anika Mukherjee and reviewed and edited by Dr. Shannon Bainbridge-Whiteside.

Manuscript 2: Automated segmentation of villi in histopathology images of placenta

Dr. Adrian Chan was the principal investigator for the study. This study was conceptualized by Dr. Adrian Chan, Dr. Eran Ukwatta, Dr. Shannon Bainbridge-Whiteside, and Dr. David Grynspan. Whole slide images from placenta tissue sections were manually annotated by Anika Mukherjee and validated by Dr. David Grynspan. All codes for segmenting villi were written by Sina Salsabilli. The manuscript was prepared by Sina Salsabilli and Anika Mukherjee and revised by Dr. Adrian Chan, Dr. Shannon Bainbridge-Whiteside, and Dr. David Grynspan. This manuscript was published in Computers in Biology and Medicine (Comput Biol Med. 2019 Aug 30;113:103420).

Manuscript 3: Application of Machine Learning to Classify Distinct Patterns of Placenta Histopathology: A Proof-of-Concept Using Cases of Preeclampsia

Dr. Shannon Bainbridge-Whiteside and Dr. David Grynspan were the principal investigators for the study. Dr. Eran Ukwatta provided sponsorship for access to Compute Canada High Performance Computing resources to be able to run the programs. Codes for data augmentation and machine learning were written by Anika Mukherjee. Sina Salsabilli applied the code developed in Manuscript 2 and extracted clinically relevant features from segmented placenta villi. Anika Mukherjee extracted textural features from the same samples for comparison with clinically relevant features. This manuscript was prepared by Anika Mukherjee and reviewed by Dr. Shannon Bainbridge-Whiteside.

Ethics Statement

This study was granted research ethics approval by the University of Ottawa Office of Research Ethics and Integrity. Anika Mukherjee was added as an additional co-investigator to perform a sub-analysis of the data collected for the work presented in Leavey et. al 2016. Ethics approval was granted on August 24th, 2018 under the file H-08-18-1023 for the project titled Identification of Molecular Subclasses of PE. Approval was renewed April 15th, 2019. Tri-Council Policy Statement: Ethical Conduct for Research Involving Humans Course on Research Ethics (TCPS 2:CORE) was completed on September 26th, 2016. Certificates of ethics approval for the study and TCPS 2: CORE course completion are included in Appendix A.

Table of Contents

List of Abbreviations

AJCC	American Joint Committee on Cancer
ANN	Artificial Neural Networks
BRIEF	Binary Robust Independent Elementary Features
CAD	Computer Aided Diagnosis
CC	Cytotrophoblasts Cells
CIE L*a*b*	Commission internationale de l'éclairage – Lightness*, Red-Green*, Blue-Yellow*
CHEO	Children's Hospital of Eastern Ontario
CHTN	Cooperative Human Tissue Network
CNN	Convolutional Neural Network
CT	Healthy Controls
CV	Computer Vision
CVD	Cardiovascular Disease
DAB	3,3'-Diaminobenzidine
DL	Deep Learning
EO-PE	Early Onset Preeclampsia
EVT	Extravillous Cytotrophoblast

FAST	Features From Accelerated Segment Test
FGR	Fetal Growth Restriction
FN	False Negative
FP	False Positive
GA	Gestational Age
GLCM	Grey-Level Co-Occurrence Matrix
H&E	Hematoxylin and Eosin
HELLP	Hemolysis, Elevated Liver Enzymes, Low Platelets
HSI	Hue, Saturation, Intensity
HSV	Hue, Saturation, Value
ISOMAP	Isometric Feature Mapping
IUGR	Intrauterine Growth Restriction
IV	Intervillous Space
LBP	Local Binary Pattern
LDA	Linear Discriminant Analysis
LLE	Local Linear Embedding
LOO	Leave-One-Out Cross Validation
LO-PE	Late Onset Preeclampsia

LPQ	Local Phase Quantization
LTSA	Local Tangential Space Embedding
MeSH	Medical Subject Headings
MCT	Mesenchymal Connective Tissue
MDS	Multiple-Dimensional Scaling
MIL	Multiple Instance Learning
ML	Machine Learning
MPFD	Massive Perivillous Fibrin Deposition
MRP	Mean Rank Plots
MVM	Maternal Vascular Malperfusion
ORB	Oriented FAST and Rotated BRIEF
PCA	Principal Component Analysis
PE	Preeclampsia
PMD	Placenta Mediated Disease
RCWIH	Research Centre for Women's And Infants Health
REB	Research Ethics Board
RGB	Red Green Blue
SA	Spiral Arteries

SC	Syncytiotrophoblast Cells
SE	Structuring Element
SIFT	Scale-Invariant Feature Transform
STR	Villous Tree Stroma
SURF	Speeded Up Robust Features
SVM	Support Vector Machine
TCGA	The Cancer Genome Atlas
TCPS 2: CORE	Tri-Council Policy Statement: Ethical Conduct for Research Involving Humans Course on Research Ethics
TMA	Tissue Microarray
TN	True Negative
TP	True Positive
VC	Villi Core
VPRS	Variable Precision Rough Sets
VUE	Villitis of Unknown Etiology
WSI	Whole Slide Images
XAI	Explainable Artificial Intelligence

List of Figures

Chapter 1

Chapter 2

Chapter 3

Chapter 4

Appendices

List of Tables

Chapter 1

Chapter 2

Chapter 3

Chapter 4

Thesis Outline

Chapter 1: Introduction

The introduction provides the relevant background information and rationale for the thesis. Further, the overarching hypothesis and specific research objectives are presented.

Chapter 2 (Manuscript 1): Computer Aided Classification of Histopathology Images: A Systematic Review to Inform Best Practices

The first manuscript addresses specific research aim 1. To address the current gap in the literature, this article presents a systematic review of machine learning methods previously published for used on histopathology images.

Chapter 3 (Manuscript 2): *Automated segmentation of villi in histopathology images of placenta*

The second manuscript addresses specific research aim 2, sub-aim 1. This article presents a novel approach to digitally segmenting individual villi from placenta histology slides. This manuscript has been published (*Comput Biol Med*. 2019 Oct;113:103420).

Chapter 4 (Manuscript 3): *Application of Machine Learning to Classify Distinct Patterns of Placenta Histopathology: A Proof-of-Concept Using Cases of Preeclampsia*

The third manuscript addresses specific research aim 2, sub-aim 2. This article tests three feature extraction methods identified in Chapter 2 to develop a machine learning model capable of accurately classifying placenta histopathology images from healthy controls and cases of preeclampsia.

Chapter 5: General Discussion

The discussion connects the findings from all three manuscripts with a critical interpretation of the results in connection to the overarching hypothesis for the thesis. The significance of the findings as well

as limitations and future directions are included in this chapter along with a discussion related to the interdisciplinary nature of this project.

Chapter 1

Introduction

1.1 The Human Placenta

The human placenta is disk-shaped organ exclusively used throughout the gestational period by the developing fetus. It is responsible for transporting all gases, nutrients and metabolites to the fetus, ensuring appropriate development, growth and ultimately survival. The placenta further acts as a critical endocrine organ, producing hormones that regulate essential maternal adaptations to pregnancy [1]. The human placenta can be divided into two functional compartments (Figure 1.1): the extravillous compartment (the site of uterine attachment); and the villous compartment (the site of maternal-fetal exchange). Extravillous cytotrophoblast (EVT) cells of the placenta invade the uterine wall and participate in transforming the uterine spiral arteries into low-resistance vessels compatible with the high placenta blood flow required to support rapid fetal growth in late gestation [2]. Maternal blood exiting the uterine spiral arteries flows into the convoluted intervillous space, which is surrounded by branching villous structures coated by a single multinucleated layer of fetal syncytiotrophoblast cells (SC). Under the SC layer is a discontinuous layer of proliferative villous cytotrophoblast cells (CC) and fetal capillaries embedded in the villous core made up of mesenchymal connective tissue [1]. These villi are tree-like structures and are the site of exchange between maternal blood in the intervillous space and fetal blood perfusing the dense capillary networks of the villi [3]. Histological sections of the placenta show a series of cross-sections through these villous structures surrounded by the "empty/white" intervillous space, which would normally be filled with maternal blood in vivo [4]. Across gestation these villous structures continue to elongate and branch, increasing the maternal-fetal exchange surface area of the organ and decreasing the thickness of the exchange barrier between the maternal and fetal circulations [1].

1.2 Placenta-Mediated Diseases of Pregnancy

A healthy placenta is essential for a healthy pregnancy. Compromised placental development and/or function can have significant impacts on the health of both the fetus and mother and are collectively

coined **placenta-mediated diseases**. Placenta-mediated diseases play a causal role in the majority of serious obstetrical complications faced in our health care system today, including the most common conditions of preeclampsia (PE) and fetal growth restriction (FGR). Collectively, placenta-mediated diseases are responsible for half of all pre-term deliveries in Canada [5] and increase the risk of complications in subsequent pregnancies [6]. This places a substantial burden on our health care system, with each baby born pre-term as a result of placental disease costing the Ontario Health Care System up to 50-times that of a healthy baby born at term ($6,500-$90,000 per neonate [7]). While tremendous strides are being made in the early identification and management of pregnancies affected by placenta-mediated disease, there is much that we still do not understand with regards to the divergent underlying causes of these disorders.

1.3 Preeclampsia

1.3.1 Clinical Burden of PE

PE is a life-threatening disorder of pregnancy, characterized by new onset hypertension and multi-organ dysfunction. This disorder affects 3-8% of all pregnancies and is responsible for 63,000 maternal deaths worldwide per year [8]. FGR, defined as failure of a fetus to attain optimal intrauterine growth, is a common co-morbidity in cases of PE. It places the fetus at high risk of pre-term delivery and perinatal morbidity [9]. Furthermore, many of these babies demonstrate life-long health consequences, with increased risk of obesity and cardiovascular disease (CVD) in later life [10]. The maternal health burden of PE also extends well past the perinatal period, as PE is a significant risk factor for CVD in later life [11–13]. Compared to uncomplicated pregnancies, women with PE have higher rates of premature CVD-related death [11] and a 2-fold increased risk of future heart disease and stroke [14].

The placenta is central to the etiology of this disorder, and currently the only cure for PE is the delivery of this organ. Clearly, if severe disease arises early in gestation this cure can put the fetus in considerable danger due to the iatrogenic effects of preterm delivery. Conversely, if the pregnancy is

maintained, maternal health can become significantly compromised. In severe cases mothers can go in to organ failure (ex. HELLP Syndrome) or go on to develop eclampsia – the onset of seizures due to dangerously high blood pressure [15]. For this reason, a primary focus of maternal-fetal health research is on better understanding the mechanisms of disease progression in PE and the identification of effective prevention and intervention therapeutic options.

1.3.2 Placental Disease in PE

PE is most commonly described as a hypertensive disorder of pregnancy, but the underlying cause of the disease is placenta mediated, particularly in severe disease [16–19]. Insufficient placental invasion of the uterine wall and insufficient remodeling of the uterine spiral arteries is thought to results in poor blood flow to the placenta [20,21]. The oxygen-starved placenta then releases a mix of stress-induced factors (i.e. pro-inflammatory cytokines, anti-angiogenic factors) into the maternal circulation [22–25].These factors, released at the level of the uterus, cause damage to the maternal immune and cardiovascular systems, ultimately leading to clinical maternal disease [26,27]. In this well-characterised 'two-stage' model of PE [27], abnormalities in placental development and function early in pregnancy are translated into pathologies within the mother at later stages of pregnancy. However, clinical presentation, pregnancy outcomes and observed placental pathologies are all extremely variable between women with PE [28–31], suggesting that this paradigm of pathophysiology may not be true for all cases of PE.

1.3.3 Evidence of Disease Subclasses in PE

PE is a highly heterogeneous disorder, with differences in the time of disease onset, severity of maternal symptoms, impact on fetal growth trajectories, pregnancy outcomes and types of placental damage observed during the placenta pathology examination [32]. The observations of clinical and pathological heterogeneity observed across the spectrum of PE cases are now viewed as clues to the presence of distinct subpopulations of PE patients. In this vein, it is hypothesized by several groups [29] that PE is a

spectral disorder with several possible underlying disease processes that converge to commonly cause maternal disease. In the clinical context, PE subtypes are often acknowledged by separation of "early onset" versus "late onset" disease. This is an important distinction, as women with early onset PE (<34 weeks) have a 20-fold higher rate of maternal mortality compared to women who develop PE closer to term [33,34]. Fetal growth is more often adversely affected within this group, with ~ 20% of early onset PE pregnancies demonstrating evidence of FGR [35]. However, this dichotomous split of PE patients still cannot account for the all heterogeneity observed in PE. A vast "grey zone" of maternal and fetal outcomes and long-term health risk blurs the line between these two groups.

Detailed placental profiling carried out by our research group recently has demonstrated the presence of at least 3 distinct and clinically relevant PE subclasses with divergent underlying forms of placental disease [18,36]. Using unsupervised clustering analysis of placental gene expression and placental histopathology profiles, three different type of PE pathophysiology were described, including: 1) "Canonical PE" – resulting from insufficient blood flow and hypoxia within the placenta; 2) "Immunological PE" – resulting from heightened inflammatory response at the maternal-fetal interface; and 3) "Maternal PE" – resulting from maternal maladaptation to pregnancy, with minimal involvement of the placenta. The ability to clearly delineate the disease process underlying a woman's PE diagnosis is critical to the discovery of effective therapeutic interventions, and to best council patients with respect to recurrence risks for future pregnancies and long-term health risks.

1.4 The Role of Histopathology Analysis in Understanding Placenta-Mediated Diseases

Standard of care for pregnancies impacted by a placenta-mediated disease includes the submission of the placenta for a detailed pathology examination following delivery [37]. During this examination both gross anatomical descriptions and microscopic observations from histopathology specimens are recorded and summarized in a narrative pathology report which is included in both the mothers and

infants' medical charts for interpretation by their clinical care teams [38]. These examinations can be instrumental in understanding the underlying reason for the adverse pregnancy outcome, allowing the visual damage to the placenta – termed "placental lesions" – to tell a story regarding the disease process across pregnancy [16,39]. While the gross anatomical descriptions are useful, the bulk of this "story" really comes from the observations made at the cellular level in the histopathology specimens.

To generate histopathology specimens, full thickness sections from the fixed placenta are mounted onto glass slides and stained with chemical dyes that highlight morphological features of interest [40]. Hematoxylin and Eosin (H&E) is most commonly used because it stains all cellular components pink or blue depending on whether they are acidophilic or basophilic [41]. Understanding the structural morphology of the placenta in healthy cases and comparing them with the morphology in cases of placenta-mediated disease can help determine which cellular and molecular processes are failing across pregnancy and provide insight into how to best therapeutically target this disease in the future. In practice, pathologists look for common visual patterns in histology slides and combine this information with clinical findings to report on sources of disease progression [39]. Broadly, most placental lesions can be classified according to ten broad categories of placental disease process, which include: Maternal vascular malperfusion (MVM); maternal decidual vasculopathy; implantation site abnormalities; ascending intrauterine infection; placental villous maldevelopment; fetal vascular malperfusion; utero-placental separation; fibrinoid deposition; intervillous thrombi; and, chronic inflammation [42,43]. Brief descriptions of these disease process categories, along with distinct placental lesions indicative of these categories are detailed in Table 1.1.

1.4.1 Placental Histopathology in PE

The most common type of placental injury observed and reported in cases of PE is Maternal Vascular Malperfusion (MVM) [16,44]. MVM represents a recognizable pattern of placental injury related to

altered uterine and intervillous blood flow dynamics and placental tissue oxygenation [45]. Historically this constellation of lesions were thought to be the result of simple underperfusion of the placenta by the poorly remodelled uterine spiral arteries, however more recent understanding of this type of placental injury has expanded to include high velocity and turbulent blood flow into the intervillous space [46]. Many of the hallmark placental lesions of MVM can be found throughout the villous compartment of the placenta, each with a distinct visual appearance. Placental lesions associated with MVM include: Placental Infarcts (glossy discoloured region of the placenta caused by necrosis, thrombosis, or fibrin deposition [47]); Distal Villous Hypoplasia (sparse, widely spaced distal villi around thin intermediate villi [48,49]); Increased Syncytial Knots (aggregates of syncytial nuclei on outer surface of tertiary villi [50]); Advanced Villous Maturation (presence of mature appearing villi for gestational age [51]); and, Villous Agglutination (clusters of fused terminal villi connected by fibrin or bridging syncytial knots [16]) (Figure 1.2).

However, as indicated above, PE is highly heterogeneous in its clinical presentation, with variability extending into the types of placental lesions observed across the spectrum of disease [36]. In fact, work carried out by our group has indicated that the MVM lesions were restricted to the “canonical PE” subtype, which encompassed many of the “early onset” cases. Conversely, the “immunological PE” subclass instead demonstrated placental injury consistent with chronic inflammation and fibroid deposition – histopathology lesions typically observed in the context of an allograft rejection, suggesting a maternal-fetal immune incompatibility in this group of PE women. In this small subclass of PE, accounting for approximately 12% of PE cases examined [18,36], the primary placental lesions observed were villitis of unknown etiology (VUE) and massive perivillous fibrin deposition (MPFD). These two lesions also carry a distinct visual appearance, with VUE displaying diffuse areas of lymphohistocytic infiltration in the villous stroma [52,53] and MPFD characterized by extensive fibrinoid extracellular material in the intervillous space [54]. Finally, in the third PE subclass identified, the “maternal PE”

subclass, very minimal evidence of placental histopathology was observed. The majority of cases had no sign of placental injury, with some demonstrating very mild forms of MVM.

1.4.2 Current Challenges Faced in Applied Placenta Pathology

The use of placenta pathology examinations, and histopathology examination in particular, has offered considerable insight into the complexity of placenta-mediated disease pathophysiology and is a highly informative clinical tool for the management and counselling of patients following an adverse pregnancy outcome [39,55]. However, this practice is not without its challenges and limitations. Unfortunately, placenta pathology has historically been plagued by a lack of standardization in diagnostic definitions and criteria, and institutional practices [56–58]. The Amsterdam Consensus, a working paper put out by leading experts in this field [59], has sought to directly combat the issue of standardization through a published series of diagnostic definitions and criteria to be followed around the globe. However, the examinations proposed by this group require a high degree of sub-specialty training, primarily limiting the clinical application and utility of these examinations to tertiary care centres.

Further, the placenta is a highly complex organ that is changing across gestation and whose appearance can be altered by a variety of environmental factors like smoking and nutrition [60,61]. Perinatal pathologists must consider a variety of clinical correlates when interpreting placental morphology in any one case. They may analyze hundreds of tissue specimens in a day, most of which are complicated cases [62,63]. This practice is both costly in hospital resources and can cause fatigue in the analyst. Studies on clinician fatigue found that agreement between pathologists declined with increased levels of fatigue [64,65].

In order to address some of these challenges, several clinical aids have been proposed and developed. One such aid produced by our group is an online synoptic reporting tool that includes Amsterdam Consensus definitions and diagnostic criteria, along with representative images of different placental

lesions [42,59]. While this tool certainly addresses issues of clinical practice standardization across users, even those with lower levels of subspecialty training, it does not address the significant issue of workload management and pathologist fatigue. Across all fields of health care there is a push to incorporate computer aided diagnosis or artificial intelligence into standard of care workflows, to target issues of resource allocation and practice standardization [62,66,67]. Based on the current challenges faced in the area of placenta pathology, and the immense clinical utility to improve the health of mothers and babies, this field is ripe for exploration into how this technology could be applied in the context of placenta-mediated diseases.

1.5 Applying Machine Learning to Histopathology Specimens

1.5.1 Brief Overview of Machine Learning

Machine learning is the foundational building block for designing artificial intelligence and is based on the notion that computer algorithms can identify patterns in data and create data-driven models with minimal human involvement [68,69]. These models perform tasks such as retroactively classifying existing data, predicting future trends based on old data, or identifying patterns in the data. Machine learning differs from older methods of statistical modelling because it is developed using automatic rule-building based on inherent characteristics in the data [70]. With older methods, bias could easily enter into a model since the algorithm would be based on approximate interpretations of the data from the developer or researcher. Machine learning addresses much of the bias problem because the algorithm adapts directly to the data, effectively removing the intermediary bias introduced with human interpretation of the data [71].

There are two broad categories of machine learning which differ in the structure of the data and objective of the project [72,73]. Supervised machine learning models are trained on patterns in a labelled dataset (ex. placenta histopathology images with associated case and control labels) [70,74].

The trained model can subsequently be provided with unlabelled data and make accurate label predictions based on the learning it did in the training phase. Conversely, an unsupervised machine learning model will identify patterns in unlabelled data (ex. placenta histopathology images with no associated labels) in order to uncover structure in seemingly disordered data [70,75]. In this type of learning, the model is trained uniquely on inherent characteristics of the dataset. Unsupervised machine learning removes all human bias from the model and is often used to explore and identify novel patterns in complex datasets.

A detailed discussion of the various methods used for supervised machine learning, particularity in the context of histopathology image analysis, is provided in Chapter 2.

1.5.2 Machine Learning in a Healthcare Setting

Machine learning tools are currently being developed and applied in many different areas of healthcare, including computerized diagnostic aids (CAD)[67,76–78], personalized medicine[79–82], and patient decision aids [82]. The healthcare setting is ideal for the exploration and application of machine learning, as there is a wealth of collected data, human health and disease is complex, and healthcare resources are currently stretched to their limits. There is no question that artificial intelligence will be completely integrated into all facets of the healthcare system of the future, likely bringing with it considerable advances in screening, diagnosis, therapeutic interventions and patient engagement in health decisions.

With these exciting advances, however, comes a number of challenges and concerns that will need to be faced head on. First and foremost is the issue of patient privacy and confidentiality. Privacy regulation is changing in a direction favorable for future secondary use of healthcare data that would benefit owners of the data [83–87]. This push for publicly accessible healthcare data was born out of the desire for transparency, advancement of knowledge generation, and research and development opportunities

[83,86]. As well, our need for human interaction, interpretation, and compassion in a healthcare setting may become compromised in the realm of automation-driven healthcare. In order to combat this problem, we must engage in societal dialog regarding the importance of placing audits and regulations on the ways we allow new technologies to permeate the patient interactions with care providers.

Despite these concerns, significant success has been achieved by several groups leading the push to profit from this new technology in a health care setting. In Chapter 2, a comprehensive overview of the application of machine learning in the field of onco-histopathology is provided – highlighting the advantage of using this technology to detect and classify a variety of tumors using digitally captured histopathology images.

1.5.3 Machine Learning in the Context of Placental Histopathology

As detailed in Chapter 2, the application of machine learning to histopathology specimens has almost exclusively fallen within the realm of onco-histopathology. To date, only a few groups have developed automated tools to digitally assess components of the placenta, but in all instances these tools focused on a small number of specific placental lesions (ex. syncytial knots, distal villous hypoplasia) and they did not employ a machine learning approach [49,88]. The current MSc. thesis project specifically addresses this gap in the literature, aiming to design an automated classification tool using machine learning on placental histopathology images.

Having accurate computerized models that could classify placenta specimens in a matter of seconds could improve issues of inter-observer variability, standardization of practice, and resource pressures. Further, it would open the door to comprehensive pathology examination in low resource settings where highly trained perinatal pathologists may not be available. From a research perspective, computer-driven pattern recognition in placental histopathology images from cases of placenta-

mediated disease may help identify novel avenues of investigation as we seek to better understand the underlying pathophysiology.

1.6 Rationale

The placenta is a vital organ of pregnancy, critical to fetal development and survival. Abnormalities in the development and/or function of placenta can lead to an umbrella of placenta-mediated diseases of pregnancy, including PE. Our ability to properly identify placental disease processes underlying obstetrical complications, and properly council patients on issues of recurrence and long-term health risks, heavily relies on highly trained perinatal pathologists to perform a comprehensive examination of the placenta at the histological level following delivery. However, the clinical utility of this examination is highly dependent on the subspecialty training on the reviewer and resources allocated. Further, this field is plagued with issues of poor standardization and reviewer fatigue. Machine learning modelling has been identified and tested as a tool to address similar limitations in other domains of pathology, with the field of onco-pathology leading the charge in the development and application of automated machine learning tools for clinical application. To date the application of similar machine learning tools have been applied in a very limited scope to the field of obstetrics, with no clinical applications to date focused on the examination of the placenta following delivery. If placenta image models are successful in automatically detecting lesions of interest, they can help automate aspects of placenta pathology and aid in the classification of placenta mediated diseases – ultimately addressing the previously mentioned limitations.

1.7 Hypothesis

A computerized model developed with machine learning can recognize distinct morphological features in human placenta histopathology images and could be applied to automate detection of placenta-mediated diseases.

1.8 Research Aims

Research Aim 1: To perform a systematic review of the literature to identify different machine learning methods that have been successfully applied to histopathology specimens.

- **Sub-aim:** To propose best practices for methodology selection when applying machine learning models to histopathology related research questions.

Research Aim 2: To apply and compare different methods of supervised machine learning to detect morphological features in human placenta histopathology images.

- **Sub-aim 1:** To develop an automated segmentation tool capable of identifying and extracting unique features of relevance from individual chorionic villi structures in human placenta histopathology images.
- **Sub-aim 2**: To apply and compare two supervised machine learning algorithms in the classification of human placenta histopathology images from healthy controls and cases of PE.

In this thesis, a series of manuscripts will be presented, each of which addresses one of the research aims and/or sub-aims.

1.9 Tables and Figures

Table 1.1. Description of Tissue-Level Placenta Disease Processes and Associated Lesions

Category of placental disease process	**Description**	**Representative lesions** [42]
Maternal vascular malperfusion (MVM)	A recognizable pattern of placental injury related to altered uterine and intervillous blood flow dynamics and placental tissue oxygenation [45]	• Placental infarct • Distal villous hypoplasia • Accelerated villous maturation • Increased syncytial knots • Villous agglutination
Maternal decidual vasculopathy	Abnormal transformation of the uterine vascular structure in the decidua [89]	• Insufficient vessel remodelling • Fibrinoid necrosis
Implantation site abnormalities	Abnormal trophoblast invasion depth or site [90]	• Microscopic accreta
Ascending intrauterine infection	Compromised cervical mucus barrier, permitting ascension of pathogens into the uterine cavity [91]	• Maternal inflammatory response (stage, grade) • Fetal inflammatory response (stage, grade)
Placental villous maldevelopment	Either a predominance of non-branching angiogenesis resulting in long filamentous	• Chorangiosis • Chorangiomas

	terminal villi with unbranched capillary loops or knob-like clusters of richly developed and hyper vascularized terminal villi resulting from low-grade hypoxia [92]	• Delayed villous maturation
Fetal vascular malperfusion	An obstruction in fetal blood flow in any location of the placenta vascular tree from the umbilical vessels to the terminal villi [93]	• Avascular fibrotic villi • Thrombosis • Intramural fibrin deposition • Villous stromal-vascular karyorrhexis • Stem villous vascular obliteration • High grade fetal vascular malperfusion
Utero-placental separation	Premature separation of the placenta from the uterine lining likely due to abnormal trophoblast invasion and rupture of spiral arteries [94]	• Chorionic hemosiderosis • Presence of retroplacental adherent hematoma

Fibrinoid deposition	Overabundance of extracellularly deposited fibrin-containing material within the intervillous space [95]	• Increased focal perivillous fibrin deposition • Massive perivillous fibrin deposition
Intervillous thrombi	Pathologic coagulation of blood within intervillous space which often displaces chorionic villi [96]	• Intervillous thrombi
Chronic inflammation	Infiltration of lymphocytes, plasma cells and histiocytes in the villous tree, basal plate, extraplacental chorioamniotic membranes, and chorionic plate of the placenta [97]	• Villitis of unknown etiology • Chronic intervillositis • Chronic plasma cell deciduitis • Chronic chorioamnionitis (Grade, stage)

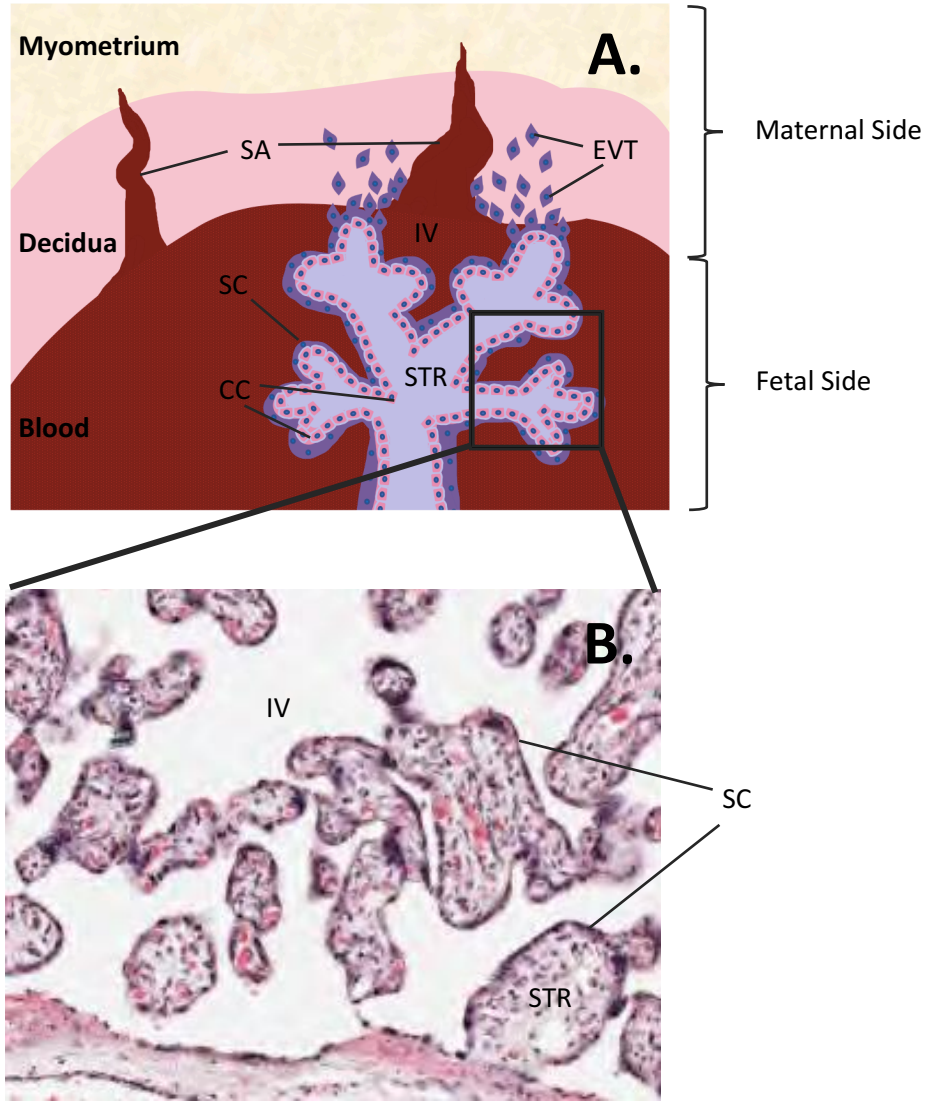

Figure 1.1. Anatomy and histology of the maternal-fetal interface of the human placenta. A. Illustration of the interface between the villous compartment (fetal side) and the surrounding extra villous compartment of the human placenta. Three types of differentiated trophoblasts cells are shown: a multinucleated single cell layer of syncytiotrophoblast (SC) cells forming the boundary between the villous tree and the intervillous space (IV), cytotrophoblasts (CC) within the villous tree stroma (STR), and extravillous trophoblasts (EVT) anchoring the placenta to the decidua and remodelling the spiral arteries (SA). **B.** Cross section of the villous tree at 40x magnification of terminal villi surrounded by intervillous space.

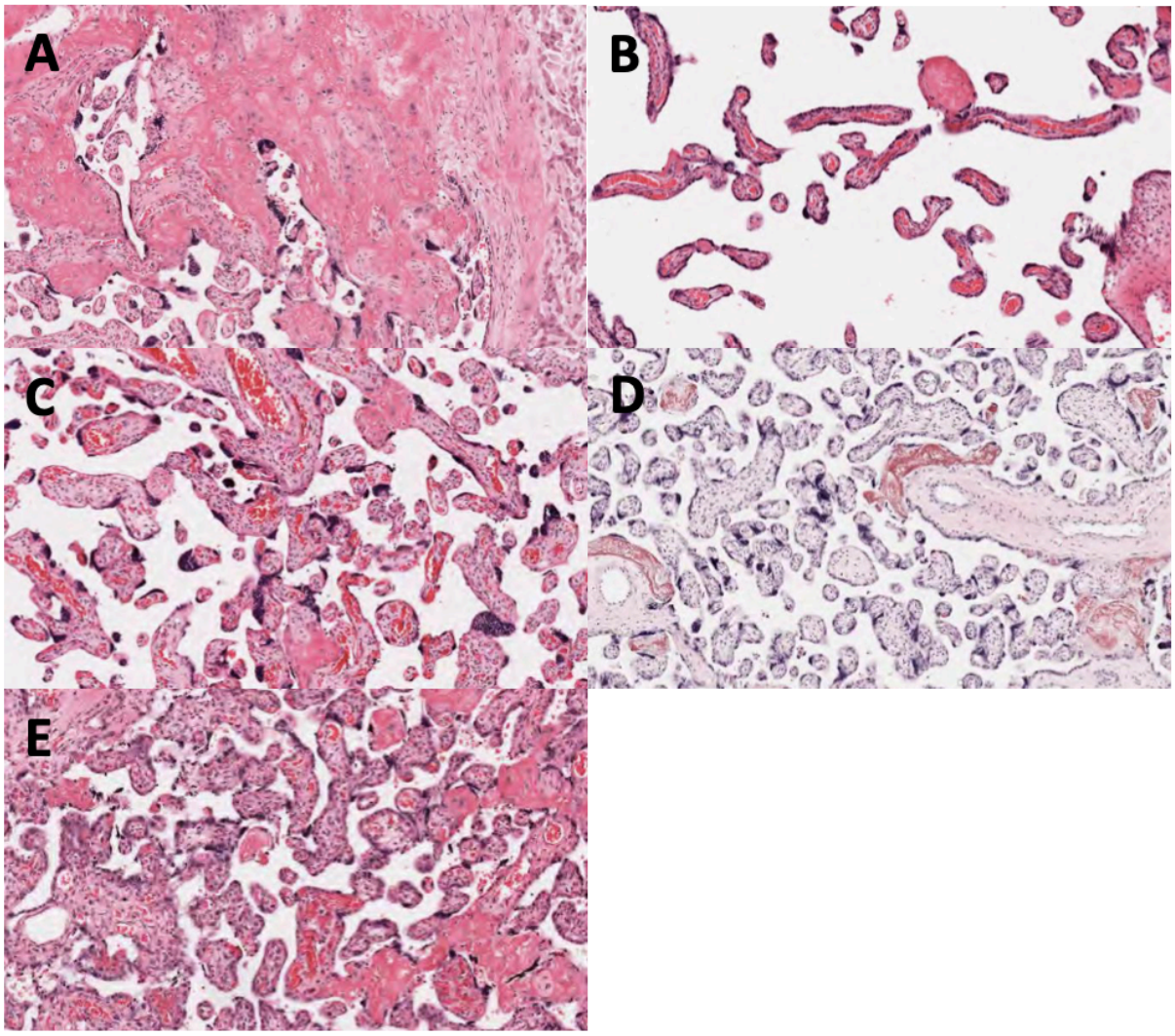

Figure 1.2. Placenta histopathology - lesions of maternal vascular malperfusion. Digital images of placentas from PE pregnancies captured at 20X magnification in Aperio Scanscope. **A)** Placenta Infarcts: villous crowding and coagulation in intervillous space observed in a week 31 placenta. **B)** Distal Villous Hypoplasia: appearance of thin sparse intermediate villi surrounded by small terminal villi in a week 33 placenta. **C)** Increased Syncytial Knots: clusters of syncytiotrophoblast nuclei seen on outer layer of terminal villi in a week 32 placenta. **D)** Advanced Villous Maturation: small villi with increased syncytial knots and increased fibrin deposition observed for gestational age in a week 33 placenta. **E)** Villous Agglutination: bridges formed between terminal villi with syncytial knots or intervillous fibrin in a week 29 placenta.

Chapter 2

Computer Aided Classification of Histopathology Images: A Systematic Review to Inform Best Practices

Mukherjee A[1], Leckie M[2,3], Patnaik P[1], Chan ADC[4], Grynspan D[3,5], Bainbridge SA[1,6].

[1]1Interdisciplinary School of Health Sciences, University of Ottawa, Ottawa, Ontario, Canada.

[2]Department of Physiology, University of Toronto, Ontario, Canada.

[3]Department of Pathology and Laboratory Medicine, Children's Hospital of Eastern Ontario, Ottawa, ON, Canada.

[4]Department of Systems and Computer Engineering, Carleton University, Ottawa, Ontario, Canada.

[5]Department of Pathology, Vernon Jubilee Hospital, Vernon, British Columbia, Canada.

[6]Department of Cellular and Molecular Medicine, University of Ottawa, Ottawa, Ontario, Canada.

This manuscript was formatted for submission to the peer-reviewed journal *Archives of Pathology & Laboratory Medicine*.

Abstract:

Context: Computer-aided diagnosis (CAD) has revolutionized several domains of medical image analysis over the past few decades but has yet to be adopted into clinical pathology practice. Clinical histopathology examination is a prime candidate for CAD-based applications, as issues of procedural and diagnostic standardization have plagued this field for years due to the subjective nature and high degrees of intra- and inter- personal/institutional discrepancies in reported diagnoses. A significant deterrent to clinical adoption in pathology is the lack of a standardized protocol for CAD model development for applications to histopathology images, which makes safety and efficacy testing a challenge. Having a standard protocol for the development of such tools is necessary to provide a gold-standard against which models can be evaluated, and once in place, it would facilitate their transition to clinical use.

Objective: To conduct a systematic review of the current methods of CAD development and application to histopathology image datasets and provide recommendations for best practice.

Data Sources: The databases Medline, Embase, Scopus, and IEEE Explore were used to identify all applicable articles.

Methods: A total of 230 articles were retrieved from a MeSH term search in the 4 academic databases listed above. After three authors conducted full text screening with moderate agreement (weighted Kappa scores of 0.47-0.71), 18 articles remained to be analyzed. Articles were assessed for common methodological elements and for the performance of machine learning classifiers on histopathology image. The results reported, discussion in the articles, and information from current literature was used to propose a set of recommendations to guide researchers in applying the 5 steps to develop machine learning tools on histopathology images.

Results: All studies that passed through screening had 5 common methodological elements: image acquisition, image preprocessing, tissue feature extraction, pattern recognition and classifier training, and algorithm testing. One or more recommendations were proposed for each of the 5 elements based on the findings in the articles and the available literature.

Conclusions: While a wide variety of approaches were used, all studies followed a 5-step workflow to develop classification models for histopathology images. The articles assessed focused uniquely on onco-histopathology images, but due to the adaptive nature of machine learning, the techniques presented can be applied to datasets relevant to other disease states. The guidelines proposed should be used to inform experimental design in future machine learning projects on histopathology images across pathology domains.

Introduction:

Histopathology analysis is one of the primary methods for assessing disease progression in a variety of tissues, but continues to face challenges in an ever evolving clinical environment[1,2]. Analysis of whole slide images (WSI) captured from histological specimens requires pathologists to detect subtle visual patterns in complex tissues, which can be challenging, time-consuming, and lead to high rates of inter-observer reporting differences[3,4]. As such, a strong case has been made for the development and integration of computer aided diagnostic (CAD) tools for clinical histopathology image analysis[3,5,6]. CAD applications in the field of pathology use mathematical models to classify an input image according to a clinical output of interest, such as diagnosis or prognosis, helping to standardize the evaluation of clinical specimens and provide decision support for pathologists[3–5]. Historically, developing such mathematical models on histopathology images was nearly impossible due to the complexity and size of high-resolution WSI[4,7,8]. However, the increasing popularity and accessibility of machine learning (ML) model development has rendered CAD applications within reach for this clinical domain[9].

Supervised machine learning algorithms allow for automated model development with minimal human intervention, with the model "learning" inherent characteristics in the training dataset.[10–12] In the case of histopathology image analysis, a branch of machine learning termed Computer Vision is applied, in which the model is trained to recognize distinct *visual* features in the images that are unique to the labeled clinical outcome of interest (i.e. diagnosis, prognosis, etc). [13–15] Once the model is adequately trained, it can predict (i.e. classify) the clinical outcome of interest in a set of unseen and ultimately unlabeled images, based on the absence or presence of these same visual characteristics[16]. Machine learning model development and assessment, in the context of Computer Vision applications, typically follows 5 fundamental steps [4] (Figure 1):

Step 1) *Image acquisition and data preparation*[4,8,14,17,18] – Digital images are captured from clinical specimens of interest. Tissue samples can be acquired from large public databases or from private hospital collections. Images are annotated or labeled according to the desired clinical categories to be predicted by the model. At this stage, all original annotated image data can be split into model training, validation and testing datasets.

Step 2) *Image pre-processing*[4,14] - Image transformations and data augmentation are conducted on all images. These transformations help to normalize non-biological visual variations across specimens and to augment the size of the original dataset to ensure robust model development.

Step 3) *Tissue feature extraction*[4,14,17] – Automated extraction of visual features of interest is conducted, ideally extracting features that may be different across the groups of clinical interest[17]. Dimension reduction is often applied at this step[4,19], aiming to reduce the computational power required to process all of the data and remove redundant features.

Step 4) *Pattern recognition and classifier training (**model development**)*[4,14,17,18] – An iterative process in which the algorithm "learns" visual characteristics in each image, unique to the clinical labels applied to the training dataset. The model is punished for errors in classification until the rate of correct classification improves and reaches a stable classification accuracy[4,20]. The resulting product is a trained classifier (model) that can predict a clinical classification label based on the rules adopted during training. Cross-validation can be applied to fine-tune model training and can provide a reliable estimate of classifier performance [21,22].

Step 5) *Model testing*[4,14] - The developed classifier is tested on an unseen image dataset – the testing subset[22]. Model classification performance is assessed through comparison of model outputs to ground truth image labels.

Despite considerable advances in CAD-based research focused on clinical applications, to date we have yet to see a translation of this technology into clinical practice. The highly technical language used in the majority of papers on this topic, coupled to a lack of standardized protocols for the development, application and assessment of histopathology-based CAD tools have certainly been limiting factors for clinical translation. A 2013 survey on CAD support systems declared insufficient testing and validation as the primary barrier for clinical adoption[23], with the identification of published systematic methods for developing and assessing the utility of these tools identified as key to overcoming this barrier. As such, the purpose of this systematic review was to provide a comprehensive review of the CAD model development and validation protocols that have been reported to date for clinical histopathology image analysis. It is anticipated that by consolidating this information and proposing an accessible standard guideline for best practices, the barriers for clinical adoption of CAD technology in histopathology can be overcome.

In the current review, a systematic analysis of 18 articles which applied the above-mentioned Computer Vision workflow for purposes of histopathology analysis is presented, including a comparison of model performance according to methods used. The findings are an important first step in the identification of the best practice for applying commuter-aided diagnosis in the clinical pathology environment.

Methods:

Search strategy

The York protocol for systematic reviews[24] was employed, using a search of 4 primary biomedical, clinical science, and engineering databases (Medline, Embase, Scopus, and IEEE). A combination of relevant MeSH terms, keywords, and word variants were used (Supplementary Table 1). A scan of all identified articles was performed to remove any duplicate articles.

Inclusion/Exclusion Screening

All articles were assembled in reference manager software (Mendeley), and 3 reviewers (A.M., D.G., and M.L.) performed the initial screening of titles and abstracts for inclusion/exclusion criteria. Primary inclusion/exclusion criteria were: 1) a primary research aim which included image segmentation or image classification; 2) methods that were being applied to digital histopathology specimens from humans; 3) primary objective related to clinical utility of CAD technology (not solely for the purpose of basic scientific investigation). All tissue and disease subtypes were included provided they met the above criteria. Conference proceedings, provided all other criteria were met, were included, however reviews, book chapters, and papers discussing methods that are not routinely used in clinical pathology practice (ex. focused exclusively on nuclear texture, immunohistochemistry quantification, or prognostic immunohistochemistry) were excluded. The level of reviewer agreement was assessed by comparing screening decisions from each reviewer and measured using a weighted Kappa score[25]. Disagreements were resolved through joint discussion until a consensus was reached. Subsequently, a full-text screening was performed by 2 reviewers (A.M and M.L.) on articles that passed the initial screening to ensure they met the inclusion/exclusion criteria listed above.

Data Extraction

Following a full-text screening of each article, author A.M. identified seven recurring methodological themes: description of cancer tissue type (ex. brain, thyroid, etc.), image pre-processing methods, feature extraction methods, dimension reduction methods, classifier(s) used, cross-validation method, training/classifier performance. With this list of themes in mind, an excel data extraction template was devised to enable consistent data collection from each article. The data extraction template contained the list of studies on one axis and the list of common elements on the second axis so that the same raw data would be collected for each study, regardless of the author extracting the data and regardless of whether a method was absent in a particular article. Authors A.M. And M.L. systematically extracted methods presented in each article along the dimensions in the excel template.

The raw data from the excel template was later refined (ex. Dimension Reduction was grouped with Tissue Feature Extraction) to fit into the five standard steps of a computer vision workflow (Figure 1): 1) Image Acquisition, Image Pre-processing, Tissue Feature Extraction, Pattern Recognition and Classifier Training, and Algorithm Testing. The results were then extracted into tables (Tables 2-6) summarizing the different methods used in each step along with which articles used said methods.

Quality Assessment

A risk of bias and assessed applicability analysis of each article was performed using the QUADAS-II tool for diagnostic tests of accuracy (under the Cochrane Guidelines for Systematic Reviews)[26]. To our knowledge, there are no quality assessment tools unique to CAD-based diagnostic application, however the flexibility with QUADAS-II tool allowed for customization of this analysis to the current literature dataset. Reviewers A.M. and P.P. assessed the following categories for each paper: 1) Patient Selection, 2) Index Test (new diagnostic test), 3) Reference Standard (original validated protocol for diagnosis), and 4) Flow and Timing (process patient undergoes to compare reference standard and index test). Risk of

bias for articles for the Reference Standard and Flow and Timing criteria were judged to be unclear when there was no information on how the pathologists assigned ground truth labels.

Results:

Article Selection

The initial article search yielded 230 articles, with 209 removed following screening of the title and abstract and another 3 removed following full text screening for inclusion/exclusion criteria. Reviewer agreement on the inclusion of articles during screening was moderate to good based on weighted kappa scores[27]. Weighted kappa scores between reviewers were: 0.71 (A.M. - D.G.), 0.55 (D.G. - M.L.), and 0.47 (A.M. - M.L). 10 articles were discussed for discrepancies in screening to reach a consensus on articles to be included. The final dataset comprised of 18 articles that met the specific criteria outlined above (Figure 2). A list of the papers included for analysis by author and year is included in Table 1. All 18 articles applied their methods to cancer-related histopathology specimens including brain, breast, colon, kidney, larynx, ovary, prostate, skin, and thyroid cancer (Table 2).

Computer Vision Methodology

i. Primary Research Aim

All articles analyzed had a primary research aim of automating diagnostic classification of clinical histopathology images. Small differences in identified research objectives stemmed from differences in tissue and/or disease subtypes included in the datasets. For example, prostatic adenocarcinoma severity is measured using the Gleason scale[28], so training labels/classifiers used were in reference to the corresponding Gleason scores[29,30]. All articles used either a non-biased approach, using textural patterns in the histopathological images[31], or relied on explicit segmentation of biologically relevant features (i.e. nuclei)[32]. In individual instances, articles explored both approaches described above, along with many different classifiers, and reported and compared the results from each[33]. Most papers used visual

elements of an image to train an image classifier, with the goal of automating prediction of clinical diagnosis in unseen images (ex. Benign vs malignant tumor). However, Ninos et al.[34] and Yu et al.[35] used their classifiers to predict patient survival rates, and were included as the methods used followed the same 5-step computer vision workflow described (Figure 1).

Image classification categories (i.e. labels) reported in the included papers were: Gleason score[29,30], benign vs malignant tumor[33,36], glioblastoma stages[37,38], American Joint Committee on Cancer (AJCC) melanoma stages[31], ovarian carcinoma subtypes[39], renal carcinoma subtypes[40], tumor vs non-tumor[35,41–43], thyroid follicular adenoma vs. thyroid follicular carcinoma vs. healthy thyroid[36], colorectal cancer subtypes[44], good vs. poor prognosis[34,35], low vs. high grade laryngeal cancer[45], and healthy thyroid vs. papillary thyroid carcinoma[32].

ii. Image Acquisition (Computer Vision Workflow Step 1)

A number of studies used large publicly available histopathology image databases for image acquisition. These included the BreakHis dataset[33,38], The Cancer Genome Atlas (TGCA)[35,46,47], the Trans Canadian Ovarian Cancer Dataset[39], the Stanford TMA database[35], the Cooperative Human Tissue Network (CHTN)[31] and the PETAACC-3 dataset[44]. The articles that did not use a public database retrieved and digitized a small number of archived samples from a local hospital or university[29,34,36,45,48] or did not specify the origin of the histopathology images used[40–42,49,50]. Sample sizes varied widely across studies (Table 1), ranging from 7-742 individual patients and 15-21860 individual images, with some groups failing to indicate the number of patient samples used[37,43]. Only Xu et al[43]. mentioned using a sample size for each class that reflects the true prevalence of the lesion(s) in question.

Histopathology specimens were prepared from original tissue samples using standard procedure: tissue fixation, embedding in paraffin wax, and sectioning with a microtome[51]. Embedded tissue sections were then mounted on glass slides, stained with H&E, p63, Feulgen stain, or DAB, covered with a glass slip,

and digitally scanned. Images were taken with a light microscope paired with an RGB digital camera or with a high-resolution glass tissue slide scanner, most commonly at a magnification of 40X. Some databases had previously acquired images at multiple resolutions (40X, 100X, 200X, 400X). The digital image file types most commonly used were Whole Slide Images (WSI) and Tissue Microarrays (TMA), and were in the SVS file format which contains a pyramid of images at multiple magnifications[52]. Images included in the pyramid usually range from 240x240 pixels to 1024x768 pixels. SVS files of scanned histopathology tissue were often greater than 1 Gb in size[7].

iii. Image Pre-processing (Computer Vision Workflow Step 2)

Image pre-processing is the process of applying a series of transformations to images before feeding them to a classifier. This step is often done in preparation for feature extraction to ensure all images are uniform[4]. Four pre-processing techniques were identified in the article dataset: 1) augmentation; 2) colour transformations; 3) data cleaning; and, 4) automatic segmentation. All articles used some combination of these four methods. Yang et al.[36] did not report using any preprocessing on their data. Table 3 contains a summary of image pre-processing methods used in each article. Selective discarding of poor-quality tissue sections or images is included as a separate category in Table 3, however, for simplicity it is categorized under data cleaning in the description below.

Data augmentation involves increasing the number of examples a classifier can learn from. Data augmentation is achieved through random image transformations such as rotation, flipping, and stretching at each round of training and/or by extracting multiple image patches from the original image prior to training, increasing the size of the training dataset[18,53]. Data augmentation is particularly crucial in computer vision applications, allowing developers to address the requirement for large training datasets in the face of ethical and/or financial constraints which may limit the number of original patient samples available for ML development[53,54]. This technique also provides an opportunity to address

inherent problems in a dataset, such as class imbalance. In this case, under-represented clinical classes can be specifically augmenting in the dataset, removing any possible bias introduced in the model training phase through uneven class distribution[54,55]. In articles reviewed, fifteen of eighteen articles reported using data augmentation in their workflow. The primary method of data augmentation was multiple image patch extraction. Extracted image patches ranged in size from 32x32 to 2000x2000 pixels, sometimes capturing hundreds of small overlapping patches from across the original image, or randomly selecting a small number (10-20) of representative patches from each original image. In some cases, the augmentation method used included the extraction of patches from the same image at multiple magnifications[33]. Bayramoglu et al.[38] also described rotating and flipping images as part of their augmentation method, further helping a classifier learn more variations of image features.

Many articles reported manipulating the image colour in the pre-processing step. Either the images were converted to greyscale, or they were converted to HSI (Hue, Saturation, Intensity), HSV (Hue, Saturation, Value), or CIE L*a*b* (Commission internationale de l'éclairage – Lightness*, Red-Green*, Blue-Yellow*) colour spaces[55,56]. Converting images to greyscale reduces the complexity of an image, reducing the image from 3-4 channels (ex. red, green, blue (RGB)) to 1 channel (grey)[55]. Greyscaling images also helps to highlight dark areas, which can facilitate segmenting objects of interest, such as nuclei[37,55]. Non-greyscale colour transformations, such as converting an RGB image to HSV format, were used in one article that tried to mimic the process a pathologist would use to analyze images[42]. In this article, colours closer to those interpreted by the human eye were chosen, rather than simply RGB colours[55]. Three groups deconvolved the images into separate hematoxylin and eosin channels because they found less redundancy in the features extracted from those channels as opposed to the RGB channels. DiFranco et al.[30] tested several colour channels to determine which (alone or in combination) yielded better classification results and found that b* channel features from a CIE L*a*b* colour space provided optimal results.

Data cleaning is another pre-processing step that involves inspection of the data in order to remove outliers and images containing little or unusable data[4]. In the case of histopathology images this could include artefacts on slides, folds in tissue, areas of inconsistent staining[57], or poor scanning quality[52]. To mitigate this problem, several authors chose to have a pathologist manually select regions of interest within slides[30,33,34,38,42,48], discard images or patches of poor quality[33,38,42,48], automatically discard images containing too little information[39,48], or exclude objects based on size threshold[45]. In the context of computer vision, data cleaning may also include reducing the complexity of images. Articles in this search reported using smoothing, noise reduction, and increasing contrast of image datasets to amplify important patterns and facilitate feature selection. For histopathology images, normalization during the data cleaning stage of pre-processing can specifically address a common issue unique to histopathology specimens - differences in staining intensity[58]. Normalization involves modifying the intensity of the pixels in an image by a scaling factor to achieve consistency between different images[18,58,59]. A common approach was Min-Max scaling, which shifts the possible pixel values to a consistent range for all images[60].

While some articles chose to classify images based on the global appearance of images, others felt it more pertinent to segment objects of interest prior to classification. Automatic segmentation is used to pre-select and extract objects or regions of interest within an image that are relevant to the clinical outcome (ex. nuclei from malignant cancer cells)[61]. Seven articles reported using segmentation to isolate regions of interest in images prior to classifier training. Open source and commercial software packages, such as CellProfiler, OpenCV, and MATLAB, are currently available to aid in image segmentation, and were used in several of the reviewed articles[33–35,37,39,40,62]. Algorithms used to segment nuclei included random field graph cut[63], active contours[64], fuzzy c-means clustering[65], PSO-based Otsu level thresholding[66], density-based clustering[67], and curvelet transform[29]. Most of the algorithms described above are available through free software such as ImageJ[68], or can be implemented with common

coding languages such as Python. However, Curvelet transform was a novel method developed by Lin et al.[29]

iv. Tissue Feature Extraction (Computer Vision Workflow Step 3)

Feature extraction involves converting an image from a raw set of pixels to a numeric representation of an image with real-world relevance (ex. number of cancerous nuclei in an image), or that is less computationally expensive to analyze (ex. quantifying textures found in an image)[4]. In the reviewed articles, global texture feature extraction[30,31,33,36,41,42,44] or object level (clinically relevant) feature extraction[48,49] methods were employed, with some groups testing and comparing both approaches[29,34,35,37,39,40]. As well, two articles extracted keypoint descriptors, which are points of interest in an image that can be used to identify it at any scale[33,43]. Ninos et al.[34] additionally included patient information as a feature to train their classifier.

To carry out global textural and spatial feature extraction there are several programs available to researchers, with the feature extraction toolboxes provided in MatLab and CellProfiler[62] used in some of the reviewed articles to extract over 9000 features[30,31,34,35,40,43]. Global features described in the articles retrieved can be categorized into: Local Binary Pattern (LBP)[69], Local Phase Quantization (LPQ)[70], Grey-Level Co-occurrence Matrix (GLCM)[71], Haralick features[71], wavelet features[72], and Gabor features[73], and keypoint descriptors[74,75]. The most commonly used Keypoint descriptors include SIFT[76], SURF[77], ORB[78], FAST[79], and BRIEF[33,80]. We direct the reader to Spanhol et al.[33] for a description of LBP, LPQ, GLCM, and keypoint features, and to the Appendix in Wang et al.[48] for a brief description of Haralick features, wavelet features, and Gabor features.

A total of 9 articles instead used an object level feature extraction approach, with common extracted features including area, convexity, and circularity[29,34,35,37,39,40,45,48,49]. Object level features are attractive for analysis on histopathology images because they are computed on objects pre-determined to be

clinically relevant in an image (ex. nuclei, tumour regions)[4,81]. The drawback is that this step may introduce human bias or error into a classifier if objects of interest are manually segmented, or if thresholds for automatic thresholding are inappropriate. Object level features include elliptical, convex hull, bounding box, boundary, and other shape features[37]. Table 1 in Fukuma et al.[37] presents a comprehensive list of object level features and their organization into the five categories listed above. These shape features are commonly used to distinguish cancer and healthy samples in digital pathology, and they describe shape elements such as area, perimeter, convexity, and eccentricity of an object[48].

The articles we examined reported extracting between 10 – 9878 features per image. When too many features are used, some may be redundant and no longer help the classification algorithm discriminate between classes. In these cases, dimensionality reduction is used to reduce the length of the feature vectors that describe each image and increase the efficiency of classification[82]. Dimension reduction methods reported in the articles retrieved include: Greedy Hill Climbing[83], Pearson's Correlation[84], mRMR[85], Linear Discriminant Analysis (LDA)[86], Dissimilarity Matrix[87], Fisher Score[88], Wilcoxon's Correlation[89], Variable Precision Rough Sets (VPRS)[90], Mean Rank Plots (MRP)[91], Principal Component Analysis (PCA)[92], Multiple-Dimensional Scaling (MDS)[93], Local Linear Embedding (LLE)[94], Isometric Feature Mapping (ISOMAP)[95], Local Tangential Space Embedding (LTSA)[96], Point Biserial Correlation[97], and Information Gain Ratio[98]. Yang et al.[36] tested MDS, PCA, LLE, ISOMAP, and LTSA with 3 to 4000 dimensions and reported that ISOMAP performed the best. Jothi et al.[99] described and tested the VPRS based b-reduct methods with a closest matching rule classifier and achieved 100% classification accuracy. Rough Set Theory[100] (the basis of VPRS) has previously been used to reduce image features in various medical image types such as mammograms, Computed Tomography, and Magnetic Resonance Images[99]. An alternative approach described by Yu et al.[35] and Orlov et al.[31] was to determine the optimal number of features using the cross-validation results. DiFranco et al.[30] also used a random forest classifier, which provides feature importance by counting the number of times a feature is selected in

each decision tree. (See Results – Classifiers and cross-validation). Table 4 includes a summary of feature extraction and dimensionality reduction methods included in each paper.

v. Pattern Recognition and Classifier Training (Computer Vision Workflow Step 4)

Classifier training is the fundamental stage in developing an ML model where it sets rules by which the algorithm will distinguish between classes[4]. Fine-tuning of the training is carried out using cross-validation methods which can provide a reliable estimate for how well the model is performing by plotting a learning curve that shows the rate of improvement of performance on a portion of the training data over rounds of training. A summary of classifiers and cross-validation methods used in the selected articles is included in Tables 5. Types of classifiers applied in the selected articles were: Support Vector Machine (SVM)[101], Nearest Neighbors[102], Decision Tree[103] and Random Forests[104], Bayesian[105], Boosting[106], Neural Networks[107], Multiple Instance Learning (MIL)[108], Discriminant Functions[109], and novel classifiers[32]. Differences between classifiers lie in the mathematical approach to creating a decision boundary. Some articles chose to apply ensemble-based learning, where the output from multiple classifiers was used to improve the overall accuracy[30]. Support vector machine (SVM) was a popular choice of classifier in the article dataset, appearing in at least one experiment in 11/18 articles[29,30,33,35–37,39,42–44,48]. The SVM classifier finds a set of hyperplanes in the n-dimensional feature space that has the longest distance to the nearest training points of other classes[48]. They can be paired with different kernels (linear, quadratic, radial based Gaussian) to fit the data better. This classifier works well for large feature spaces, which usually is the case for histopathological image data.

In 8 articles reviewed[30,33–36,43,45,48], cross validation methods were used to fine tune the parameters used during the training phase and assess computational needs using a learning curve, although some articles[29,31,32,37–40,44] only reported using cross validation to evaluate model performance (*Computer Vision Workflow Step 5*) or employed both uses of cross validation[34,36,43,45,48]. Broadly, this method

involves splitting the training dataset into smaller training/validation sets (ex. training set split into 80% for training and 20% for validation) and evaluating the rate of improvement of performance on the portion of data reserved for validation in order to tune parameters and assess how much computing resources are required for a project. Types of cross-validation methods reported in the reviewed articles included K-fold[110], Leave-One-Out (LOO)[111], Sequential Backwards Selection[112], Jackknife[113], and Bootstrap[113]. Differences between cross-validation methods stem from how training dataset is split at each round of training. LOO, Bootstrap and Jackknife cross-validation involve testing every possible split of data to obtain optimal results, whereas the others involve splitting the data into a discrete number of portions for validation.

vi. Algorithm Testing (Computer Vision Workflow Step 5)

To assess the performance and generalizability of a developed ML model, an unseen test dataset is fed into the model and the predicted output labels are compared against the "Ground Truth" labels of the dataset. All articles reviewed were retrospective studies comparing image classification based on manual pathology evaluation (ground truth) vs. ML model evaluation on the same task. ML model performance was measured as a combination of true positives (TP), true negatives (TN), false positives (FP), and false negatives (FN). These can be combined in many ways to punish errors that are less acceptable in a given problem. In the articles analyzed, accuracy ((TP + TN) / number of images) was most commonly used as the primary performance measure[29,31,33,34,36–42,44,45,48,49]. Reported accuracies for the methods presented ranged from 65% - 100%. Orlov et al.[31], Wang et al.[48], and Jothi et al.[32] reported achieving 100% accuracy in at least one developed model. They used a nearest neighbor classifier, an SVM, and an SVM and Decision tree combination respectively to achieve these results. A summary of the optimal model performance achieved in each article is summarized in Table 6.

Risk of Bias

The QUADAS-II tool was used to assess the risk of bias and applicability of the included articles, with the results summarized in Figure 3. Overall, the risk of bias was low for all articles, except for rare cases where one of four categories of assessment were considered high risk[37,40,42–44]. In most cases, the reason for the high risk of bias was that it was unclear whether or not patient selection was biased[40,42–44]. Several of the articles accessed cancer histopathology images from a database of samples previously collected, and authors did not disclose whether they recruited representative patients, whether patients were randomly enrolled, or whether there were any inappropriate exclusions of patients. The articles by Budinska et al.[44], Mete et al.[42], and Yu et al.[35] were deemed to have a high risk of bias for the Patient Selection criterion, as they did not describe how patients were selected and did not include a clinically representative distribution of cases. Yu et al.[35] explicitly stated in their discussion that because they obtained their cases from a public database (TCGA), there was an overrepresentation of cases where morphological patterns of disease were obvious and might not reflect what a pathologist would see in clinical practice[35].

For the most part, we found that articles scored low on the risk of bias for the Index Test criterion. Contrary to a standard diagnostic test of accuracy, where a clinical researcher would be applying a new test and comparing it to previous standards, in the articles retrieved, a computer performed the new test analysis. An automated tool removes subjectivity and ensures the reproducibility of results. In some articles, it was unclear whether regions of interest were selected or discarded systematically, so the risk of bias for the index test criterion could not be definitively assessed. The article by Fukuma et al.[37] demonstrated a high risk of bias, as they did not split their data into training and test sets and they did not report results from all classifiers. If their classifier was evaluated on the same data it was trained on, the accuracy would be falsely high. The assignment of ground truth labels was often unspecified in cases where images were obtained as a secondary source from a database. Finally, there were few concerns

regarding the applicability of the articles to the original research question for this study, as very stringent inclusion and exclusion criteria were applied to article selection in respect to this criterion.

Discussion:

The application of computer vision as a CAD aid in the field of clinical histopathology has tremendous potential, yet the complexity and wide array of methods available in this domain make the translation of these tools into the clinical environment a daunting task. One of the primary challenges in bringing histopathology CAD tools to the market is the lack of standardization in the methods used to develop the models, making it difficult to determine which models would be best suited and have the highest performance metrics in a clinical setting[23]. While a large variety of methods were observed in the systematic review of the literature on this topic, a clear 5-step workflow was identified as the common thread to all studies (Figure 1). Interestingly, the application of a 5-step workflow was not used as an explicit inclusion criterion for this review, but instead was an inherent characteristic of the all reviewed study designs. While a clear consensus on best practices to be used within the 5-step workflow framework was not apparent in the individual studies reviewed, the high-level overview provided through this systematic evaluation has allowed for the generation of recommendations of current best practices for each of the 5 workflow steps, as described below (Table 7).

Image Acquisition (Computer Vision Workflow Step 1)

The articles reviewed had a common research aim of developing a computerized model that can take a histopathology image as an input and output a clinically relevant label of interest, such as diagnosis or prognosis. Despite not having excluded any type of histopathology samples in the screening criteria, the articles represented in the search were overwhelmingly focused on cancer diagnostic aids. This was not surprising considering the large publicly available digital image databases dedicated to cancer-specific pathologies (ex. The Cancer Genome Atlas), facilitating these types of CAD-application initiatives. A considerable strength of using image datasets from these public repositories is access to large datasets

with minimal costs and often a high degree of quality control as it relates to image quality and annotation – aspects that can be highly variable in smaller, institution-based collections. This can allow for better model comparison across research groups as well. Unfortunately, similar large-scale, highly annotated public image datasets for tissue types and pathologies outside of cancer are not currently available, a considerable limitation that has no doubt hindered paralleled progress in the development of CAD-based tools for other important clinical domains, such as perinatal pathology, dermatology, gastrointestinal and hepatic pathology.

While there is no gold standard for sample size calculations that can be easily applied to determine optimal numbers of patient samples required for ML model development, it is generally acknowledged that model accuracy improves with increasing sample sizes[114,115 116]. The complexity of the machine learning algorithm being used is an important consideration, with traditional machine learning models, such as SVM, requiring fewer input images compared to more complex deep learning models. And finally, in the context of histopathology datasets, the baseline degree of variability that may be observed in the tissue of interest in both healthy and sick populations need to be considered, ensuring the dataset used for training adequately represents this variability. A small number of studies have proposed statistical methods for calculating optimal sample size, using either characteristics of the data such as number of classes and number of features (model-based approach)[117] or by learning from the rate at which the model improves over training (inverse power law approach)[118,119]. However, even these methods yield considerable variations in estimated sample sizes, in the magnitude of hundreds of images, providing little clarity to a researcher requiring guidance in experimental design. In the reviewed articles, digital image sample sizes ranged from 15 to > 21,000, originating from 7-742 distinct patient samples – demonstrating a clear lack of guidance and consensus on sample size determination for ML model development in this domain.

A clear description of how patient samples are selected for inclusion in a study and what parameters were used for ground truth sample classification are also important considerations. To generate a robust CAD model with widespread generalizability in the clinical context, one must be sure that the patient samples being used for model development were truly representative of the clinical population of interest and that the methods used to classify each sample were clear, appropriate and reproducible. Unfortunately, these descriptions were often lacking in the reviewed articles on this topic, properly described in only 4 of the 18 articles reviewed (Figure 3). Further, the highly subjective nature of pathological evaluations – used as ground truth classification of images – must be considered. While in the field of onco-pathology the degree of inter- and intra- evaluation variability may be lower, in other fields of study this variability can be quite high and would therefore greatly impact the performance metrics of the developed ML model.

Recommendation 1a: The use of highly annotated, publicly available digital image databases is the current gold standard for image acquisition in the development of CAD-based machine learning model development, allowing for wide access to large, high quality datasets. Consolidated efforts should be undertaken to generate large scale, highly annotated digital image databases for tissue types and pathologies outside of cancer to ensure the progress being made in the field of oncology can likewise be realized in other domains of pathology.

Recommendation 1b: Researchers should aim to maximize the number of individual samples included when developing machine learning models, applying data augmentation techniques to further increase training sample size and assess data size impact on model development through the generation of learning curves. Further efforts in this field should be focused on developing reliable methods of samples size determinations for ML model development experiments.

Recommendation 1c: Groups developing CAD-based machine learning models for histopathology purposes need to be explicit in how the image dataset was sourced and annotated.

Image Pre-processing (Computer Vision Workflow Step 2)

Image pre-processing includes 3 major activities, each of which was included to varying degrees in the reviewed articles: 1) data augmentation, 2) image normalization, and 3) data cleaning. Of these three activities, the biggest challenges in protocol standardization efforts will likely be focused on the first two. As indicated previously, the development of a robust model requires a considerably large image dataset in order to properly train the algorithm to detect class-specific differences in extracted features. Unique to the realm of medical imaging, access to large, highly annotated image datasets of clinical specimens can be a major limitation to CAD model development. An important technique used to overcome this challenge is data augmentation. A common approach to data augmentation is the use of a sliding window image patch extraction, in which a number of smaller overlapping images are captured from across the entire original image. This method was employed in a total of 3 articles reviewed[29,42,43], augmenting dataset up to 7,000 fold. For researchers with limited access to samples, a sliding window approach offers a fast and systematic way to augment data. A similar approach, which attempts to mimic a pathologist's approach, extracts a smaller number of image patches from distinct or representative regions of the original image, and in the case of the reviewed articles, augmented datasets by a factor of 10-3,000 fold[40,44,45]. Importantly, the process of data augmentation through patch extraction also addresses another major barrier currently faced in histopathology image analysis – the large file sizes of these high-resolution digital images. Scanned images used in histopathology analysis often contain over a gigabyte of information[7], presenting an enormous computational task. The use of image patch extraction can reduce the size of these files to the magnitude of hundreds of kilobytes (or

hundreds- thousands of pixels squared), sizes that are compatible with current computing power availability for most users. Further, opting for the development of a traditional machine learning classifier (vs. a deep learning classifier) with pre-extracted image features, as seen in 15 of 18 articles review, can also minimize the required computational power needed. Bayramoglu et. al. was the only article to mention using image modifications such as rotation and flipping to their dataset as a form of data augmentation. This is somewhat unsurprising, as it is a technique more commonly used in deep learning where it is typically embedded in the training process as a random image generator that would produce different transformations at each round of training[31,38,45]. Although this technique is useful in increasing variability and size in a smaller dataset[120], one must be careful when applying some image manipulations (i.e. stretching), always keeping in mind the biological importance of morphological features in the tissue of interest.

Image normalization is an important consideration when working with histopathology specimens. Differences in tissue staining intensity and/or lighting differences in the captured digital images can have a considerable impact on model classification accuracy. The articles reviewed combatted this problem using a variety of image normalization strategies. In some of the articles reviewed, color transformation processes were compared[30,31,42,48], indicating that there was no clear choice for which colour space to use. Orlov et. al. compared classifier performance using RGB, CIELab, and deconvolved H&E colour spaces and found that the H and E colour space outperformed the other two by far, achieving an accuracy of 95% compared to 75% and 72% for the RGB and LAB spaces, respectively. However, the method of color normalization applied for any CAD model development will need consideration to ensure that that the features of highest relevance are being adequately highlighted for classifier training. In addition to image normalization, data cleaning includes routinely scanning for artifacts and poor quality until automating the detection and removal of histopathology-specific artifacts becomes commonplace and efficient. Data cleaning with manual removal of images or regions in 11/18 articles

and was used to ensure that the features subsequently extracted represent the true morphological differences between groups, unconfounded by differences in staining or artifacts[30–35,37,41,42,45,48].

Recommendation 2a: The adoption of sliding window image patch extraction is a reasonable data augmentation approach to considerably increase the size of the training dataset, while minimizing computational power required.

Recommendation 2b: Image modifications incorporated through a random image data generator during classifier training can be used for deep learning experiments to increase size and variability of image datasets.

Recommendation 2c: While model-specific considerations must be used, H&E channel and l*a*b* color normalization methods demonstrate optimal results in their ability to best highlight distinct tissue morphology in histopathology specimens used for ML model development.

Tissue Feature Extraction (Computer Vision Workflow Step 3)

Tissue feature extraction demonstrated the highest degree of methodological variability in the review of the literature. If a fully automated approach is used for feature extraction, the introduction of human bias into model development can be minimized. However, the mathematical descriptors used to identify and extract features from each image may not necessarily be driven by the biology and/or pathophysiology underlying disease mechanism. On the contrary, if manual or semi-automatic feature extraction was guided by the expertise of a clinical pathologist - highlighting tissue areas or feature of highest relevance - clarity on how classification decisions were being mediated by the ML model can better be achieved. However, this method can be highly time-consuming and heavily influenced by human biases. Interestingly, the performance of machine learning models was similar across both

feature extraction approaches in the reviewed literature, with some reviewed articles reporting classification accuracy of 100% for both approaches. This would suggest that both approaches demonstrate promise, and ultimately the developer will need weigh the pros and cons of each approach considering the research question at hand. That being said, in order to move this technology into clinical practice, a move towards full automation of feature extraction would likely be required to address clinical work-load management. Moving forward, removing the feature extraction phase entirely, and instead having feature extraction integrated into classifier development will likely yield the most robust and clinically relevant CAD models. Historically, integrated feature extraction which is used in deep learning, has demonstrated improved model performance when applied to non-medical image datasets (ex. for facial recognition or self-driving cars) compared to traditional machine learning algorithms[121–125].

Recommendation 3: Both manual/semi-automated and fully automated feature extraction methods work well in histopathology-focused CAD tool development. A move towards fully automated, and ultimately fully integrated, approaches to feature extraction is recommended to best accommodate translation of these tools into a clinical setting.

Pattern Recognition and Classifier Training (Computer Vision Workflow Step 4)

Two distinct architectures for machine learning models exist, each with advantages and disadvantages: 1) traditional machine learning classifiers with extracted features, 2) deep learning classifiers with integrated feature extraction. In the reviewed articles, multiple classifying algorithms were tested and compared for both machine learning and deep learning algorithms. Support vector machine (SVM) and probabilistic neural network were by far the most commonly used, and while SVM demonstrated the highest ML model performance convolutional neural network (CNN) demonstrated the highest deep learning performance metrics. Although deep learning algorithms have been shown to outperform

traditional classifiers on image classification tasks, a current limitation of this approach is the inability to determine which image features were weighted more heavily in classification decisions. Deep learning is suitable in practical situations where a very high level of accuracy is essential but may pose a challenge in a clinical setting where it is crucial to be able to justify a diagnosis. However this limitation of deep learning is the primary focus of explainable artificial intelligence (XAI), a relatively new but increasingly important field of study, which will allow for the integration *and* understanding of deep learning models in a healthcare setting [126,127].

Eight of 18 articles used cross-validation to assess the rate of improvement of classification accuracy over the course of training, or the "learning", by plotting a curve of error decrease over training epochs[30,33–36,43,45,48]. Although several articles also reported using cross validation to evaluate model performance (Table 5), the results are reported and a recommendation is provided in *Computer Vision Workflow Step 4* because the topic of whether it should be used for parameter tuning or model evaluation appears to still be under debate, but a 2006 study addressing this problem found that using cross validation to evaluate a model and test its generalizability to new data gives a "significantly biased estimate of error" when it is also used to tune training algorithm parameters [128]. Moreover, two of the articles using cross-validation to estimate model performance highlighted the a major limitations to this approach which is the potential for the model to overfit to the training data and fail at generalizing to new data[30,40]. In the reviewed articles, the most widely used method of cross-validation for parameter tuning, but not model evaluation were 5-fold cross validation and leave-one-out cross validation.

Recommendation 4a: Deep learning models represent optimal model architecture when working with complex histopathology image data. However, due to current lack of transparency with deep learning models and the computing resources required, traditional machine learning algorithms are currently better for use with histopathology image data, with SVM classifiers shown to produce equally strong performance metrics.

Recommendation 4b: 5-fold and leave-one out cross validation are common and reasonable methods for fine tuning ML model development for histopathology application, helping to optimize model parameters such as number of rounds of training, sample size, and computing resource allocation.

Algorithm Testing (Computer Vision Workflow Step 5)

Standard practice for ML model development is to reserve a portion of the available dataset as the "test dataset", used strictly for the purposes of final model performance assessment. In total, only 3 of 18 articles explicitly stated following this standard practice, with the size of the testing dataset ranging from 0.016%-50% of the total dataset [40,43], in line with the industry standard of reserving at least 50% of the data for training with room for adjustment if the dataset is too small[129]. Performance was reported as accuracy in all articles except for 3, with other reported metrics including F-1 score and area under the curve. As all these metrics are permutations of the true positives, true negatives, false positives, and false negatives and can be interconverted, they are all reasonable to report. However standardizing reporting guidelines would help with quick comparisons of results across studies.

Surprisingly, in 13 of the 18 articles reviewed, a separate testing dataset was not used to assess model performance, or it was unclear in the text whether or not the data was split. Instead, these articles (aside from the two where the data structure was unclear) reported using cross-validation to evaluate model performance. While cross-validation can provide a reasonable estimate, true model performance metrics are measured when the model is tested on a previously unseen dataset – allowing the determination of a model's generalizability. A likely cause for the adapted use of cross-validation for evaluation purposes was small image dataset sizes[128,129], however this is not typical of standard of ML modelling workflows due to problems related to data overfitting, and ultimately inflated model performance accuracy estimates.

Recommendation 5a: Ideal experimental design for ML model development for histopathology application includes reserving 20% of the original dataset for model performance testing.

Recommendation 5b: Accuracy and F-1 score are standard model performance metrics that should be routinely presented in articles on histopathology CAD-tool development. Standardization in reporting practices will allow for head-to-head comparisons of developed models and expedite translation of these tools into the clinical setting.

Conclusion:

The findings of the current systematic review highlight expanding and promising development of CAD-based tools that can be applied in the domain of clinical histopathology. To date, this work has been focused entirely in the realm of cancer pathologies, identifying the expansion of this technology into other branches of pathology as important opportunities for the future. While CAD-based advances show tremendous promise for clinical utility, rigorous research protocols must be developed which can clearly demonstrate the value machine learning in a clinical setting in order to realize this clinical utility of these tools. Recommendations provided in this research article should provide orientation for researchers developing CAD tools and for clinical pathologists interested in adopting this technology into their practice and should serve as a basis for the creation of evidence-based guidelines.

References:

1. Kamel HM. Trends and Challenges in Pathology Practice: Choices and necessities. *Sultan Qaboos Univ Med J*. 2011;11(1):38-44. https://www.ncbi.nlm.nih.gov/pubmed/21509206.

2. Rabe K, Snir OL, Bossuyt V, Harigopal M, Celli R, Reisenbichler ES. Interobserver variability in breast carcinoma grading results in prognostic stage differences. *Hum Pathol*. 2019. doi:https://doi.org/10.1016/j.humpath.2019.09.006

3. Wang S, Yang DM, Rong R, et al. Artificial Intelligence in Lung Cancer Pathology Image Analysis. *Cancers (Basel)*. 2019;11(11). doi:10.3390/cancers11111673

4. Jimenez-del-Toro O, Otálora S, Andersson M, et al. Chapter 10 - Analysis of Histopathology Images: From Traditional Machine Learning to Deep Learning. In: Depeursinge A, S. Al-Kadi O, Mitchell JRBT-BTA, eds. Academic Press; 2017:281-314. doi:https://doi.org/10.1016/B978-0-12-812133-7.00010-7

5. Hipp J, Flotte T, Monaco J, et al. Computer aided diagnostic tools aim to empower rather than replace pathologists: Lessons learned from computational chess. *J Pathol Inform*. 2011;2:25. doi:10.4103/2153-3539.82050

6. Bhargava R, Madabhushi A. Emerging Themes in Image Informatics and Molecular Analysis for Digital Pathology. *Annu Rev Biomed Eng*. 2016;18:387-412. doi:10.1146/annurev-bioeng-112415-114722

7. Komura D, Ishikawa S. Machine Learning Methods for Histopathological Image Analysis. *Comput Struct Biotechnol J*. 2018;16:34-42. doi:https://doi.org/10.1016/j.csbj.2018.01.001

8. Huisman A, Looijen A, van den Brink SM, van Diest PJ. Creation of a fully digital pathology slide

archive by high-volume tissue slide scanning. *Hum Pathol*. 2010;41(5):751-757. doi:10.1016/j.humpath.2009.08.026

9. Ilse M, Tomczak JM, Welling M. Chapter 22 - Deep multiple instance learning for digital histopathology. In: Zhou SK, Rueckert D, Fichtinger GBT-H of MIC and CAI, eds. Academic Press; 2020:521-546. doi:https://doi.org/10.1016/B978-0-12-816176-0.00027-2

10. Michie D. “memo” functions and machine learning. *Nature*. 1968;218(5136):19-22. doi:10.1038/218019a0

11. Langley P. Machine Learning as an Experimental Science.(Author abstract)(Editorial). *Mach Learn*. 1988;3(1):5. doi:10.1007/BF00115008

12. Baldi P. *Bioinformatics : The Machine Learning Approach*. (Brunak S, ed.). Cambridge, Mass.: Cambridge, Mass. : MIT Press, c1998.; 1998.

13. Ikeuchi K, ed. Computer Vision BT - Computer Vision: A Reference Guide. In: Boston, MA: Springer US; 2014:145. doi:10.1007/978-0-387-31439-6_100073

14. Klette author R. *Concise Computer Vision : An Introduction into Theory and Algorithms*. London : Springer, 2014.; 2014.

15. Montoya JC, Muñoz CQG, Márquez FPG. Chapter 9 - Remote condition monitoring for photovoltaic systems. In: Papaelias M, Márquez FPG, Karyotakis ABT-N-DT and CMT for REIA, eds. Boston: Butterworth-Heinemann; 2020:133-142. doi:https://doi.org/10.1016/B978-0-08-101094-5.00009-5

16. Kandemir M, Hamprecht FA. Computer-aided diagnosis from weak supervision: A benchmarking study. *Comput Med Imaging Graph*. 2015;42:44-50. doi:https://doi.org/10.1016/j.compmedimag.2014.11.010

17. Ritter author GX, Ritter GX. *Handbook of Computer Vision Algorithms in Image Algebra*. Second edi. (Wilson JN, ed.). Boca Raton: Boca Raton : CRC Press, 2001.; 2001.

18. Khan author S. *A Guide to Convolutional Neural Networks for Computer Vision*. Vol # 15. (Rahmani author H, Shah author SAA, Bennamoun author M (Mohammed), eds.). San Rafael, California : Morgan & Claypool, 2018.; 2018.

19. Tsagkatakis G. Dimensionality Reduction and Sparse Representations in Computer Vision. Savakis A, Amuso V, Cahill N, Rhody H, eds. 2011.

20. Masnadi-Shirazi H, Mahadevan V, Vasconcelos N. On the design of robust classifiers for computer vision. In: *2010 IEEE Computer Society Conference on Computer Vision and Pattern Recognition*. ; 2010:779-786. doi:10.1109/CVPR.2010.5540136

21. Lopez-del Rio A, Nonell-Canals A, Vidal D, Perera-Lluna A. Evaluation of Cross-Validation Strategies in Sequence-Based Binding Prediction Using Deep Learning. *J Chem Inf Model*. 2019;59(4):1645-1657. doi:10.1021/acs.jcim.8b00663

22. Gutierrez author D. *Machine Learning and Data Science: An Introduction to Statistical Learning Methods with R*. 1st editio. (Safari an OMC, ed.). Technics Publications, 2015.; 2015.

23. Belle A, Kon MA, Najarian K. Biomedical Informatics for Computer-Aided Decision Support Systems: A Survey. *Sci World J*. 2013;2013:1-8. doi:10.1155/2013/769639

24. Tacconelli E. Book: Systematic reviews: CRD's guidance for undertaking reviews in health care. *Lancet Infect Dis*. 2010;10(4):226.

25. Cohen J. A Coefficient of Agreement for Nominal Scales. *Educ Psychol Meas*. 1960;20:37.

26. Whiting PF, Rutjes AWS, Westwood ME, et al. QUADAS-2: A Revised Tool for the Quality

Assessment of Diagnostic Accuracy Studies. *Ann Intern Med*. 2011;155(8):529-536. doi:10.7326/0003-4819-155-8-201110180-00009

27. McHugh ML. Interrater reliability: the kappa statistic. *Biochem medica*. 2012;22(3):276-282. https://www.ncbi.nlm.nih.gov/pubmed/23092060.

28. Hansel DE. The Gleason Grading System: The Approach that Changed Prostate Cancer Assessment. *J Urol*. 2017;197(2):S140-S141. doi:10.1016/j.juro.2016.11.028

29. Lin WC, Li CC, Epstein JI, Veltri RW. Curvelet-based texture classification of critical Gleason patterns of prostate histological images. *2016 IEEE 6th Int Conf Comput Adv Bio Med Sci*. 2016:1-6. doi:10.1109/ICCABS.2016.7802768

30. DiFranco MD, O'Hurley G, Kay EW, Watson RWG, Cunningham P. Ensemble based system for whole-slide prostate cancer probability mapping using color texture features. *Comput Med Imaging Graph*. 2011;35(7-8):629-645. http://ovidsp.ovid.com/ovidweb.cgi?T=JS&PAGE=reference&D=med7&NEWS=N&AN=21269807.

31. Orlov N V, Weeraratna AT, Hewitt SM, et al. Automatic detection of melanoma progression by histological analysis of secondary sites. *Cytometry A*. 2012;81(5):364-373. http://ovidsp.ovid.com/ovidweb.cgi?T=JS&PAGE=reference&D=med7&NEWS=N&AN=22467531.

32. Angel Arul Jothi J, Mary Anita Rajam V. Effective segmentation of orphan annie-eye nuclei from papillary thyroid carcinoma histopathology images using a probabilistic model and region-based active contour. *Biomed Signal Process Control*. 2016;30:149-161. doi:10.1016/j.bspc.2016.06.008

33. F.A. S, L.S. O, C. P, et al. A Dataset for Breast Cancer Histopathological Image Classification. *IEEE Trans Biomed Eng*. 2016;63(7):1455-1462. doi:10.1109/TBME.2015.2496264

34. Ninos K, Kostopoulos S, Kalatzis I, et al. Microscopy image analysis of p63 immunohistochemically

stained laryngeal cancer lesions for predicting patient 5-year survival. *Eur Arch Oto-Rhino-Laryngology*. 2016;273(1):159-168. doi:10.1007/s00405-015-3747-x

35. K.-H. Y, C. Z, G.J. B, et al. Predicting non-small cell lung cancer prognosis by fully automated microscopic pathology image features. *Nat Commun*. 2016;7:no pagination. http://www.nature.com/ncomms/index.html.

36. L. Y, W. C, P. M, et al. *High Throughput Analysis of Breast Cancer Specimens on the Grid*. Vol 10. L. Yang, Dept. of Electrical and Computer Eng., Rutgers Univ., Piscataway, NJ 08544, USA.; 2007:617-625. http://ovidsp.ovid.com/ovidweb.cgi?T=JS&PAGE=reference&D=emed11&NEWS=N&AN=350325804.

37. Fukuma K, Prasath VBS, Kawanaka H, Aronow BJ, Takase H. A Study on Nuclei Segmentation, Feature Extraction and Disease Stage Classification for Human Brain Histopathological Images. In: *Procedia Computer Science*. Vol 96. ; 2016. doi:10.1016/j.procs.2016.08.164

38. Bayramoglu N, Kannala J, Heikkilä J. Deep learning for magnification independent breast cancer histopathology image classification. *2016 23rd Int Conf Pattern Recognit*. 2016:2440-2445. doi:10.1109/ICPR.2016.7900002

39. Bentaieb A, Nosrati MS, Li-Chang H, Huntsman D, Hamarneh G. Clinically-inspired automatic classification of ovarian carcinoma subtypes. *J Pathol Inform*. 2016;7(1). doi:10.4103/2153-3539.186899

40. Waheed S, Moffitt RA, Chaudry Q, Young AN, Wang MD. Computer Aided Histopathological Classification of Cancer Subtypes. *2007 IEEE 7th Int Symp Bioinforma Bioeng*. 2007:503-508. doi:10.1109/BIBE.2007.4375608

41. Doyle S, Rodriguez C, Madabhushi A, Tomaszeweski J, Feldman M. Detecting Prostatic Adenocarcinoma From Digitized Histology Using a Multi-Scale Hierarchical Classification Approach. *2006 Int Conf IEEE Eng Med Biol Soc*. 2006:4759-4762. doi:10.1109/IEMBS.2006.260188

42. Mete M, Xu X, Fan C y., Shafirstein G. Head and Neck Cancer Detection in Histopathological Slides. *Sixth IEEE Int Conf Data Min - Work*. 2006:223-230. doi:10.1109/ICDMW.2006.90

43. Y. X, J.-Y. Z, E.I.C. C, et al. Weakly supervised histopathology cancer image segmentation and classification. *Med Image Anal*. 2014;18(3):591-604. http://ovidsp.ovid.com/ovidweb.cgi?T=JS&PAGE=reference&D=medl&NEWS=N&AN=24637156.

44. Budinská E, Bosman F, Popovici V. Experiments in molecular subtype recognition based on histopathology images. *2016 IEEE 13th Int Symp Biomed Imaging*. 2016:1168-1172. doi:10.1109/ISBI.2016.7493474

45. K. N, S. K, K. S, et al. Computer-based image analysis system designed to differentiate between low-grade and high-grade laryngeal cancer cases. *Anal Quant Cytopathol Histopathol*. 2013;35(5):261-272. http://www.aqch.com/toc/auto_article_process.php?year=2013&page=261&id=23248&sn=0.

46. Weinstein JN, Collisson EA, Mills GB, et al. The Cancer Genome Atlas Pan-Cancer analysis project. *Nat Genet*. 2013;45(10):1113-1120. doi:10.1038/ng.2764

47. Fukuma K, Surya Prasath VB, Kawanaka H, Aronow BJ, Takase H. A study on feature extraction and disease stage classification for glioma pathology images. In: *2016 IEEE International Conference on Fuzzy Systems, FUZZ-IEEE 2016*. ; 2016. doi:10.1109/FUZZ-IEEE.2016.7737958

48. W. W, J.A. O, Wang W, Ozolek JA, Rohde GK. *Detection and Classification of Thyroid Follicular*

Lesions Based on Nuclear Structure from Histopathology Images. Vol 77. G. K. Rohde, Department of Biomedical Engineering, HHC 122, 5000 Forbes Avenue, Pittsburgh, PA 15232, United States. E-mail: gustavor@cmu.edu: Wiley-Liss Inc. (111 River Street, Hoboken NJ 07030-5774, United States); 2010:485-494. doi:10.1002/cyto.a.20853

49. Angel Arul Jothi J, Mary Anita Rajam V. Effective segmentation and classification of thyroid histopathology images. *Appl Soft Comput J*. 2015. doi:10.1016/j.asoc.2016.02.030

50. Xu Y, Zhu J-Y, Chang E, Tu Z. Multiple clustered instance learning for histopathology cancer image classification, segmentation and clustering. In: *Proceedings of the IEEE Computer Society Conference on Computer Vision and Pattern Recognition*. ; 2012. doi:10.1109/CVPR.2012.6247772

51. Slaoui M, Fiette L. Histopathology Procedures: From Tissue Sampling to Histopathological Evaluation. *Methods Mol Biol*. 2011;691:69-82. doi:10.1007/978-1-60761-849-2_4

52. Ameisen D, Deroulers C, Perrier V, et al. Towards better digital pathology workflows: programming libraries for high-speed sharpness assessment of Whole Slide Images. *Diagn Pathol*. 2014;9(1):S3. doi:10.1186/1746-1596-9-S1-S3

53. Aggarwal 1st Lt. Pushkar. Data augmentation in dermatology image recognition using machine learning. *Ski Res Technol*. 2019;25(6):815-820. doi:10.1111/srt.12726

54. Bang J, Hur T, Kim D, et al. Adaptive Data Boosting Technique for Robust Personalized Speech Emotion in Emotionally-Imbalanced Small-Sample Environments. *Sensors*. 2018;18(11):3744. doi:10.3390/s18113744

55. Solomon C. *Fundamentals of Digital Image Processing : A Practical Approach with Examples in Matlab*. (Breckon T, ed.). Chichester: Chichester : Wiley-Blackwell, ©2011.; 2011.

56. CIE Recommendations on Uniform Color Spaces, Color-Difference Equations, and Metric Color Terms. *Color Res Appl*. 1977;2(1):5-6. doi:10.1002/j.1520-6378.1977.tb00102.x

57. Lyon HO, De Leenheer AP, Horobin RW, et al. Standardization of reagents and methods used in cytological and histological practice with emphasis on dyes, stains and chromogenic reagents. *Histochem J*. 1994;26(7):533-544. doi:10.1007/BF00158587

58. Khan AM, Rajpoot N, Treanor D, Magee D. A nonlinear mapping approach to stain normalization in digital histopathology images using image-specific color deconvolution. *IEEE Trans Biomed Eng*. 2014;61(6). doi:10.1109/TBME.2014.2303294

59. Roy S, kumar Jain A, Lal S, Kini J. A study about color normalization methods for histopathology images. *Micron*. 2018;114:42-61. doi:https://doi.org/10.1016/j.micron.2018.07.005

60. Jayalakshmi T, Santhakumaran A. Statistical Normalization and Back Propagationfor Classification. *Int J Comput Theory Eng*. 2011;3(1):89-93. doi:10.7763/IJCTE.2011.V3.288

61. He BS, Zhu F, Shi YG. Medical Image Segmentation. *Adv Mater Res*. 2013;760-762:1590-1593. doi:10.4028/www.scientific.net/AMR.760-762.1590

62. Carpenter AE, Jones TR, Lamprecht MR, et al. CellProfiler: image analysis software for identifying and quantifying cell phenotypes. *Genome Biol*. 2006;7(10):R100. doi:10.1186/gb-2006-7-10-r100

63. Blake 1956- A, Kohli P, Rother C. *Markov Random Fields for Vision and Image Processing*. Cambridge, Mass.: Cambridge, Mass. : MIT Press, ©2011.; 2011.

64. Sakaridis C, Drakopoulos K, Maragos P. Theoretical Analysis of Active Contours on Graphs. *SIAM J Imaging Sci*. 2017;10(3):1475-1510. doi:10.1137/16M1100101

65. Peizhuang W. Pattern Recognition with Fuzzy Objective Function Algorithms (James C. Bezdek).

SIAM Rev. 1983;25(3):442. doi:10.1137/1025116

66. Poli R, Kennedy J, Blackwell T. Particle swarm optimization. *Swarm Intell*. 2007;1(1):33-57. doi:10.1007/s11721-007-0002-0

67. 13. Density-Based Clustering Algorithms. In: *Data Clustering: Theory, Algorithms, and Applications*. ASA-SIAM Series on Statistics and Applied Mathematics. Society for Industrial and Applied Mathematics; 2007:219-226. doi:doi:10.1137/1.9780898718348.ch13

68. Broeke author J. *Image Processing with ImageJ - Second Edition*. 2nd editio. (Pérez author J, Pascau author J, Safari an OMC, eds.). Packt Publishing, 2015.; 2015.

69. Huang D, Shan C, Ardabilian M, Wang Y, Chen L. Local binary patterns and its application to facial image analysis: A survey. *IEEE Trans Syst Man Cybern Part C Appl Rev*. 2011;41(6):765-781. doi:10.1109/TSMCC.2011.2118750

70. Nanni L, Brahnam S, Lumini A. Local phase quantization descriptor for improving shape retrieval/classification. *Pattern Recognit Lett*. 2012;33(16):2254-2260. doi:10.1016/j.patrec.2012.07.007

71. Haralick RM, Shanmugam K, Dinstein I. Textural Features for Image Classification. *IEEE Trans Syst man Cybern*. 1973;smc-3(No. 6):610-621. doi:10.1109/TSMC.1973.4309314

72. Pathak RS. *The Wavelet Transform*. Vol v.4. Amsterdam : Amsterdam ; 2009.

73. Schreier 1961- R. *Understanding Delta-Sigma Data Converters*. (Temes 1929- GC, John Wiley & Sons publisher, eds.). Piscataway, NJ : Hoboken, N.J. : Piscataway, NJ : IEEE Press ; 2005.

74. Ünay D, Stanciu SG. An Evaluation on the Robustness of Five Popular Keypoint Descriptors to Image Modifications Specific to Laser Scanning Microscopy. *IEEE Access*. 2018;6:40154-40164.

doi:10.1109/ACCESS.2018.2855264

75. A V, Hebbar D, Shekhar VS, Murthy KNB, Natarajan S. Two Novel Detector-Descriptor Based Approaches for Face Recognition Using SIFT and SURF. *Procedia Comput Sci*. 2015;70(C):185-197. doi:10.1016/j.procs.2015.10.070

76. Lowe D. Distinctive Image Features from Scale-Invariant Keypoints. *Int J Comput Vis*. 2004;60(2):91-110. doi:10.1023/B:VISI.0000029664.99615.94

77. Bay H, Ess A, Tuytelaars T, Van Gool L. Speeded-Up Robust Features (SURF). *Comput Vis Image Underst*. 2008;110(3):346-359. doi:10.1016/j.cviu.2007.09.014

78. Rublee E, Rabaud V, Konolige K, Bradski G. ORB: An efficient alternative to SIFT or SURF. In: *Proceedings of the IEEE International Conference on Computer Vision*. ; 2011:2564-2571. doi:10.1109/ICCV.2011.6126544

79. Mair E, Hager GD, Burschka D, Suppa M, Hirzinger G. Adaptive and Generic Corner Detection Based on the Accelerated Segment Test BT - Computer Vision – ECCV 2010. In: Daniilidis K, Maragos P, Paragios N, eds. Berlin, Heidelberg: Springer Berlin Heidelberg; 2010:183-196.

80. Calonder M, Lepetit V, Ozuysal M, Trzcinski T, Strecha C, Fua P. BRIEF: Computing a Local Binary Descriptor Very Fast. *IEEE Trans Pattern Anal Mach Intell*. 2012;34(7):1281-1298. doi:10.1109/TPAMI.2011.222

81. Gurcan MN, Boucheron LE, Can A, Madabhushi A, Rajpoot NM, Yener B. Histopathological image analysis: a review. *IEEE Rev Biomed Eng*. 2009;2:147-171. doi:10.1109/RBME.2009.2034865

82. Sarangi PK, Ravulakollu KK. Feature Extraction and Dimensionality Reduction in Pattern Recognition Using Handwriten Odia Numerals. 2014;65(3).

83. Michalewicz Z. *How to Solve It : Modern Heuristics*. 2nd ed., r. (Fogel DB, ed.). Berlin : Berlin ; 2004.

84. Pearson K. Mathematical Contributions to the Theory of Evolution. X. Supplement to a Memoir on Skew Variation. *Philos Trans R Soc London Ser A, Contain Pap a Math or Phys Character*. 1901;197(287-299):443-459. doi:10.1098/rsta.1901.0023

85. Papailiopoulos DS, Dimakis AG. Interference Alignment as a Rank Constrained Rank Minimization. *IEEE Trans Signal Process*. 2012;60(8):4278-4288. doi:10.1109/TSP.2012.2197393

86. Fisher RA. THE USE OF MULTIPLE MEASUREMENTS IN TAXONOMIC PROBLEMS. *Ann Hum Genet*. 1936;7(2):179-188. doi:10.1111/j.1469-1809.1936.tb02137.x

87. Cacciatore S, Luchinat C, Tenori L. Knowledge discovery by accuracy maximization. *Proc Natl Acad Sci U S A*. 2014;111(14):5117. doi:10.1073/pnas.1220873111

88. Duda RO. *Pattern Classification*. 2nd ed. (Hart PE, Stork DG, eds.). New York: New York : Wiley, 2001.; 2001.

89. Litchfield JT, Wilcoxon F. The Rank Correlation Method. *Anal Chem*. 1955;27(2):299-300. doi:10.1021/ac60098a038

90. Ziarko W. Variable precision rough set model. *J Comput Syst Sci*. 1993;46(1):39-59. doi:10.1016/0022-0000(93)90048-2

91. Iman RL, Davenport JM. Rank correlation plots for use with correlated input variables. *Commun Stat - Simul Comput*. 1982;11(3):335-360. doi:10.1080/03610918208812266

92. Hess AS, Hess JR. Principal component analysis. *Transfusion*. 2018;58(7):1580-1582. doi:10.1111/trf.14639

93. Kupper LL, Hafner KB. On assessing interrater agreement for multiple attribute responses. *Biometrics*. 1989;45(3):957. doi:10.2307/2531695

94. Roweis ST, Saul LK. Nonlinear dimensionality reduction by locally linear embedding. Roweis ST, ed. *Science*. 2000;290(5500):2323-2326. doi:10.1126/science.290.5500.2323

95. Wang C, Chen J, Sun Y, Shen X. Wireless Sensor Networks Localization with Isomap. In: *2009 IEEE International Conference on Communications*. ; 2009:1-5. doi:10.1109/ICC.2009.5199576

96. Teng L, Li H, Fu X, Chen W, Shen I-F. Dimension reduction of microarray data based on local tangent space alignment. In: *Fourth IEEE Conference on Cognitive Informatics 2005, ICCI 2005*. ; 2005:154-159. doi:10.1109/COGINF.2005.1532627

97. Anderson JA. Point biserial correlation. *Stata Tech Bull*. 1994;3(17).

98. Kent JT. Information gain and a general measure of correlation. *Biometrika*. 1983;70(1):163-173. doi:10.1093/biomet/70.1.163

99. Angel Arul Jothi J, Mary Anita Rajam V. *Segmentation of Nuclei from Breast Histopathology Images Using PSO-Based Otsu's Multilevel Thresholding*. Vol 325.; 2015. doi:10.1007/978-81-322-2135-7_88

100. Inuiguchi M, Hirano S, Tsumoto 1963- S. *Rough Set Theory and Granular Computing*. Vol v. 125. Berlin : Berlin ; 2003.

101. Guenther N, Schonlau M. Support Vector Machines. *Stata J*. 2016;16(4):917-937. doi:10.1177/1536867X1601600407

102. Darrell T, Indyk P, Shakhnarovich G. *Nearest-Neighbor Methods in Learning and Vision : Theory and Practice*. Cambridge, Mass.: Cambridge, Mass. : MIT Press, 2005; 2005.

103. Despontin M. Decision theory: An introduction to the mathematics of rationality: Ellis Horwood, Chichester, 1986, 448 + pages, £55.00. *Eur J Oper Res*. 1987;29(2):212-213. doi:10.1016/0377-2217(87)90113-5

104. Pavlov YL. *Random Forests*. Utrecht : Utrecht ; 2000.

105. Friedman N, Geiger D, Goldszmidt M. Bayesian Network Classifiers. *Mach Learn*. 1997;29(2):131-163. doi:10.1023/A:1007465528199

106. Mayr, Binder, Gefeller, Schmid. The evolution of boosting algorithms. From machine learning to statistical modelling. *Methods Inf Med*. 2014;53(6):419-41927. doi:10.3414/ME13-01-0122

107. De Wilde 1958- P. *Neural Network Models : Theory and Projects*. Second edi. London ; 1997.

108. Herrera F, Ventura S, Bello R, et al. *Multiple Instance Learning : Foundations and Algorithms*. Cham: Cham : Springer, 2016.; 2016.

109. Lin J-Y, Ke H-R, Chien B-C, Yang W-P. Classifier design with feature selection and feature extraction using layered genetic programming. *Expert Syst Appl*. 2008;34(2):1384-1393. doi:10.1016/j.eswa.2007.01.006

110. Fushiki T. Estimation of prediction error by using K -fold cross-validation. *Stat Comput*. 2011;21(2):137-146. doi:10.1007/s11222-009-9153-8

111. Wong T-T. Performance evaluation of classification algorithms by k-fold and leave-one-out cross validation. *Pattern Recognit*. 2015;48(9):2839-2846. doi:https://doi.org/10.1016/j.patcog.2015.03.009

112. Ruan F, Qi J, Yan C, Tang H, Zhang T, Li H. Quantitative detection of harmful elements in alloy steel by LIBS technique and sequential backward selection-random forest (SBS-RF). *J Anal At*

Spectrom. 2017;32(11):2194-2199. doi:10.1039/C7JA00231A

113. Efron B. *The Jackknife, the Bootstrap, and Other Resampling Plans*. Vol 38. (Mathematics S for I and A, ed.). Philadelphia, Pa.: Philadelphia, Pa. : Society for Industrial and Applied Mathematics SIAM, 3600 Market Street, Floor 6, Philadelphia, PA 19104, 1982.; 1982.

114. Cui Z, Gong G. The effect of machine learning regression algorithms and sample size on individualized behavioral prediction with functional connectivity features. *Neuroimage*. 2018;178:622-637. doi:10.1016/j.neuroimage.2018.06.001

115. Vapnik V. *The Nature of Statistical Learning Theory*. Springer science & business media; 2013.

116. Byrd RH, Chin GM, Nocedal J, Wu Y. Sample size selection in optimization methods for machine learning. *Math Program*. 2012;134(1):127-155.

117. Dobbin KK, Zhao Y, Simon RM. How large a training set is needed to develop a classifier for microarray data? *Clin Cancer Res*. 2008;14(1):108-114. doi:10.1158/1078-0432.CCR-07-0443

118. Mukherjee S, Tamayo P, Rogers S, et al. Estimating dataset size requirements for classifying DNA microarray data. *J Comput Biol*. 2003;10(2):119-142. doi:10.1089/106652703321825928

119. Figueroa RL, Zeng-Treitler Q, Kandula S, Ngo LH. Predicting sample size required for classification performance. *BMC Med Inform Decis Mak*. 2012;12(1):8. doi:10.1186/1472-6947-12-8

120. Tran T, Pham T, Carneiro G, Palmer L, Reid I. A Bayesian Data Augmentation Approach for Learning Deep Models. In: Guyon I, Luxburg U V, Bengio S, et al., eds. *Advances in Neural Information Processing Systems 30*. Curran Associates, Inc.; 2017:2797-2806. http://papers.nips.cc/paper/6872-a-bayesian-data-augmentation-approach-for-learning-deep-models.pdf.

121. Sun Y, Wang X, Tang X. Deep learning face representation from predicting 10,000 classes. In: *Proceedings of the IEEE Conference on Computer Vision and Pattern Recognition*. ; 2014:1891-1898.

122. Krizhevsky A, Sutskever I, Hinton GE. ImageNet classification with deep convolutional neural networks. In: *Advances in Neural Information Processing Systems*. Vol 2. ; 2012:1097-1105. https://www.scopus.com/inward/record.uri?eid=2-s2.0-84876231242&partnerID=40&md5=621b2cd1757ccc77341281f8a2f2ecaf.

123. Farabet C, Couprie C, Najman L, LeCun Y. Learning hierarchical features for scene labeling. *IEEE Trans Pattern Anal Mach Intell*. 2012;35(8):1915-1929.

124. Burlina P, Billings S, Joshi N, Albayda J, Miller FW. Automated diagnosis of myositis from muscle ultrasound: Exploring the use of machine learning and deep learning methods. *PLoS One*. 2017;12(8). doi:10.1371/journal.pone.0184059

125. Ciregan D, Meier U, Schmidhuber J. Multi-column deep neural networks for image classification. In: *2012 IEEE Conference on Computer Vision and Pattern Recognition*. IEEE; 2012:3642-3649.

126. Choo J, Liu S. Visual Analytics for Explainable Deep Learning. *IEEE Comput Graph Appl*. 2018;38(4):84-92. doi:10.1109/MCG.2018.042731661

127. Došilović FK, Brčić M, Hlupić N. Explainable artificial intelligence: A survey. In: *2018 41st International Convention on Information and Communication Technology, Electronics and Microelectronics (MIPRO)*. ; 2018:210-215. doi:10.23919/MIPRO.2018.8400040

128. Varma S, Simon R. Bias in error estimation when using cross-validation for model selection. *BMC Bioinformatics*. 2006;7(1):91.

129. Chicco D. Ten quick tips for machine learning in computational biology. *BioData Min*.

2017;10(1):35. doi:10.1186/s13040-017-0155-3

Figures:

2.1.

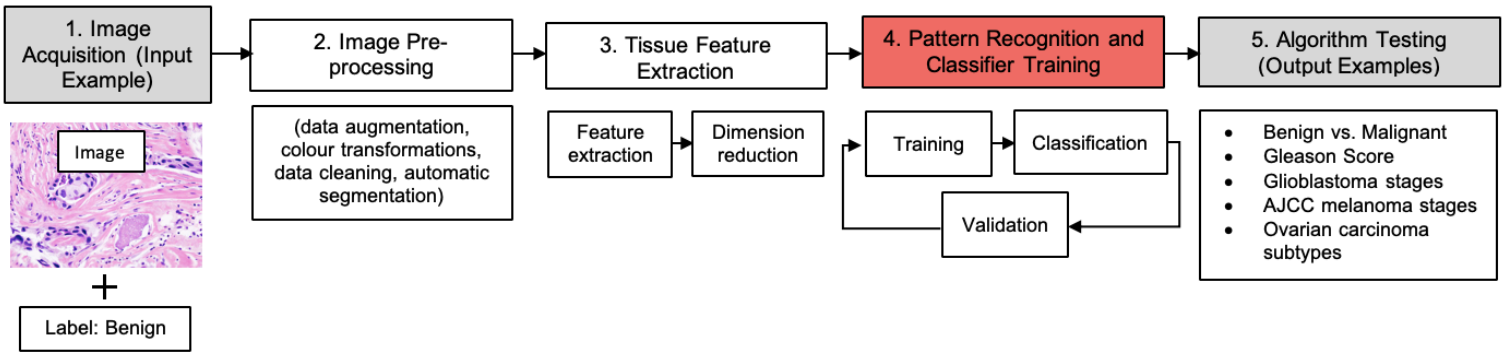

2.2.

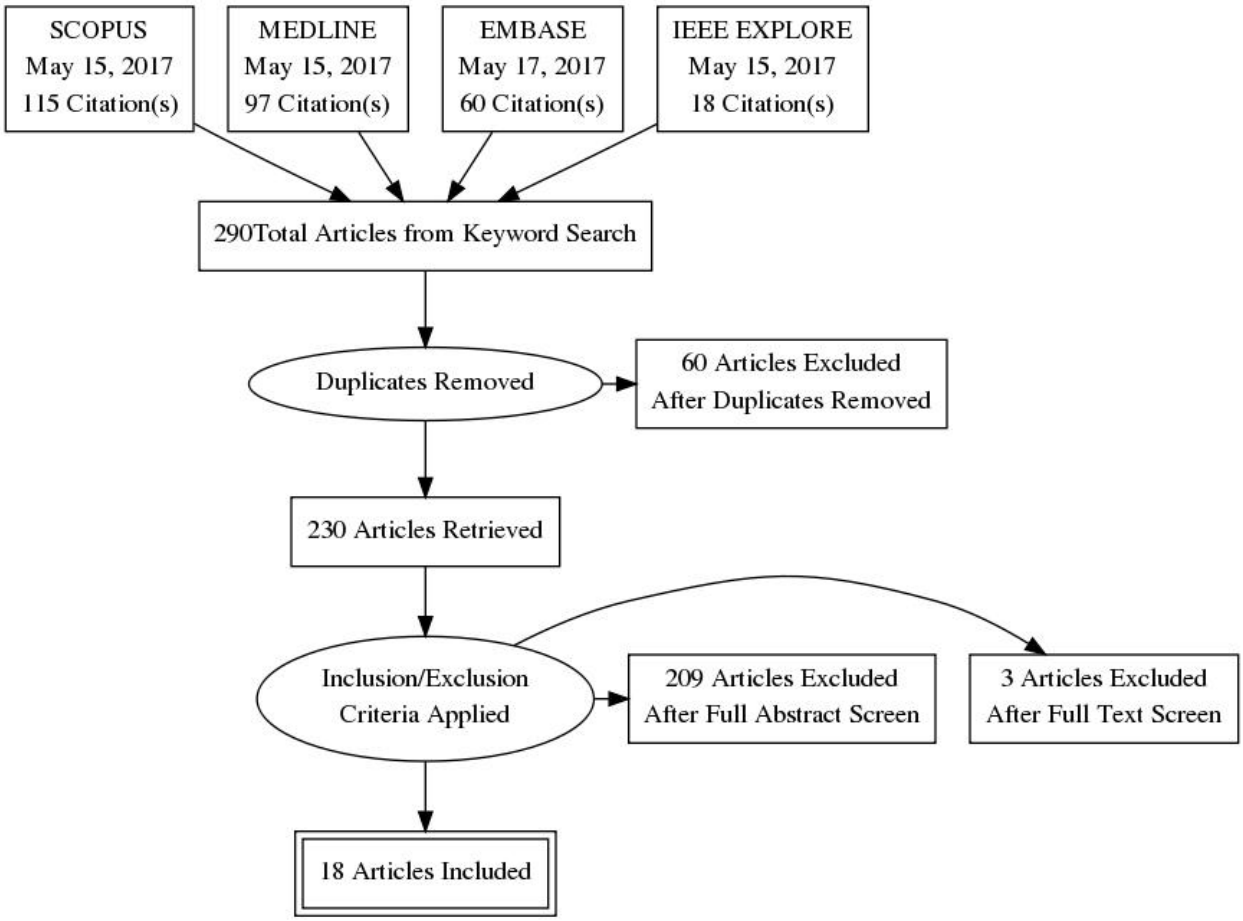

2.3.

A)

Study	RISK OF BIAS				APPLICABILITY CONCERNS		
	PATIENT SELECTION	INDEX TEST	REFERENCE STANDARD	FLOW AND TIMING	PATIENT SELECTION	INDEX TEST	REFERENCE STANDARD
Spanhol et. al.	○	○	?	○	○	○	○
Fukuma et. al.	?	○	?	?	○	○	○
Orlov et. al.	?	○	?	?	○	○	○
BenTaieb et. al.	○	○	○	○	○	○	○
Waheed et. al.	○	?	?	?	○	?	○
Ninos et. al.	?	○	○	○	○	○	○
Lin et. al.	?	○	○	?	○	○	○
Bayramoglu et. al.	?	○	?	?	○	○	?
Doyle et. al.	?	○	?	?	○	○	?
Wang et. al.	○	○	○	○	○	○	○
Jothi et. al.	○	○	○	○	○	○	○
DiFranco et. al.	?	○	○	○	○	○	○
Budinska et. al.	○	○	?	?	○	○	○
Mete et. al.	○	○	?	○	○	○	○
Yang et. al.	?	○	○	○	○	○	○
Ninos et. al.	?	?	○	○	○	○	○
Xu et. al.	○	○	○	○	○	○	○
Yu et. al.	?	○	○	○	○	○	○

○ Low Risk ○ High Risk ? Unclear Risk

B)

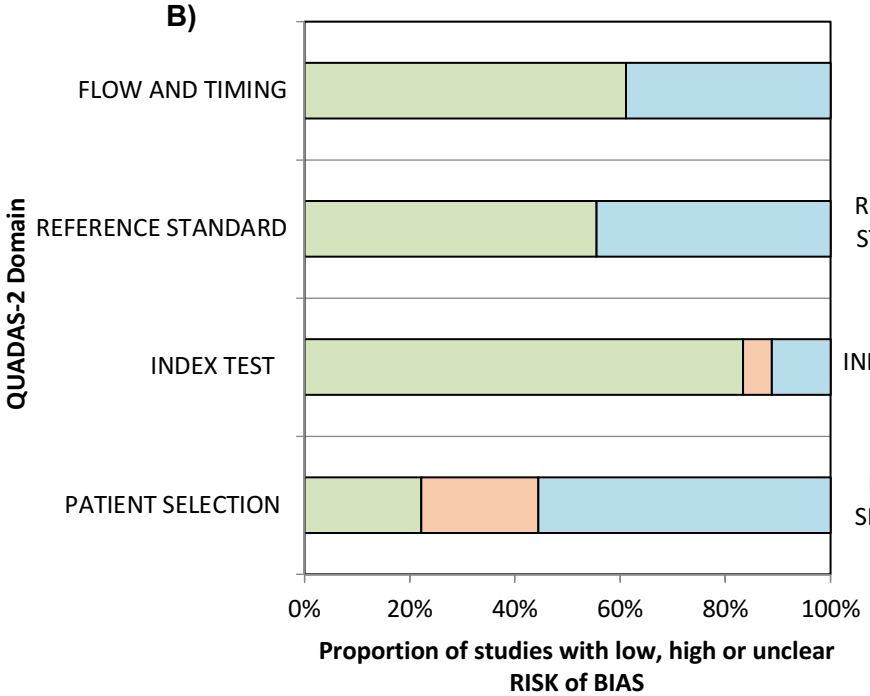

C)

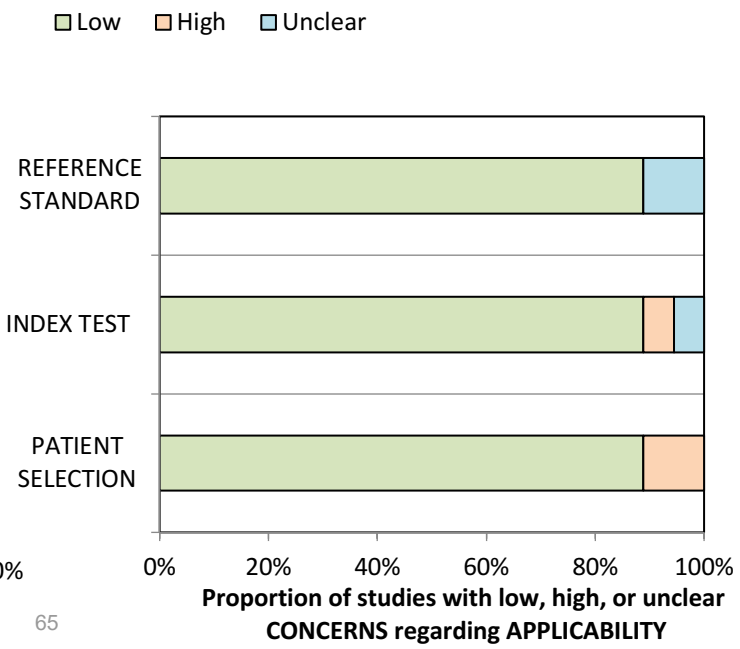

Figure Legends:

Figure 2.1. 5-Step computer vision workflow for CAD development on digital histopathology images. Upper panels show the workflow elements common to each reviewed article and beneath each panel is an example of the inputs (step 1), outputs (step 5), or tasks (steps 2-4) involved at each step.

Figure 2.2. Flow chart of article selection process. Medline, Embase, Scopus, and IEEE Explore were searched for articles relating to CAD on histopathology images. After abstract and full text screening, 18 articles remained for review.

Figure 2.3. Risk of bias summary. Risk of bias and applicability were assessed along 7 criteria outlined in the QUADAS-II tool. Low risk items are marked in green, high risk in red, and unclear in blue. **A.** Summary of risk score for each article along 4 Risk of Bias dimensions and 3 Applicability Concerns dimensions. **B.** Proportion of risk ratings along 4 Risk of Bias dimensions (Patient Selection, Index Test, Reference Standard, Flow and Timing) across all articles. **C.** Proportion of risk ratings along 3 Applicability Concerns dimensions (Patient Selection, Index Test, Reference Standard) across all articles.

Tables:

Table 2.1. Summary of articles included in analysis

	Authors	Year	Sample Size (patients)	Sample Size (images)
1	Spanhol et. al.	2016	82	7909
2	Fukuma et. al.	2016	unknown	150
3	Orlov et. al.	2012	164	14208
4	BenTaieb et. al.	2016	80	~9600
5	Waheed et. al.	2007	16	64
6	Ninos et. al.	2013	55	220
7	Lin et. al.	2016	16	1600
8	Bayramoglu et. al.	2016	82	7909
9	Doyle et. al.	2006	20	60
10	Wang et. al.	2010	10	200-400
11	Jothi et. al.	2016	12	219
12	DiFranco et. al.	2011	14	15
13	Budinska et. al.	2016	100	100
14	Mete et. al.	2006	7	7591
15	Yang et. al.	2007	300	3744
16	Ninos et. al.	2016	42	~168
17	Yu et. al.	2016	1017	21860
18	Xu et. al.	2014	unknown	100

Table 2.2. Summary of cancer types analyzed

Tissue Type	Proportion of Articles (n/18)[ref]
Brain	1[2]
Breast	3[1,8,15]
Colon/Rectum	2[18, 13]
Kidney	1[5]
Larynx	2[6,16]
Ovary	1[4]
Prostate	3[7,9,12]
Skin	3[3,14,17]
Thyroid	2[10,11]

Table 2.3. Summary of image pre-processing methods (Computer vision workflow stage 2)

Preprocessing Method	Proportion of Articles (n/18)[ref]
Data Augmentation	15[1,2,4,5,6,7,8,9,10,12,13,14,16,17,18]
Color Transformations	11[2,3,6,9,10,11,12,13,14,16,17]
Data Cleaning and Transformation	7[2,4,5,6,10,11,13]
Automatic Segmentation	7[4,6,10,11,14,16,18]
Selective Discarding of Poor-Quality Data	11[1,2,3,6,9,10,11,12,14,16,17]

Table 2.4. Summary of feature extraction and dimension reduction methods (Computer vision workflow stage 3)

Feature Extraction	Proportion of Articles (n/18)[ref]
Textural/Topological Features	15[1,2,3,4,5,6,7,9,12,13,14,15,16,17,18]
Object Level Features	9[2,4,5,6,7,10,11,16,17]
Keypoint Descriptors	2[1,18]
Other (Deep Learning)	2[16]
Dimension Reduction	**Proportion of Articles (n/18)[ref]**
None/Not applicable	10[1,2,5,7,8,9,10,13,14,18]
Greedy Hill Climbing	1[3]
Peason's Correlation	1[3]
Minimum-Redundancy-Maximum Relevance	1[3]
Linear Discriminant Analysis	1[4]
Dissimilarity Matrix	1[4]
Fisher Score	1[4]
Wilcoxon's Correlation	2[6,16]
Variable Precision Rough Sets	1[11]
Mean Rank Plots	1[12]
Principal Component Analysis	1[15]
Multi-Dimensional Scaling	1[15]
Local Linear Embedding	1[15]
ISOMAP	1[15]

Table 2.4. Summary of feature extraction and dimension reduction methods (Computer vision workflow stage 3) cont.

Local Tangent Space Embedding	1[15]
Point Biserial Correlation	1[16]
Information Gain Ratio	1[17]

Table 2.5. Summary of classifiers and cross-validation methods (Computer vision workflow stage 4)

Classifier	Proportion of Articles (n/18)[ref]
Support Vector Machine	11[1,2,4,7,10,12,13,14,15,17,18]
Nearest Neighbors	5[1,3,10,13,15]
Decision Trees and Random Forrest	6[1,2,9,12,15,17]
Bayesian	3[5,15,17]
Boosting	3[9,15,18]
Neural Networks	4[3,6,8,16]
Multiple Instance Learning	1[18]
Discriminant Function	1[1]
Novel Classifier	1[11]
Ensemble Based/Hierarchical	5[7,9,12,13,15]
Cross Validation	**Proportion of Articles (n/18)[ref]**
Unspecified	2[9,14]
K-fold	10[1,3*,8*,10**,11*,12,13*,15**,17,18**]
Leave-One-Out	6[2*,4*,5*,6**,16**,17]
Mean Decrease Gini	1[2]
Sequential Backward Selection	1[6]
Jackknife	1[7*]
Bootstrap	1[16]

*Used uniquely for model evaluation; **Used for evaluation and parameter tuning

Table 2.6. Summary of maximal performance metric according to different methods employed (Computer vision workflow stage 5)

Author	Classifier for best performance	Performance
Spanhol et al., 2016	SVM[a] with Gaussian Kernel	85.10%
Fukuma et al., 2016	Random Forest	99.80%
Orlov et al., 2012	WND	100%
BenTaieb et al., 2016	SVM with Linear Kernel	95%
Waheed et al., 2007	Multi-Class Bayesian with Maximum Likelihood Classification	98.40%
Ninos et al., 2013	Neural Network (Deep Learning)	90.90%
Lin et al., 2016	SVM with Gaussian Kernel	93.75%
Bayramoglu et al., 2016	Neural Network (Deep Learning)	83.25%
Doyle et al., 2006	Hierarchical Classifier (Adaboost and Decision Tree)	>90%
Wang et al., 2010	SVM with Gaussian Radial Basis Function Kernel	100%
Jothi et al., 2016	Closest Matching Rule	100%
DiFranco et al., 2011	SVM with gaussian Radial Basis Function Kernel and Random Forest	95% AUC
Budinska et al., 2016	SVM with Chi Squared Kernel	65%
Mete et al., 2006	SVM with Gaussian Radial Basis Function kernel	96%
Yang et al., 2007	Gentle Boosting with 8-Node CART Decision Tree	86%
Ninos et al., 2016	Neural Network (deep learning)	90.50%

Table 2.6. Summary of maximal performance metric according to different methods employed (Computer vision workflow stage 5) cont.

Yu et al., 2016	SVM with Gaussian Kernel, Random Forrest, Breiman's Random Forrest	81% AUC
Xu et al., 2014	Context-Constrained Multiple Clustered Instance Learning	F =97.2%

Table 2.7. Recommendations for computer vision methodology on digital histopathology images

Experiment Component	Recommendation
1. Image Acquisition *(Computer Vision Workflow Step 1)*	a) Publicly available histopathology image datasets are currently the best available in terms of size and reproducibility of acquisition methods. Institutions should work toward curating additional image datasets for research use. b) Learning curves should be used during model development to assess whether an appropriate sample size is being used. c) To minimize the risk of bias, developers should be explicit in the source of the histopathology images and annotations.
2. Image Pre-processing *(Computer Vision Workflow Step 12):*	a) A sliding window approach to extract image patches produces a larger dataset and represents the original images the most. b) An image data generator can be used for deep learning experiments to increase the data size and variability. Caution should be used with distortion and colour manipulation as these factors are often important to the appearance of histopathology images.

Table 2.7. Recommendations for computer vision methodology on digital histopathology images cont.

Experiment Component	Recommendation
2. Image Pre-processing *(Computer Vision Workflow Step 2)*	c) H&E stained histopathology images should be used, and images should be manually inspected for quality.
3. Tissue Feature Extraction *(Computer Vision Workflow Step 3)*	a) Manual or semi-automated and fully automated feature extraction performed well on histopathology image datasets. If computing resources allow for fully integrated feature extraction (with deep learning), this technique has been shown to perform more consistently on image data.
4. Pattern Recognition and Classifier Training *(Computer Vision Workflow Step 4)*	a) Until decisions from deep learning models can be more easily explained, the support vector machine classifier should be used as it has been found to outperform other classifiers on histopathology image data. b) Cross-validation should be used during training so that parameters such as sample size and resource allocation can be tuned to optimize model performance and computing resources required for training. 5-fold and leave-one-out cross validation are commonly used.

Table 2.7. Recommendations for computer vision methodology on digital histopathology images cont.

Experiment Component	Recommendation
5. Algorithm Testing *(Computer Vision Workflow Step 5)*	a) Reserving 20% of the dataset for testing was the most common data split used. b) To facilitate comparison of model performance with other machine learning models on histopathology data, accuracy and/or F1-score should be used to report model performance.

Supplementary Tables

Supplementary Table 2.0.1. MeSH terms and word variants searched in Medline

1. Visual pattern mining in histology image collections using bag of features.m_titl.
2. histological techniques/ or histocytochemistry/ or immunohistochemistry/
3. (histopathology adj2 imag*).tw,kf.
4. exp Diagnostic Imaging/
5. 2 and 4
6. histology ajd2 imag*.tw,kf.
7. 3 or 5
8. exp pattern recognition, automated/ or "neural networks (computer)"/ or support vector machine/
9. (pattern adj2 (recognition? or classification?)).tw,kf.
10. image segmentation.tw,kf.
11. 8 or 9 or 10
12. 7 and 11
13. limit 12 to english language

Supplementary Table 2.0.2. MeSH terms and word variants searched in Embase

1. Visual pattern mining in histology image collections using bag of features.m_titl.
2. histology/ or immunohistology/ or immunohistochemistry/
3. (histopathology adj2 imag*).tw.

4. exp diagnostic imaging/
5. 2 and 4
6. 3 or 5
7. exp automated pattern recognition/ or exp artificial neural network/ or exp support vector machine/
8. (pattern adj2 (recognition? or classification?)).tw.
9. image segmentation.tw.
10. 7 or 8 or 9
11. 6 and 10

Supplementary Table 2.0.3. MeSH terms and word variants searched in Scopus

1. TITLE-ABS-KEY ((histopathology W/2 imag*) AND ((pattern W/2 (recognition? OR classification?)) OR image AND segmentation))

Supplementary Table 2.0.4. MeSH terms and word variants searched in IEEE Explore

1. histopathology image* AND (pattern recognition* or pattern classification*) in Basic Search

Chapter 3

Automated Segmentation of Villi in Histopathology Images of Placenta

Salsabili S[1], **Mukherjee A**[2], Ukwatta E[1,3], Chan ADC[1], Bainbridge S[2,4], Grynspan D[5].

[1]Department of Systems and Computer Engineering, Carleton University, Ottawa, Ontario, Canada.

[2]Interdisciplinary School of Health Sciences, University of Ottawa, Ottawa, Ontario, Canada; Department of Pathology and Laboratory Medicine, Children's Hospital of Eastern Ontario, Ottawa, Ontario, Canada.

[3]School of Engineering, University of Guelph, Guelph, Ontario, Canada.

[4]Department of Cellular and Molecular Medicine, University of Ottawa, Ontario, Canada.

[5]Department of Pathology and Laboratory Medicine, Children's Hospital of Eastern Ontario and the University of Ottawa, Ontario, Canada.

This manuscript was published in *Computers in Biology and Medicine* in August 2019. Complete citation information for this manuscript is as follows: Comput Biol Med. 2019 Aug 30;113:103420. doi: 10.1016/j.compbiomed.2019.103420.

Computers in Biology and Medicine 113 (2019) 103420

Contents lists available at ScienceDirect

Computers in Biology and Medicine

journal homepage: http://www.elsevier.com/locate/compbiomed

Automated segmentation of villi in histopathology images of placenta

S. Salsabili [a,*], A. Mukherjee [b,c], E. Ukwatta [a,d], A.D.C. Chan [a], S. Bainbridge [e,f], D. Grynspan [g]

[a] Department of Systems and Computer Engineering, Carleton University, Ottawa, Ontario, Canada
[b] Interdisciplinary School of Health Sciences, University of Ottawa, Ottawa, Ontario, Canada
[c] Department of Pathology and Laboratory Medicine, Children's Hospital of Eastern Ontario, Ottawa, Ontario, Canada
[d] School of Engineering, University of Guelph, Guelph, Ontario, Canada
[e] Department of Cellular and Molecular Medicine, University of Ottawa, Ontario, Canada
[f] Interdisciplinary School of Health Sciences, University of Ottawa, Ontario, Canada
[g] Department of Pathology and Laboratory Medicine, Children's Hospital of Eastern Ontario and the University of Ottawa, Ontario, Canada

ARTICLE INFO

Keywords:
Histopathology
Biomedical image processing
Placenta
Image segmentation
Preeclampsia
Color image processing

ABSTRACT

Purpose: Manual analysis of clinical placenta pathology samples under the microscope is a costly and time-consuming task. Computer-aided diagnosis might offer a means to obtain fast and reliable results and also substantially reduce inter- and intra-rater variability. Here, we present a fully automated segmentation method that is capable of distinguishing the complex histological features of the human placenta (*i.e.*, the chorionic villous structures).

Methods: The proposed pipeline consists of multiple steps to segment individual placental villi structures in hematoxylin and eosin (H&E) stained placental images. Artifacts and undesired objects in the histological field of view are detected and excluded from further analysis. One of the challenges in our new algorithm is the detection and segmentation of touching villi in our dataset. The proposed algorithm uses the top-hat transformation to detect candidate concavities in each structure, which might represent two distinct villous structures in close proximity. The detected concavities are classified by extracting multiple features from each candidate concavity. Our proposed pipeline is evaluated against manual segmentations, confirmed by an expert pathologist, on 12 scans from three healthy control patients and nine patients diagnosed with preeclampsia, containing nearly 5000 individual villi. The results of our method are compared to a previously published method for villi segmentation.

Results: Our algorithm detected placental villous structures with an F1 score of 80.76% and sensitivity of 82.18%. These values are substantially better than the previously published method, whose F1 score and sensitivity are 65.30% and 55.12%, respectively.

Conclusion: Our method is capable of distinguishing the complex histological features of the human placenta (*i.e.*, the chorionic villous structures), removing artifacts over a large histopathology sample of human placenta, and (importantly) account for touching adjacent villi structures. Compared to existing methods, our developed method yielded high accuracy in detecting villi in placental images.

1. Introduction

The human placenta is a vital organ of pregnancy, exchanging all gases, nutrients, and waste products between the mother and developing fetus. This complex organ is essential for fetal survival. Developmental abnormalities and/or in utero damage to this organ can have detrimental short- and long-term health effects for both the mother and her fetus. Placental damage or dysfunction is known to play a central role in the development of fetal intrauterine growth restriction, pre-term birth, stillbirth, preeclampsia, and has also been linked to long term health outcomes, such as premature cardiovascular disease in mothers and metabolic disturbances in offspring [1–8]. The effective application of placental histopathology following a poor pregnancy outcome can inform ongoing clinical management of mothers and neonates, and offer insight into etiology of placental disease, the risk of recurrence in future pregnancies, and may provide indications regarding which mothers and offspring are at highest risk of cardio-metabolic disease later in life [9–14]. However, unlike some other fields of clinical pathology, there are a limited number of perinatal pathologists who are highly specialized in the field of placental histopathology, and the quality and

* Corresponding author.
E-mail address: sina.salsabili@carleton.ca (S. Salsabili).

https://doi.org/10.1016/j.compbiomed.2019.103420
Received 22 May 2019; Received in revised form 12 August 2019; Accepted 27 August 2019
Available online 30 August 2019

reproducibility of placental pathology examinations are currently very poor [15–17]. Collectively, this has limited the clinical utility of this diagnostic/prognostic tool. The ability to apply an unbiased quantitative approach to the field of placental histopathology would substantially reduce the high degree of inter-observer variability and quality control issues currently plaguing this field [18–20], allowing for highly reproducible and reliable findings from this clinical modality. It is anticipated that the contextually rich information that could be gained from automated forms of placental histopathology would allow for a highly integrated use of placenta pathology findings in the continuum of care – allowing for effective translation of findings from the microscope to the clinical management of mothers and babies.

In recent years, there has been increased interest in and research addressing automated detection and analysis of various features within the complex architecture of the human placenta [21–26]. The chorionic villi are the basic functional units of the placenta, anatomically described as a branched "tree-like structure" covered in a multinucleated layer of syncytiotrophoblast cells, which encases the feto-placental vasculature, embedded within a non-cellular connective tissue core. These villi structures are bathed in maternal blood, found within the intervillous space, in vivo. Previous work has focused on automated detection of the feto-placental vascular space within the villi – as poor feto-placental vascular development has been linked to several obstetrical diseases. Almoussa et al. [22] used a segmentation approach based on artificial neural networks (ANNs) to automatically extract feto-placental blood vessel features from digital histological images of the placenta. The ANNs were successful in detecting these most prominent vascular spaces within the placental villi. Chang et al. [25] proposed an automatic filtering method, which locally detects pixels containing curvilinear structures and reduces non-vessel noise. Compared to ANN-based methods, Chang et al. [25] proposed a faster and more accurate approach for feto-placental vessel detection.

A fuzzy C-means clustering method was applied successfully to distinguish cellular vs. extracellular components of the chorionic villi and to identify areas normally filled with maternal blood (intervillous space) [26]. Kidron et al. [24] used ImageJ software (https://imagej.net/) to extract features, such as size and number of chorionic villi, from histological images of the placenta and tested the feasibility of automated diagnosis of delayed or accelerated villous maturation. However, the images analyzed appear to be selective (*e.g.*, there was no indication that artifacts in the histological images were present). In addition, this method does not appear to properly segment villi that are in very close proximity, touching, or overlapping (*e.g.*, Fig. 1 in Kidron et al. [24] shows touching villi identified as a single villous structure). Swiderska-Chadaj et al. [23] described a method of automatic segmentation of placental villi structures for assessment of edema within the placenta. These authors used texture analysis, mathematical morphology, and region growing operations to extract different structures from placental images. Although they presented a comprehensive pipeline for automated analysis of placental histology, a small sample size of 50 villi from placentas with a variety of pathologies was used, with selective/optimal image selection (e.g., no image artifacts).

The objective of this paper is to describe an image analysis pipeline for automated analysis and segmentation of chorionic villi structures in histopathology images of human placentas. The main contribution of this work is the development of a new automated, segmentation protocol, which operates with a high degree of accuracy over large sample size. We also address the issue of adjacent, touching, and overlapping chorionic villi in our work, a common clinical finding that has not been properly addressed in the literature. The proposed method is validated on a set of healthy control placentas, as well as those complicated with the placenta-mediated disease of preeclampsia, to ensure the developed algorithm performs effectively for analyzing placenta specimens from healthy and diseased subjects. We also compare our work with a previously published automated method to detect villi in histological images of the placenta [24]. We apply their provided source code to our dataset and compare the results to our method.

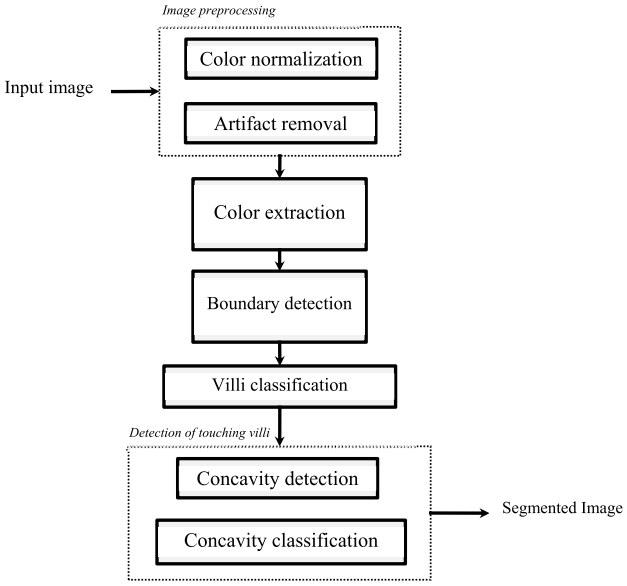

Fig. 1. Block diagram of our methodology.

2. Methodology

2.1. Placenta histopathology images

Our dataset comprises high-resolution digital scans of 12 placental histopathology specimens obtained from the Research Centre for Women's and Infants Health (RCWIH) Biobank (Mount Sinai Hospital, Toronto, ON). The ethics approval to perform sub-analyses on the Biobank samples was obtained from the Ottawa Health Science Network Research Ethics Board and the Children's Hospital of Eastern Ontario (CHEO) Research Ethics Board.

The placental specimens were fixed in paraffin wax, stained with hematoxylin, washed in a 0.3% acid alcohol solution, and counterstained with eosin following the standard protocol for hematoxylin and eosin (H&E) staining at the Department of Pathology and Laboratory Medicine at the CHEO. Slides were scanned (Aperio Scan Scope), and high-resolution color images ($20\times$ magnification) were obtained. In total, 12 placental scans were generated from three healthy term placental specimens and nine placental specimens collected from term pregnancies complicated with preeclampsia (PE). From each placental scan, three sample images of size 2740×3964 pixels were extracted, amounting to a total of 36 sample images (nine images from healthy term pregnancies and 27 from term pregnancies complicated with PE).

Manual segmentation of these images was performed using ImageJ software by A.M. and verified by D.G. (a clinical perinatal pathologist). For each sample image, a "chorionic villi mask" was manually generated by A.M (verified by D.G), identifying individual villi structures and artifact objects. These masks were generated by manually drawing a line around the area of each target object (*i.e.*, villi or undesired objects). The manual segmentation provided an estimation of adjacent villi boundaries and boundaries of undesired objects (*i.e.*, objects that are not considered villi). The manual segmentation served as a ground truth for training and evaluation. From the 36 sample images, there were 4946 villi in total.

2.2. Image segmentation

The image processing pipeline for villi segmentation in a placental image is shown in Fig. 1. The various steps are discussed in detail below.

2.3. Image preprocessing

A number of factors can contribute to variations in the color content of histological images (e.g., histochemical staining time, amount of histology stain used, etc.). We applied a comprehensive color normalization [27] to input images to compensate for such variations. Imaging artifacts might also exist in the histological images. In our work, imaging artifacts appeared as darkened areas of the image, and therefore needed to be removed prior to segmentation of the villi boundary. In Fig. 4 a, examples of these imaging artifacts are identified with blue arrows. Using Equation (1), pixels that are part of the imaging artifacts were identified; the intensity of these pixels was then adjusted to be white.

$$\begin{cases} bw_1(k,l) = \left|I_i(k,l) - I_j(k,l)\right| \le C1 \\ bw_2(k,l) = \left|I_i(k,l)\right| \le C2 \\ BW_{artifact} = bw_1 \cap bw_2 \\ where \begin{cases} i \ne j \\ i,j \in (R,G,B) \\ k \in (1,m), l \in (1,n) \end{cases} \end{cases} \quad (1)$$

In equation (1), I is an $m \times n \times 3$ intensity matrix and $I_i = \begin{bmatrix} a_{1,1} & \cdots & a_{1,n} \\ \vdots & \ddots & \vdots \\ a_{m,1} & \cdots & a_{m,n} \end{bmatrix}$ represents the ith matrix in RGB color space (i.e., red, green, and blue). The constant c_1 is a threshold to ensure that the intensity differences between the R, G, and B channels are small (*i.e.*, detected pixel is essentially grey). The constant c_2 is a threshold to ensure the detected pixels are relatively dark. The values assigned to c_1 and c_2 were 5 and 200, respectively, which were determined empirically. The $BW_{artifact}$ is a binary mask, which is the intersection of the bw_1 and bw_2 binary masks and contains all of the pixels in I that are contaminated with artifacts, which are adjusted to be white.

2.4. Color extraction

Pixels in the histological images of the placenta were divided into three classes based on color: red, white, and purple. Examples of these color classes and their subdivisions can be seen in Fig. 2. The first step in color classification is the extraction of the white class, found primarily outside of the villi, which is the maternal side of the placenta, called the intervillous space. This is deemed the background of the image. White spaces also exist within the core of some villi, primarily made of a non-cellular compartment of mesenchymal connective tissue (MCT) and/or tears in the connective tissue, which represent no specific tissue compartment. The white class is extracted using equation (2):

$$\begin{cases} bw_1(k,l) = \left|I_i(k,l) - I_j(k,l)\right| \le C3 \\ bw_2(k,l) = |I_i| \ge TH \\ BW_{white} = bw_1 \cap bw_2 \\ where \begin{cases} i \ne j \\ i,j \in (R,G,B) \\ k \in (1,m),\ l \in (1,n) \end{cases} \end{cases} \quad (2)$$

In equation (2), TH is a threshold, whose value is determined using Otsu's method [28]. This threshold ensures that the extracted pixels have high intensities (close to white). The constant $C3$ is a threshold to ensure that the intensity difference between the R, G, and B channels is small. The value assigned to $C3$ was 15, which was determined empirically. The BW_{white} is a binary mask, which is generated by the intersection of bw_1 and bw_2 binary masks, and contains the white class pixels.

The second step was the extraction of the red class. The red regions represent areas rich in fetal red blood cells, found within the feto-placental blood vessels encased within villi. In this work, all placental samples were washed several times during histological processing to remove blood from the tissue; however, some red blood cells often remain in each specimen. The combination of the red and white regions within the core of villi is referred to as the villi core (VC). The realization of the red class transformation is illustrated in Fig. 3. A transformed matrix T is computed (equation (3)), which highlights the red class, and a threshold is applied to extract the red class. The value for this threshold "TH" is determined using Otsu's method [28].

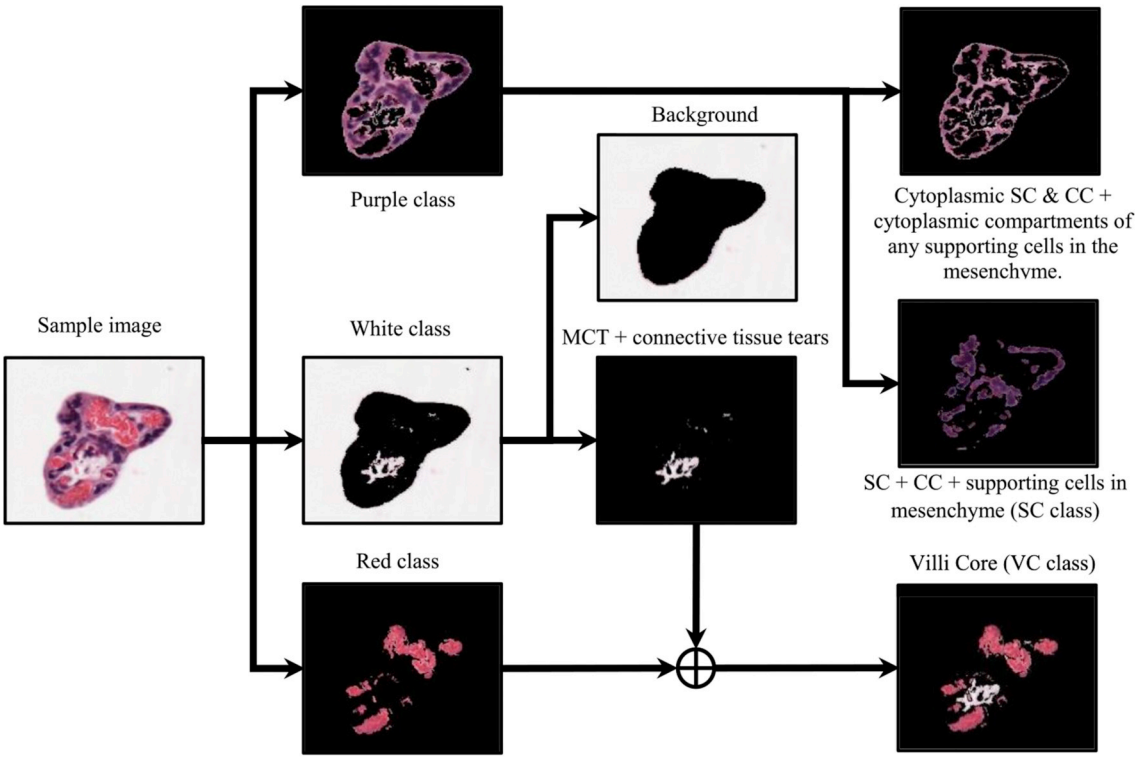

Fig. 2. Classification of color content in H&E stained images, including: syncytiotrophoblasts cells (SC) and cytotrophoblasts cells (CC) in the purple class; non-cellular mesenchymal connective tissue (MCT) in the white class; and fetal red blood cells within the villi core vasculature in the red class.

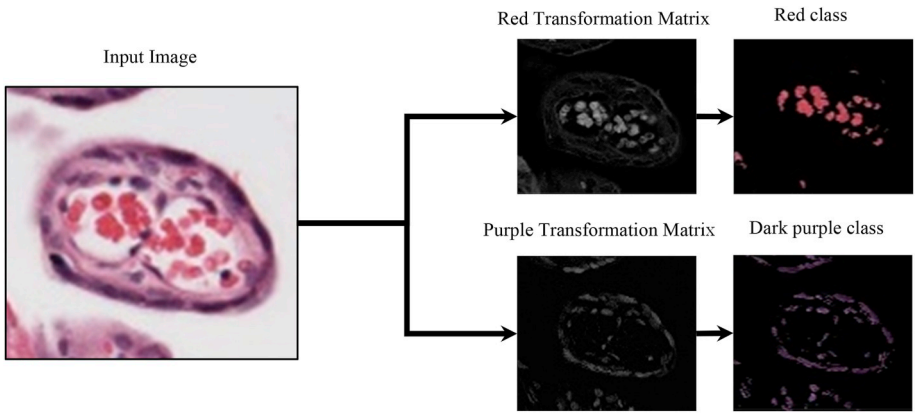

Fig. 3. Example of the red and dark purple class color extraction.

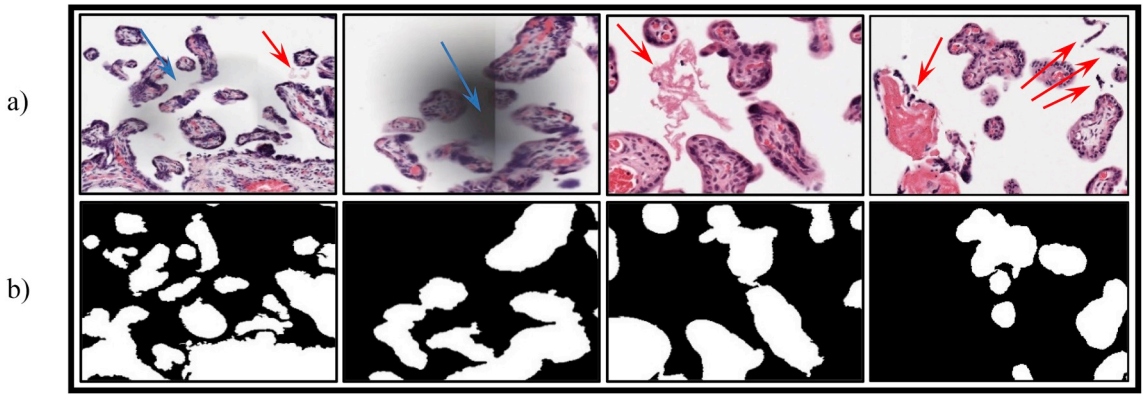

Fig. 4. a) Examples of artifacts and undesired objects. The blue arrows show the areas that are affected by artifacts and the red arrows show the undesired objects. b) the villi classification steps output that shows the removal of artifacts and undesired objects.

$$\begin{cases} T \triangleq I_R - mean(I_G + I_B) \\ BW_{red} = (T \geq TH) \end{cases} \quad (3)$$

The remaining pixels are assigned to the purple class, which represents several other cellular compartments. The dark purple regions primarily identify the nuclei of the syncytiotrophoblasts cells (SC), cytotrophoblasts cells (CC), along with the nuclei of any supporting cells, which might be present in the mesenchyme connective tissue core (i.e., fibroblasts, immune cells). SCs and CCs are densely packed along the villi borders. Nuclei of mesenchymal support cells, on the other hand, have a sparse appearance in the core regions of the villi. Therefore, the dense appearance of dark purple areas in non-border regions of a contour indicates that this is likely a border subdividing two villi in close proximity within the contour. The light purple area identifies the cytoplasmic compartment of the SCs and CCs, along with mesenchymal support cells.

The purple class is further classified into dark purple and light purple classes. For simplicity, we call the dark purple class the "SC class". Equation (4) is used to extract the SC class, where T is the transformed matrix, and "TH" is a threshold, whose value is determined using Otsu's method [28]. The transformation of the purple class can be seen in Fig. 3. The remaining pixels are assigned to the light purple class.

$$\begin{cases} T \triangleq I_B - mean(I_G + I_R) \\ BW_{SC} = (T \geq TH) \end{cases} \quad (4)$$

2.5. Boundary detection

After extraction of the color content, the input image was separated into the background (*i.e.*, white class) and foreground (*i.e.*, all classes excluding the white class). The foreground can be adopted as a rough estimate of the boundary of the objects in the image. The binary mask from the foreground was used as initial contours in the level set algorithm, based on the Chan-Vase formulation [29], to obtain the exact boundary of each contour. The algorithm accurately segments objects of interest (i.e., villi candidates).

2.6. Villi classification

To be considered "placental villi", objects of interest needed to surpass a minimum threshold size of 1000 μm [2]. This threshold size was selected based upon well-established, healthy placenta villi dimensions previously described in the literature [30,31]. This villi size threshold is the same as the one used in work by Kidron et al. [24], which is of relevance as we are comparing our method to their method. Objects of interest <1000 μm [2] might include red and white blood cells found in the intervillous space, fibrin deposition, syncytial knots (pieces of apoptotic placenta shed from the villi surface), or artifacts from tissue processing and histological preparation.

It is important to note that there are undesired objects of interest >1000 μm [2], as demonstrated in Fig. 4a. Therefore, further descriptors

needed to be included in order to identify true placenta villi objects versus undesired objects. Mature placenta villi contain white and/or red regions within their core, indicative of the presence of connective tissue and fetal vasculature and/or fetal red blood cells (VC class). Moreover, placental villi are surrounded by a continuous layer of SC cells and a sparse underlying layer of CC cells, all of which contain dark purple nuclei (*i.e.*, SC class). Conversely, undesired objects do not have these anatomical features and therefore demonstrate a considerably different density profile for the SC and VC classes. The SC and VC class density thresholds were tuned over the training set, using density profiles of the SC and VC class of true placenta villi objects (ground truth) – as identified through manual segmentation.

2.7. Detection of touching villi

In this work, a novel approach was used to detect pairs of touching villi. The postulated boundary separating the two touching villi was identified using the presence of concavity at the site where the two villi meet, which is visually distinguishable from other concavities in a standard villous structure. Specifically, at these concave sites, you additionally see the dense presence of dark purple nuclei within the SC class. Fig. 5a shows a representative example of four placenta villi that are touching each other, with three red arrows highlighting the visual features of the concave sites of separation. In this work, villi separation boundaries were identified in two steps: 1) detection of candidate concavities through contour analysis, and 2) acceptance or rejection of each candidate concavity as a separate villous boundary, through color analysis (*i.e.*, density of different color classes in the boundary area, and the density of color classes in the two resultant villi).

1) Detection of candidate concavities

The concavity detection step employs the top-hat transform, which is defined as the subtraction of the original contour from its opening with a structuring element (SE) [32]. This definition of top-hat transform can be interpreted as an attempt to cover the areas within the contour by fitting a SE into the contour, under the condition that the entirety of the SE remains within the boundary of the contour. The areas that cannot be covered by the fitted SE are the concavities/convexities in the contour. An example is shown in Fig. 5c, where the regions that are marked in red show convexities/concavities in the contour. The output of the top-hat transform (Fig. 5d) might contain the candidate concavity (Fig. 5e), which must satisfy two conditions: 1) the removal of the candidate concavity from the contour must divide the contour into two new contours, and 2) the size of each of these new contours must satisfy the minimum villi size threshold (i.e., 1000 μm [2]). Fig. 5e shows the target concavity, which satisfies these two conditions.

Identifying candidate concavities using the top-hat transform depends on the characteristics of the SE (*i.e.*, size, shape, and alignment). Fig. 6 shows the effect of varying the characteristics of the SE on the detection of candidate concavities. In our work, an elliptical SE with different sizes and orientations (*i.e.*, 0°, 45°, 90°, and 135°) is used to detect concavities in the contour.

The procedure of changing the characteristics of the SE is continued until a candidate concavity is identified, or the top-hat transform of the contour becomes equal to the contour itself. This might happen if the size of the structuring element becomes large enough that the opening of the contour with the SE can become zero (i.e., the contour is completely eroded by the structuring element). As a result, the top-hat transform of the contour (*i.e.*, subtraction of the contour from its opening with a SE) becomes equal to its opening. If a candidate concavity is identified, the candidate concavity is removed to produce two new contours, and the concavity detection process is iteratively applied on these contours. Algorithm 1 shows the pseudocode for concavity detection.

2) Color analysis

Not all of the identified candidate concavities are actual separation boundaries between two villi. Only candidate concavities that possess certain color features are accepted as the separation boundaries. Based these color features, the border regions of a villous structure have: 1) a high density of SC cells and CC cells (*i.e.*, SC class), and 2) sparse appearance of the VC class. Therefore, candidate concavities that have high SC-class density and low density of VC-class are labeled as sepa-

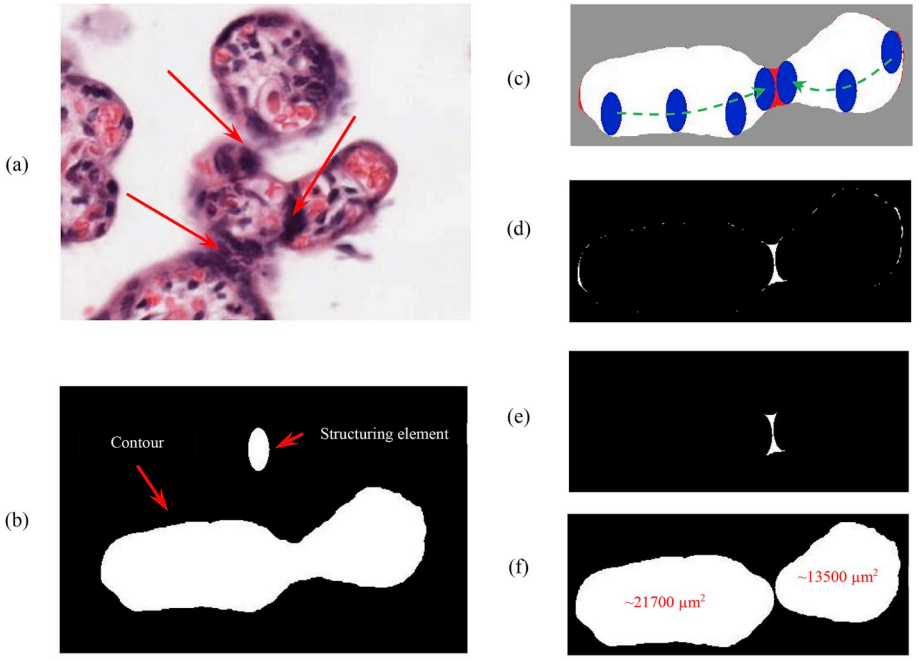

Fig. 5. (a) Examples of attachment areas in villi. (b) A sample contour and an elliptical-shape structuring element to be used in calculation of top-hat transform. (c) The interpretation of the top-hat transform by fitting the SE inside the contour. The areas that cannot be covered by SE are shown in red. These areas are the output of top-hat transform (d) The output of the top-hat transform, which represents all of the convexities and concavities in the contour. (e) The candidate concavity, which is the only concavity in the contour that its removal divide the original contour into two separate contours. (f) The resultant contours of removing the candidate concavity from the original contour. Both contour satisfied the minimum size threshold of a villous.

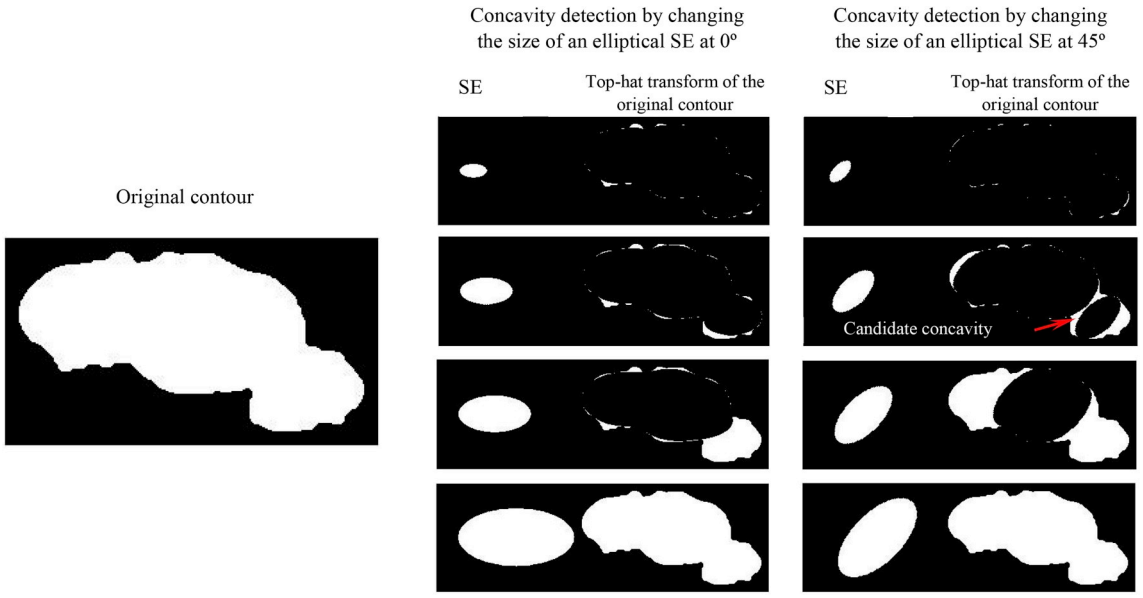

Fig. 6. An example of detecting the candidate concavity by changing the characteristics of the SE. In this example, two rotation is considered for a given elliptical-shape structuring element (*i.e.*, 0°, 45°). The size of the SE is changed for each rotation to the point that the top-hat transform of the input contour becomes equal to the input contour itself. As it can be seen in this figure, the candidate concavity cannot be detected in 0° rotation. On the other hand, in 45° rotation increasing the size of the SE leads to appearance of the candidate concavity in the top-hat transform of the contour.

Algorithm 1: Concavity detection

***Input*:** Binary mask (BW), elliptical structuring element (SE)

Output: A binary mask with all candidate concavities removed

Initialization:

Label the contours in BW → $L = \{L_0, L_1, \ldots, L_N\}$, N = number of contours

for each contour in L

  $SE = 1$

  loop of SE characteristics

    for each alignment of $SE = \{0^o, 45^o, 90^o, and\ 135^o\}$

      Calculate the Top-hat transform for contour L_i using $SE \rightarrow T_i$

      if $T_i = L_i$

        Exit nested loop of SE characteristics and go to next contour → L_{i+1}

      end if

      if the candidate concavity found in T_i

        Remove the candidate concavity from L_i to produce two new contours

        Replace L_i with one of the new contours

        Add the other new contour L_{N+1} to $L \rightarrow L = \{L_0, L_1, \ldots, L_N, L_{N+1}\}$

        Increment the number of contours $N = N + 1$

        Exit nested loop of SE characteristics and start analyzing the new contour L_i

      end if

    end for

    $SE = SE + 1$

  end loop

end for

ration boundaries. The thresholds for SC-class density and VC-class density were tuned over the training set of images, using the manual segmentation as ground truth.

2.8. Evaluation

Our data set consisted of nine images obtained from healthy term pregnancies and 27 placenta images from term pregnancies complicated with PE. We performed stratified 5-fold cross-validation, assigning the images into training and test sets with a 2:1 ratio (*i.e.*, six images from healthy patients and 18 images from PE patients were assigned to the training set, and three images from healthy patients and nine images from PE patients were assigned to the test set).

Villi detection accuracy was determined using manual segmentation as ground truth. The F1 score and sensitivity were calculated based on the following definitions:

$$Sensitivity = TP/(TP + FN) \tag{5}$$

$$F1\ score = (2 \times TP)/(2 \times TP + FP + FN) \tag{6}$$

- True positive (TP): number of villous structures identified correctly
- True negative (TN): number of objects in the binary mask generated in the boundary detection step that are correctly labeled as other objects (*i.e.*, non-villi)
- False positive (FP): number of villous structures identified incorrectly
- False negative (FN): number of villi structures identified in the manual segmentation that were not detected

For instance, if a contour contained two villi based on manual segmentation, and our algorithm correctly detected these two villi, the algorithm scored two TPs. However, if the algorithm detected only one or none of the villi, the algorithm scored one TP and one FN, or two FNs, respectively. When a contour contained only one villus based on manual segmentation, but our algorithm detected two villi, the case was scored as one TP and one FP.

2.9. Comparison to a previous method

The results of our method were evaluated against a recently published method [24] for placenta villi segmentation, based on the ImageJ software platform. The authors of the previous method publicly provided their source code online. In this previously published method, the authors extracted boundaries of villi to determine the number of existing villi in a given image, and standard color thresholding was used to segment the villi; we optimized this threshold over our training set. To achieve a fair comparison, we used the same values for the common thresholds in both methods (*i.e.*, villi size threshold, which is set to 1000 μm [2]). We then evaluated their method by comparing algorithm-generated results with manual segmentation. We also evaluate our method's segmentation results against manual segmentation and compare it with generated results from the previous method.

As stated in section II.C, TNs are defined as the number of objects in the binary mask that correctly labeled as non-villous objects. TNs were not computed for this comparison method, as it does not have a similar binary mask that would allow for a sensible TN comparison.

3. Results

As is typically observed in clinically relevant image datasets, our experimental image dataset contained artifacts and undesired objects, including imaging artifacts and maternal red blood cells in the intervillous space (12 out of 36 images were contaminated by imaging artifacts (Fig. 4)). In the villi classification step, the contours were classified based on their size and density of VC class and SC class. The proposed pipeline was able to recognize desired contours with 92.86% accuracy

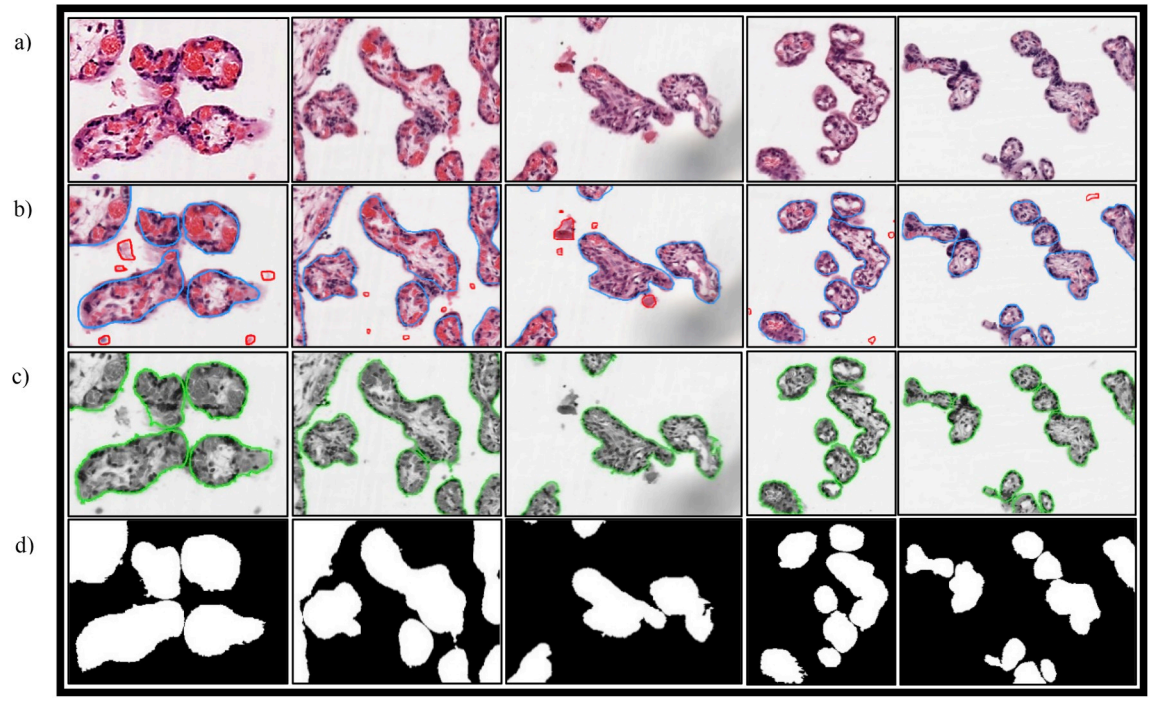

Fig. 7. Sample segmentation of villi, a) The original image, b) The manual segmentation. The boundary of a villous structure is annotated in blue. The red annotation shows undesired objects, c) The segmentation results of our proposed method. The boundaries of villi is annotated in green. d) The generated binary mask showing the final segmentation results.

Table 1
A comparison between our proposed method and the previous work. The results are presented for each fold for health term pregnancies and pregnancies complicated with PE. The TN row for the previously published work is not applicable as explained in section II.D.

		Healthy					Diagnosed with PE				
		fold #1	fold #2	fold #3	fold #4	fold #5	fold #1	fold #2	fold #3	fold #4	fold #5
Proposed method	***TP***	227	255	246	228	247	421	532	518	541	572
	TN	96	176	102	150	134	227	177	193	261	247
	FP	50	69	68	46	57	128	141	131	132	161
	FN	42	28	68	29	23	138	124	144	133	92
	F1 score (%)	83.15	84.02	78.34	85.88	86.06	75.99	80.06	79.02	80.33	81.89
	Sensitivity (%)	84.39	90.11	78.34	88.72	91.48	75.31	81.10	78.25	80.27	86.14
Previously published method [24]	***TP***	133	209	163	170	189	253	370	312	331	410
	TN	–	–	–	–	–	–	–	–	–	–
	FP	23	43	38	27	50	76	85	70	92	128
	FN	136	74	151	87	81	306	286	350	343	254
	F1 score (%)	62.59	78.13	63.30	74.89	74.26	56.98	66.61	59.77	60.35	68.22
	Sensitivity (%)	49.44	73.85	51.91	66.15	70.00	45.26	56.40	47.13	49.11	61.75

Table 2
Overall F1 score and sensitivity of the previous method, the proposed method without detection of touching villi algorithm, and the proposed method with touching villi detection algorithm. The results are reported as the weighted average of five fold cross validation.

	F1 score	*Sensitivity*
Previously published method [24]	65.30%	55.12%
Proposed method without detection of touching villi	74.58%	61.28%
Proposed method with detection of touching villi	80.76%	82.18%

(3625 out of 3904 contours were correctly identified).

Concavity detection was an important step in the detection of touching villi step. In comparison to manually identified concavities by experts, our algorithm detected concavities with an accuracy of 95.47% (3908 out of 4093 concavities were correctly identified).

Fig. 7 shows multiple sample segmentation of villi, which is performed by our proposed method. Table 1 shows the F1 scores, sensitivity, and truth table components of a recently published method [24] and the proposed method, separating the results for healthy control patients and patients diagnosed with PE. In Table 2, the overall results across all placental images are presented. In comparison to the previous method, our method yielded an F1 score and a sensitivity that are 15.46% and 27.06% higher, respectively. In order to highlight the impact that detection of touching villi has on the overall performance of our proposed method, the overall result of the proposed method without detection of touching villi is also included in Table 2.

As it is defined in Eq. (5), the sensitivity of a method depends on the total number of FNs. In this work, the majority of FN cases are generated when multiple villi are located in close proximity of each other, and the algorithm is not able to discern these as separate villi. As can be observed from the sensitivity column in Table 2, the difference gap between the previous work's sensitivity and the proposed method without detection of touching villi step is 6.68%. The comparison between the sensitivity of the proposed method with and without detection of touching villi shows a considerably large difference of 20.9%. The great improvement in sensitivity over the previous method is primarily achieved by applying the detection of touching villi step in our proposed algorithm.

The processing time required for a complete analysis of each image was approximately 21 min per image on a Core i7-6700 CPU at 3.4 GHz. We observed that this processing time is quite reasonable as the developed algorithm can run in the background without the need for any user interactions. Although we have used parallel processing in the feature-based analysis stage, the rest of the programming code is not optimized. The villi density in each image and the convexity of the extracted contours were two of the most influential factors in the determination of the processing time required for each analysis. Most of the processing time (approximately 80%) was required for the boundary detection step, which can be substantially improved by parallel (GPU) processing.

4. Discussion

An initial step for automated analysis of placental images is segmenting the chorionic villi – the functional unit of the placenta – within the histological specimens. Villi segmentation allows extraction of key features (e.g., villi count, size distribution, shape feature) for an objective assessment of placental images. Due to the complexity of villous structures and the presence of imaging artifacts, segmentation of individual villi in a placental image is a difficult task. However, the proposed method successfully identifies complex villous structures in a large series of images with high accuracy. Our proposed method yielded an F1 score of 80.76% and sensitivity of 82.18% for a dataset comprising of 4946 sample villi, which considerably outperformed a previously published method [24].

Two major contributing factors in obtaining better results in our method compared to the previous method were: 1) comprehensive artifact removal; and 2) the ability to detect and properly segment touching villi. The second factor had a large influence on the results, particularly the sensitivity score. A commonly recognized feature of the placental disease in PE is "villous agglutination" – a condition in which neighboring villi structures adhere to one another [33]. This feature of placental images from pregnancies complicated with PE likely contributed to the decreased performance of the previously published segmentation method when compared to healthy controls. Importantly, our algorithm yielded high and comparable performance when applied to histopathology cases from healthy controls (weighted average F1 score of 83.37%) or pathological cases of preeclampsia (weighted average F1 score of 79.61%) – providing confidence for the utility of this automated process in a clinical setting.

The most important limitation of our work was including connective tissue tears in VC. In our work, the calculation of fetal red blood cells density played a key role in multiple steps of our algorithm. The placental specimens used had been washed, so a considerable amount of red regions (fetal blood cells) inside placental vasculature (within the core of the villi structure) had been removed and replaced by white/light pink regions. Therefore, we also included these white regions in the calculation of VC density. However, some included areas were related to connective tissue tears, which represent no particular tissue.

The long-term goal of our work is to develop an algorithm that has the ability to process the whole placenta scan. This can be achieved by block analysis. With the scans used in our dataset, on average, around 50 extracted images would be required to cover the whole scan. Although the presented pipeline has the potential to analyze the entire scans (i.e., analysis of ~50 images per scan), in our study, we only present the results from three images from each placental scan. Manual segmentation,

to establish a ground truth, is a time-consuming process, and it was believed that it was more important for this study to have images that better capture the variability across scans than within a scan.

5. Conclusion

In this study, a fully automated method for segmentation of chorionic villi structures in histopathology images of the human placenta was presented. The proposed method has the ability to identify complex villous structures, including touching and overlapping villi, by performing color analysis on the detected concavities of the villi structures. Our proposed method yielded an F1 score of 80.76% and sensitivity of 82.18% for a dataset comprising of nearly 5000 sample villi, considerably higher performance than previously published methods. In addition, the proposed method has a comparable performance on placental samples from healthy and pathological pregnancies, a critical consideration in determining clinical utility.

With the help of an accurate and robust automated analysis method, pathologists might be presented with a set of otherwise inaccessible morphometric values for each image, such as the distribution of specific structures (physically and class-wise) and presence or absence of certain histological features/findings within identified structures. The pathologist can use these values to help make a final diagnosis. Although we focused only on histopathology images of the placenta, it might be possible to generalize this tool across multiple fields of clinical pathology. This could result in a marketable tool that would substantially reduce the subjectivity that exists in current practice.

Conflicts of interest

None.

Acknowledgments

This work is supported in part by the Ontario Trillium Scholarship (OTS) and Natural Sciences and Engineering Research Council (NSERC) of Canada.

References

[1] B. Huppertz, Placental pathology in pregnancy complications, Thromb. Res. (2011), https://doi.org/10.1016/S0049-3848(11)70026-3.
[2] R.I. Sava, K.L. March, C.J. Pepine, Hypertension in pregnancy: taking cues from pathophysiology for clinical practice, Clin. Cardiol. (2018), https://doi.org/10.1002/clc.22892.
[3] M. Kovo, L. Schreiber, A. Ben-Haroush, E. Gold, A. Golan, J. Bar, The placental component in early-onset and late-onset preeclampsia in relation to fetal growth restriction, Prenat. Diagn. (2012), https://doi.org/10.1002/pd.3872.
[4] J.M. Roberts, C. Escudero, The placenta in preeclampsia, Pregnancy Hypertens (2012), https://doi.org/10.1016/j.preghy.2012.01.001.
[5] T.K. Morgan, Role of the placenta in preterm birth: a review, Am. J. Perinatol. (2016), https://doi.org/10.1055/s-0035-1570379.
[6] R. Bukowski, M. Carpenter, D. Conway, et al., Causes of death among stillbirths, JAMA, J. Am. Med. Assoc. (2011), https://doi.org/10.1001/jama.2011.1823.
[7] L. Bellamy, J.-P. Casas, A.D. Hingorani, D.J. Williams, Pre-eclampsia and risk of cardiovascular disease and cancer in later life: systematic review and meta-analysis, BMJ (2007), https://doi.org/10.1136/bmj.39335.385301. BE.
[8] H a de Boo, J.E. Harding, The developmental origins of adult disease (Barker) hypothesis, Aust. N. Z. J. Obstet. Gynaecol. (2006), https://doi.org/10.1111/j.1479-828X.2006.00506.x.
[9] R.W. Redline, Classification of placental lesions, Am. J. Obstet. Gynecol. 213 (4) (2015) S21–S28, https://doi.org/10.1016/j.ajog.2015.05.056.
[10] A. Chen, D.J. Roberts, Placental Pathologic Lesions with a Significant Recurrence Risk - what Not to Miss! *APMIS*, 2017.
[11] J.M. Catov, C.M. Scifres, S.N. Caritis, M. Bertolet, J. Larkin, W.T. Parks, Neonatal outcomes following preterm birth classified according to placental features, Am. J. Obstet. Gynecol. (2017), https://doi.org/10.1016/j.ajog.2016.12.022.
[12] M.T. Vinnars, J. Nasiell, G. Holmström, M. Norman, M. Westgren, N. Papadogiannakis, Association between placental pathology and neonatal outcome in preeclampsia: a large cohort study, Hypertens. Pregnancy (2014), https://doi.org/10.3109/10641955.2013.842584.
[13] A.M. Roescher, A. Timmer, J.J.H.M. Erwich, A.F. Bos, Placental pathology, perinatal death, neonatal outcome, and neurological development: a systematic review, PLoS One (2014), https://doi.org/10.1371/journal.pone.0089419.
[14] K.M. Chisholm, A. Heerema-Mckenney, Fetal thrombotic vasculopathy: significance in liveborn children using proposed society for pediatric pathology diagnostic criteria, Am. J. Surg. Pathol. (2015), https://doi.org/10.1097/PAS.0000000000000334.
[15] R.W. Redline, The clinical implications of placental diagnoses, Semin. Perinatol. 39 (1) (2015) 2–8, https://doi.org/10.1053/j.semperi.2014.10.002.
[16] P. Kelehan, A. Maes, E.M. Mckay, T.K. Morgan, P.G.J. Nikkels, Sampling and Definitions of Placental Lesions, vol. 140, 2016, https://doi.org/10.5858/arpa.2015-0225-CC. July.
[17] R.W. Redline, Placental Pathology: A Systematic Approach with Clinical Correlations, vol. 22, 2008, pp. 86–91, https://doi.org/10.1016/j.placenta.2007.09.003.
[18] R.W. Redline, Villitis of unknown etiology: noninfectious chronic villitis in the placenta, Hum. Pathol. (2007), https://doi.org/10.1016/j.humpath.2007.05.025.
[19] G. Turowski, L.N. Berge, L.B. Helgadottir, E.M. Jacobsen, B. Roald, A new, clinically oriented, unifying and simple placental classification system, Placenta (2012), https://doi.org/10.1016/j.placenta.2012.10.002.
[20] B. Hargitai, Best practice NO 178: examination of the human placenta, J. Clin. Pathol. (2004), https://doi.org/10.1136/jcp.2003.014217.
[21] S.L. Warsof, P. Gohari, R.L. Berkowitz, J.C. Hobbins, The estimation of fetal weight by computer-assisted analysis, Am. J. Obstet. Gynecol. (1977), https://doi.org/10.1016/0002-9378(77)90058-8.
[22] N. Almoussa, B. Dutra, B. Lampe, et al., Automated vasculature extraction from placenta images, Proc. SPIE-Int. Soc. Opt. Eng. 7962 (2011), https://doi.org/10.1117/12.878343, 79621L-79621L - 10.
[23] Z. Swiderska-Chadaj, T. Markiewicz, R. Koktysz, S. Cierniak, Image processing methods for the structural detection and gradation of placental villi, Comput. Biol. Med. (April) (2017) 1–11, https://doi.org/10.1016/j.compbiomed.2017.08.004.
[24] D. Kidron, I. Vainer, Y. Fisher, R. Sharony, Automated image analysis of placental villi and syncytial knots in histological sections, Placenta 53 (2017) 113–118, https://doi.org/10.1016/j.placenta.2017.04.004.
[25] J.M. Chang, N. Huynh, M. Vazquez, C. Salafia, Vessel enhancement with multiscale and curvilinear filter matching for placenta images. International Conference on Systems, Signals, and Image Processing, 2013, pp. 125–128, https://doi.org/10.1109/IWSSIP.2013.6623469.
[26] P. Palee, B. Sharp, L. Noriega, N.J. Sebire, C. Platt, Image analysis of histological features in molar pregnancies, Expert Syst. Appl. 40 (17) (2013) 7151–7158, https://doi.org/10.1016/j.eswa.2013.06.034.
[27] G.D. Finlayson, B. Schiele, J.L. Crowley, Comprehensive colour image normalization, in: Lecture Notes in Computer Science (Including Subseries Lecture Notes in Artificial Intelligence and Lecture Notes in Bioinformatics), 1998, https://doi.org/10.1007/BFb0055685.
[28] O. Nobuyuki, A threshold selection method from gray-level histograms, IEEE Trans. Syst. Man Cybern. (1979), https://doi.org/10.1109/TSMC.1979.4310076.
[29] T.F. Chan, L.A. Vese, Active contours without edges, IEEE Trans. Image Process. 10 (2) (2001) 266–277, https://doi.org/10.1109/83.902291.
[30] F. Stoz, R.A. Schuhmann, A. Schmid, Morphometric investigations of terminal villi of diabetic placentas in relation to the White classification of diabetes mellitus, J. Perinat. Med. 440 (1987) 193–198.
[31] S. Chaikitgosiyakul, M.J. Rijken, A. Muehlenbachs, et al., A morphometric and histological study of placental malaria shows significant changes to villous architecture in both *Plasmodium falciparum* and *Plasmodium vivax* infection, Malar. J. (2014) 1–13.
[32] R.M. Haralick, S.R. Sternberg, X. Zhuang, Image analysis using mathematical morphology, IEEE Trans. Pattern Anal. Mach. Intell. (1987), https://doi.org/10.1109/TPAMI.1987.4767941.
[33] M.W. Stark, L. Clark, R.D. Craver, Histologic differences in placentas of preeclamptic/eclamptic gestations by birthweight, placental weight, and time of onset, Pediatr. Dev. Pathol. 17 (3) (2014) 181–189, https://doi.org/10.2350/13-09-1378-OA.1.

Chapter 4

Application of Machine Learning to Classify Distinct Patterns of Placenta Histopathology: A Proof-of-Concept Using Cases of Preeclampsia

Mukherjee A[1], Salsabilli S[2], Ukwatta E[2,3], Chan ADC[2], Grynspan D[4,5], Bainbridge SA[1,6].

[1]1Interdisciplinary School of Health Sciences, University of Ottawa, Ottawa, Ontario, Canada.

[2]Department of Systems and Computer Engineering, Carleton University, Ottawa, Ontario, Canada.

[3]Department of Biomedical Engineering, Guelph University, Guelph, Ontario, Canada.

[4]Department of Pathology and Laboratory Medicine, Children's Hospital of Eastern Ontario, Ottawa, ON, Canada.

[5]Department of Pathology, Vernon Jubilee Hospital, Vernon, British Columbia, Canada.

[6]Department of Cellular and Molecular Medicine, University of Ottawa, Ottawa, Ontario, Canada.

This manuscript was formatted for submission to the peer-reviewed journal *Journal of Pathology Informatics*.

Abstract

Background: Placenta mediated diseases (PMD) affect up to 20% of pregnancies and are the leading cause of maternal and fetal morbidity and mortality. Histopathology analysis is critical to understanding the physiology underlying placenta-induced pregnancy complications. However, a major challenge in perinatal pathology is the variable findings in histopathological analysis of the placenta. This finding is particularly true of preeclampsia (PE) – one of the most severe types of placenta mediated diseases with high heterogeneity in clinical presentation and underlying placental disease and damage. Given the heterogeneity of PE, consistent histopathological analysis of these placentae may be improved through the application of machine learning (ML) models which may be capable of differentiating distinct subclasses of PE patients with divergent forms of placental disease. The current study sought to determine the utility of ML to identify distinct patterns of placental disease, using cases of PE as a proof-of-concept. More broadly, machine learning could be applied to the entirety of placental pathology, lending to the development of computer-aided diagnostic tools in this field.

Methods: Supervised ML algorithms were used to develop classification models for the identification of PE or PE subclasses using digital images of placenta histopathology specimens. Three experimental designs were used to examine different feature extraction methods, ranging from a high degree of human involvement through to fully integrated automation (deep learning). Classification performance of each ML model was assessed, with the inclusion or omission of gestational age at delivery as an additional feature used for classification purposes.

Results: All 3 experimental models achieved maximum performance in the classification of PE cases vs controls (55-73%), with moderate performance in the identification of PE disease subclasses (41-73%). The inclusion of gestational age at delivery as a feature of relevance typically increased model

performance. The deep learning method tested demonstrated the poorest performance on all classification tasks (41%-55%).

Conclusions: The current study has determined that ML models can classify cases of PE with considerable success. However, significant variability exists in model performance, depending on the method of feature extraction used, and the reference labels being used (binary clinical outcome vs. disease subclass classification). With additional validation, the automated screening tools presented have the potential to optimize the time pathologists spend analyzing placenta histopathology images and improve the agreement of diagnoses between pathologists.

Keywords: placenta, preeclampsia, pathology, histopathology, digital pathology, machine learning, supervised machine learning, deep learning, support vector machine, convolutional neural networks, image classification, medical imaging, computer vision, feature extraction, Whole-slide imaging

Background

Preeclampsia (PE) is a hypertensive disorder of pregnancy, clinically defined by new onset hypertension after 20 weeks of gestation combined with evidence of maternal end organ dysfunction. [1,2] This disorder affects 3-8% of all pregnancies, [3] and is a leading cause of maternal and infant mortality worldwide. There is currently no cure for PE, other than delivery of the causative organ – the placenta. [1] Rates of PE are increasing across North America, likely as a result of increased maternal age and/or increased incidence of pre-disposing co-morbidities (i.e. chronic hypertension, obesity, diabetes). [3]

Preeclampsia is a highly heterogeneous placenta-mediated disorder, with a wide spectrum of clinical presentation, observed placental pathologies and maternal and fetal health outcomes. [3–5] Mounting evidence indicates this heterogeneity is the result of distinct PE disease subclasses with divergent underlying placental and maternal pathophysiology. [6] Commonly, this pregnancy disorder is classified according to time of disease onset and severity of maternal symptoms. [7,8] “Early-onset” or “severe” PE is characterized by maternal symptom onset at less than 34 weeks of gestation, and is associated with increased rates of pre-term delivery, fetal growth restriction and severe maternal complications (i.e. HELLP) when compared to “late-onset” PE. [7] However, this simple dichotomous split of PE cases does not completely resolve the high degree of heterogeneity observed, indicating further subclasses of disease may exist. Work conducted by our group demonstrates the presence of at least three distinct molecular subclasses of PE, each with a unique clinical and placenta pathology profile. [5,6] The largest subclass (coined “canonical PE”) demonstrates placental gene expression and histopathology findings consistent with maternal vascular malperfusion of the placenta, with a more severe maternal disease phenotype and earlier delivery. [5] A smaller immunological subclass of PE was also identified, demonstrating placental gene expression and histopathology findings consistent with an allograft rejection of this critical organ of pregnancy. [5] Interestingly, this subclass of PE demonstrated the most severe fetal phenotype of disease, with a large number of growth restricted infants in this subclass. The

final PE subclass previously described demonstrated minimal evidence of placental pathology, the mildest degree of maternal disease, and normal fetal outcomes, and we speculate that in these cases maternal maladaptation to pregnancy may be the underlying etiology of PE. [5]

The ability to critically evaluate the placenta at the histological level following a PE pregnancy, through clinical placenta pathology examination, can help diagnose PE disease subtypes (underlying disease etiology) and can inform the clinical team in regards to recurrence risk and/or future health risks for both the mother and infant. [5,9] However, placenta pathology examinations are resource intensive with requirements for sub-specialized pathologist expertise and heavy workload demands because of high volume and complexity of placenta-mediated diseases. [10,11] Further, it is well documented that clinical placenta pathology is plagued by a high degree of inter-observer variability – the result of differences in institutional practices, pathologist sub-specialty training and lack of diagnostic and practice standardization. [12,13] The Amsterdam collective has made tremendous strides towards improving standardization of diagnostic criteria and reporting practices [14], however the integration of diagnostic aids in this clinical field would no doubt improve the clinical utility of these examination and relieve some of the workload pressures pathologists face [15] – freeing up resources for the examination of more challenging cases. [13,16] More specifically, standardized automation of some aspects of the placenta pathology examination may clarify some confusion surrounding the heterogeneity of a PE diagnosis, leading to more personalized and effective post-partum counselling and intervention strategies for women following a PE pregnancy. [17]

Computer-aided diagnostic (CAD) tools can assist physicians in interpreting medical images, and have been shown to improve diagnostic efficiency and reproducibility in highly heterogeneous and complex diseases, including tumor detection from histopathology slides, ischemic lesions from brain magnetic resonance imaging, and tuberculosis screening from X-ray images. [15,18–21] While their clinical utility has been clearly demonstrated for many forms of radiological images, the application of CAD to digital

histopathology images is still in its infancy – with very limited attempts to apply these techniques to placenta pathology specimens in a research context. [22,23] Despite this, substantial efforts in the field of onco-histopathology demonstrate considerable promise of CAD applications for automated disease subclassification, staging/grading of disease, and prediction of disease trajectory (prognosis). [24] In most cases, the CAD tools are developed using a supervised machine learning approach, in which a computer is trained to recognized visual patterns (or features) in a large number of diagnostically-labelled digital histopathology images (i.e. benign vs. malignant). [16,25–27] The lack of widely available, highly annotated digital image banks of placenta-mediated disease cases, of a size required for machine learning applications, has limited the progress of applying these same successful approaches to the clinical placenta pathology domain.

In a proof-of principle, the current study sought to test and compare three different supervised machine learning approaches to accurately identify PE disease and/or PE disease subtypes, using a highly annotated dataset of digital placenta histopathology images from women who spanned the clinical spectrum of PE. The approaches tested varied in degree of researcher-input, ranging from semi-automated to fully integrated approaches, and included: 1) supervised machine learning on manually extracted features of biological relevance (i.e. chorionic villi size and density); 2) supervised machine learning on automatically extracted spatial and textural features in the images; and 3) supervised hierarchical feature learning (deep learning). It was hypothesized that machine learning models trained with the three image feature extraction approaches mentioned above would be capable of not only automatically distinguishing cases of PE from controls, but also distinguish between subclasses of PE. This study is an important first step in a move towards automating aspects of clinical placenta pathology – an effort that will undoubtedly improve the reproducibility and utility of this important diagnostic modality in cases of complex placenta-mediated disease.

Methods

Digital Image Dataset Acquisition and Patient Characteristics

This study has received research ethics board approval from the University of Ottawa Research Ethics Board (H-08-18-1023) and Mount Sinai Hospital (13-0212-E). Original paraffin-embedded placenta histopathology specimens were purchased from the Research Centre for Women's and Infant's Health (RCWIH) Biobank at Mount Sinai hospital (Toronto, ON). A total of 148 specimens were collected from patients with PE (n=79) and healthy controls (n=69), with each paraffin block containing four chorionic villous biopsies from each quadrant of the placenta. As previously described by our group [5,6], the collected PE specimens spanned the clinical spectrum of disease, including early-onset/severe cases of PE (n=50) and late onset cases of PE (n=29) as well as cases with (n=33) and without (n=46) small for gestational age infants (Table 4.1). Sectioned tissue was mounted on glass slides and stained following a standard histopathology protocol with Hematoxylin and Eosin (H&E) at the Department of Pathology and Laboratory Medicine at the Children's Hospital of Eastern Ontario (CHEO). Slides were scanned at 20x magnification with an Aperio Scanscope digital scanner and saved in the SVS format.

Our group has previously carried out detailed characterization of the clinical and placental phenotype of all cases used in the current study, and as such each digital image was linked to an annotated dataset that included maternal and fetal clinical demographics, pregnancy outcome and molecular subclassification of PE disease (based on gene expression and detailed histopathology profiling of each placenta) (Table 4.2) [5,6]. This annotated dataset was used in the generation of the different class labelling schemes, described below, that were used to supervise the developed machine learning models.

Supervised Machine Learning

Three supervised machine learning approaches were tested, each with decreasing user-input during the feature extraction phase of model development: 1) manually extracted features of biological relevance (Approach #1 – semi-automatic); 2) automatically extracted spatial and textural features of unknown biological relevance (Approach #2 – automatic); or 3) automatically extracted features of increasing complexity in a hierarchical fashion (Approach #3 - deep learning). Approaches #1 and #2 were also tested with the use of gestational age as an additional fed in feature to see if results would improve. Approach #3 did not include gestational age, as with all deep learning models, features are simultaneously extracted from the image and used to train the model, so only inherent features of the image can be used. Figure 4.1. provides a summary of the machine learning workflow elements for each approach.

For all three approaches applied, a series of different image class labels were tested to supervise the learning. These included: a) Binary pregnancy outcome (CT, PE); b) Pregnancy outcome according to disease onset/severity (CT, EO-PE, LO-PE); and, c) Molecular subclassification of PE (subclass 1 – canonical PE, subclass 2 – inflammatory PE, subclass 3 – maternal PE). In all cases, labeled training images (70% of total image dataset) were used to teach the model to recognize features of relevance to each class, such that the model could then classify unseen and unlabeled images into their appropriate output class (disease category). Through a feedback mechanism, which iteratively minimizes classification errors, the model progressively improves at the task.

Machine learning models for approaches #1 and #2 were trained with Support Vector Machine (SVM) classifiers [28] and the models for approach #3 were trained with Convolutional Neural Networks (CNNs) [29]. All machine learning protocols and data processing was implemented in Python 2.7 except where explicitly specified. Table 4.3 includes a summary of python libraries and modules used. Model development was processed on a 1.8 GHz Intel Core i5 processor for all three machine learning approaches.

Approach #1 – Semi-Automated Supervised Machine Learning

The semi-automated supervised machine learning approach was inspired by the clinical workflow that perinatal pathologists typically use in the microscopic component of the clinical placenta pathology exam. In this approach, all images were pre-segmented as previously describe to extract measurements of morphological features believed to be of relevance to the pathophysiology of PE [30]. Subsequently all machine learning was performed on these pre-extracted features, supervised according to the different classification label schemes described (Table 4.2).

a) Image pre-processing

The image pre-processing and segmentation was conducted as previously described. [30] Briefly, color normalization was performed in MATLAB with the Comprehensive Image Normalization approach described in Finlayson et. al [31] to account for differences in staining intensity. Using K-means clustering [32], three colour profiles (white, purple, and red) were extracted to delineate the foreground, with the identification of intervillous space, trophoblastic nuclei (both syncytiotrophoblast and cytotrophoblast) and the mesenchymal core of the villous tissue. Subsequently a top-hat transform [33] was used to identify concave regions in the perimeter of objects to properly segment distinct villi structures in each image.

b) Feature extraction

Using the pre-segmented images, measurements of four pre-defined villous structure features were extracted, including: 1) average villi size (pixels^2); 2) villi density (1/pixel); 3) syncytial trophoblast density (1/pixel), and 4) average villi circularity (scale of 0-1 with 1 being a perfect circle). These specific features were selected, in consultation with a trained perinatal pathologist (DG), due to their potential morphological relevance to PE pathophysiology. Measurements were mean values from across the

entire whole-slide image. Feature measurement extraction was automated and implemented in MATLAB as previously described. [30]

c) Machine learning model development

Extracted features were normalized using a Min-Max Scaler (SciKit Learn library, Python 2.7) to equally weight the magnitude of each feature prior to being passed into the machine learning model. Following normalization, samples were split into training (70%) and testing sets (30%) such that the model could be tested on unseen data (SciKit Learn library, Python 2.7). The training set was labeled according to the classification label scheme described above and the extracted features from each image were passed through a support vector machine (SVM) learning model (SciKit Learn library, Python 2.7). The SVM model was run three separate times, to test the 3 different classification labeling schemes: (a) CT, PE; (b) CT, EO-PE, LO-PE; (c) subclass 1, 2, 3. The SVM model was also trained with each of these three classification labeling schemes, taking into account gestational age at delivery as an additional feature of relevance for each image. All six trained SVM models were applied to the unseen test data set (remaining 30% of dataset), to assess the ability of the machine learning model to accurately classify the unseen images. Classification performance metrics were visualized using confusion matrices (SciKit Learn Library, Python 2.7), with outputs: true positives (TP), true negatives (TN), false positives (FP), and false negatives (FN). Performance metrics of accuracy, precision, recall and F1 score were calculated using classification outputs with the following equations:

(1) $Accuracy = \frac{TP+TN}{TP+TN+FP+FN}$

(2) $Precision = \frac{TP}{TP+FP}$

(3) $Recall = \frac{TP}{TP+FN}$

(4) $F1\ Score = 2 \cdot \frac{Precision \cdot Recall}{Precision+Recall}$

Approach #2 – Automated Supervised Machine Learning

In the second approach tested, feature identification and extraction was automated using SIFT keypoint descriptors , based entirely on spatial and textural differences in the images, which may or may not have biological relevance. [34] In this way, no human bias was introduced in the selection of features of interest, however control was maintained with respect to the total number of key points identified across the image set. This approach did not require a pre-segmentation step, further simplifying the application of this approach.

a) Image pre-processing

All images were cropped to five overlapping 1200x1200 pixel patches (Figure 4.2), thereby increasing the number of images available for training the machine learning model to 740, a method which has been shown to improve classification accuracy. [35] Color on each image was normalized through conversion to greyscale (SciKit Learn library, Python 2.7).

b) Feature extraction

Features were extracted using a scale-invariant feature transform (SIFT) – a well described feature detection algorithm commonly used in computer vision (Open CV library, Python 2.7). Five hundred SIFT keypoints were extracted per image, as per previously published protocols. [16] Images with fewer than 500 keypoints were excluded from model development for too little tissue-containing area, resulting in a remaining dataset size of 624 images. Each SIFT keypoint descriptor contains 128 data points that describe the texture at a particular point in an image, resulting in a matrix of dimensions 500x128 describing each image. The median value of each of the 128 features at each of the 500 keypoints in the image was preserved to create a flat feature vector of dimensions 1x128 describing each image.

c) Machine learning model development

Feature normalization, training/test set splitting of data, SVM model testing according to the different class labelling schemes and classifier performance measurements were carried out as described in Approach #1.

Approach #3 - Supervised hierarchical feature machine learning (deep learning)

The final approach tested was entirely automated, with feature extraction integrated into the machine learning model training process. Full integration is accomplished through deep learning, where a convolutional neural network (CNN) is used to optimize and select image features that result in the best classification accuracy. This approach requires the least human involvement, as the computer algorithm executes the entire process after initial image pre-processing (for quality assurance and data augmentation).

a) Image pre-processing

Whole-slide images were split into training (60%), validation (20%) and test (20%) sets for model development. Images are cropped to 2400x2400 pixels to exclude areas on slides that did not contain placental tissue. Deep learning models perform better with larger datasets, so it is common for developers to augment data before training a machine learning model. [36][37] Therefore, 225 smaller overlapping patches of 300x300 pixels were automatically extracted using a sliding window approach. All patches were passed through an additional data augmentation phase, using a directory image data generator (Keras Library, Python 2.7) which applies a random set of manipulations to the input images, including: rescaling of pixel values to be between 0 and 1, flipping and rotating. To ensure that only images that contained sufficient placental tissue were used in the deep learning approach, all images that contained fewer than 500 detectable SIFT keypoints were excluded from model training.

b) Feature extraction and machine learning model development

The Keras CNN framework, with model architecture described in Table 4.4, was used to simultaneously develop a model that can accurately discriminate between classes and optimize the features that differentiate each class. The neural network used contained 15 layers comprising convolutional, pooling, and dense layers. Loss functions are used to calculate the cost of errors in classification and are integrated into the CNN models to drive improvements in classification at each round of training. A binary cross entropy loss function was used to calculate the rate of error decline for binary classification models (ex. CT, PE), and a categorical cross entropy loss function was used for multiple class models (ex. CT, EO-PE, LO-PE). [37] The performance metric accuracy was captured at every round of training to be able to track progress in model development. Fifty rounds of training were used, with early stopping enabled if model accuracy was no longer improving with increased training. Every iteration of training was evaluated on the validation set to track model improvement and for guidance on what parameters could be adjusted to increase training accuracy. The final trained model was evaluated on the test dataset. The entire CNN workflow was implemented in Python 2.7 with the Keras library. Confusion matrices (Figure 4.3) were generated to analyze types of classification errors (ex. false positives vs. false negatives).

Results

Performance metrics for all machine learning models developed and tested using both machine learning approaches and all 3 feature extraction methods are presented in Figure 4.3 and Table 4.5 respectively. The semi-automated and automated machine learning approaches (#1-2) yielded classification accuracies that ranged from 55-73%, depending on which classification labelling scheme was used. The semi-automated approach (approach #1) demonstrated the highest degree of classifying accuracy using the categorical "pregnancy outcomes according to onset/severity" labelling scheme (CT, EO-PE, LO-PE), whereas the automated approach (approach #2) had highest classification accuracy using the binary "pregnancy outcomes" labelling scheme (CT vs. PE). In both cases, the addition of gestational age at delivery into the model as an additional image feature improved the accuracy observed (73% accuracy for both models). On the whole, the automated approach (approach #2) typically outperformed the semi-automated approach across all class labelling schemes, however the differences in performance were minimal. The deep learning modeling approach (approach #3) demonstrated the poorest performance metrics across all classification labelling schemes, with accuracies ranging between 41-55%, with the binary "pregnancy outcome" labelling scheme demonstrated the greatest classification performance.

Machine learning models that utilized categorical class labelling schemes demonstrated one class that contributed most to lower accuracies. After examination of confusion matrices normalized for class imbalance, it appears that classes with the fewest representative cases were consistently poorly classified. Across all three approaches, models demonstrated poor performance in the proper classification of "LO-PE" (0-59% true positives) and "Molecular Cluster 3" (0-27% true positives). The most accurately predicted classes varied across approaches. Using the approach which most closely mimics a pathologist's workflow (Approach #1), the model was best able to pick out placentas with PE, using categorical pregnancy outcomes based on onset information (accuracy of 73%). Using the

automated machine learning approach (approach #2), the model was best able to classify placentas with PE when a binary pregnancy outcome label was used (accuracy of 73%). In both approaches #1 and #2, including gestational age as an additional feature resulted in better classification accuracy. Finally, using the deep learning approach (approach #3), the model was best able to identify placentas labelled as "PE" (accuracy of 55%), but was not able to distinguish between early-onset/severe and late-onset cases of PE (accuracy <50%) or molecular subclass of PE (<50%).

Conclusions

In the current proof-of principle study, three different supervised ML approaches were applied to a highly annotated placenta histopathology image dataset that included cases of PE that spanned the clinical spectrum of disease. It was hypothesized that ML models would be capable of distinguishing histological features within the placenta that could not only identify cases vs. controls but would further be capable of distinguishing subclasses of PE disease. Both the semi-automated and automated supervised machine learning models tested (approaches #1-2) demonstrated success in the classification of cases vs controls, however, the ability to distinguish distinct subclasses of placental disease within the PE cases was limited. Surprisingly, the highly robust deep learning model tested, demonstrated the weakest classification performance on this dataset, correctly classifying only one half of the cases and controls collectively. Despite the limited success of the described approaches, several avenues for further optimization of the presented machine learning protocols have been identified. With reflection, this body of work will no doubt serve as a solid foundation upon which to move this field forward.

The three approaches tested differed with regards to the degree of user engagement in the selection of features, and in the complexity of features used in the ML model. In the first semi-automated approach, there was a high degree of user input into which features would be used in the classification model, an

attempt to mimic most closely what is manually looked for by perinatal pathologists during a clinical placenta pathology examination – namely morphological features deemed to be of relevance to PE pathophysiology. As PE is often characterized by pathological features including placental infarcts, syncytial knots, advanced villous maturation and villous agglutination [38], it was hypothesized that measurements of size, shape and density of the villous structures within the tissue would be of relevance for image classification. In order to capture these features, however, all images needed to be pre-segmented to identify all distinct villous structures across each image. While our group has developed an algorithm to automate this process [30], this is still a time-consuming pre-processing effort which may limit integration into a clinically useful workflow. Despite this, this approach worked quite well in distinguishing healthy and PE placentas as a binary outcome, with a mild increase in classification performance when disease onset/severity was taken into account (accuracy of 73%). However, the model demonstrated relatively poor performance in classifying images according to the molecular subclass of disease (accuracy of 57%). This finding was unexpected by our group, as we have previously demonstrated distinct placental pathology lesion profiles across these PE disease subtypes [5]. This outcome may simply be the result of small sample size, as the smallest molecular subclass (subclass 3) only had 12 cases included in the dataset, which significantly contributed to lowering the average classification accuracy. It could be that this number is simply too small for training purposes in ML models. In support, this same subclass was incorrectly classified by all three approaches tested. In addition, the biased approach taken to identify features of interest inherently ignored morphological features found to be of relevance to this small subclass of “immunologically-driven” PE, which is poorly described in the mainstream literature on PE pathophysiology. In fact, our group has described placental lesions of chronic inflammation (villitus of unknown etiology, massive perivillous fibrin deposition, chronic deciduitis) as the predominant placental pathologies observed in this group [5] – all of which would likely not be captured by the selected features used in this approach. An important evolution to

this approach moving forward would be to incorporate morphological measurements that may better encompass the highly heterogeneous nature of placental lesions seen across the PE population.

The results obtained from the first approach do, however, provide a strong argument for the removal of human bias in the selection of features that may differentiate cases from controls, and were the basis of the automated approach (approach #2) and the deep learning approach (approach #3) tested. In these approaches, a feature extraction algorithm (SIFT) or the model itself (CNN classifier) was used to detect visual features of relevance in an unbiased fashion. It was anticipated that the deep learning models would outperform the automated machine learning models, due to the exhaustive feature identification process inherently built into deep learning classifiers – allowing for complex and interconnected features to be identified and used for classification. Contrary to our expectations, the automated machine learning approach yielded the best results of the two unbiased approaches (#2 and #3), with a maximum accuracy of 73% in the classification of healthy and PE cases. Interestingly, similar performance metrics were observed in the identification of PE subtypes, whether they be distinguished based on disease onset/severity or molecular subclass of disease (accuracies of 69% and 68% respectively). In both instances, classification errors were predominant to one PE subtype – either the LO-PE or the molecular subclass 3 (immunological PE). LO-PE cases were usually misclassified as healthy controls (Figure 3), and this could be explained by the fact that this subtype of PE is considered a milder form and so visible effects in the placenta may be relatively small [7]. Molecular subclass 3 was frequently misclassified as either of the other subclasses, which suggests that the reason was not due to inherent characteristics of the images, but rather a sample size too small to properly train an ML algorithm. Given that the classification errors have possible sources that could be mitigated, the automated machine learning approach has the potential to yield stronger results with sample size augmentation and model optimization.

Deep learning models have become the industry standard for image classification, due to the ability of neural networks to model very complex data with a high degree of accuracy. [39] Neural networks train on inherent characteristics in a dataset (i.e. raw pixel data) as opposed to features extracted by investigators. Integrated feature extraction reduces the risk of bias, and automatically optimizes the number and weight of features included in the model. [29] Given the size and complexity of placenta histopathology images, it was expected that this classifier would achieve the best results. However, this was not observed, with classification accuracies from this model hovering around 50%. These results may be explained in part by an intrinsic disadvantage of deep learning models – the requirement for extensive computational power. The presented deep learning models were allowed to "learn" across a maximum of 50 epochs of training. Early stopping was used to halt the training process when classification accuracy did not further improve over 10 consecutive rounds of training. Without enabling early stopping, computer memory resources may be wasted when classification accuracy is no longer improving. Future work, with access to increased computing power will enable a more complete training phase to be executed for the deep learning models with a wider buffer for model stopping, likely increasing model performance.

Moreover, a major improvement to our deep learning model may be achieved through the inclusion of a transfer learning phase into our ML workflow. Transfer learning is a relatively new machine learning paradigm that leverages auxiliary image data from additional sources in order to improve the classification model. [40] In a transfer learning workflow, the deep learning model focuses the earlier layers of the network, where it is learning low-level image information (ex. edges, contrast, etc.), on a large and highly robust external image dataset (ex. ImageNet Large Scale Visual Recognition Challenge datasets; http://www.image-net.org/). The model is then transferred to the dataset of interest for the later layers of the network, where it is learning more complex image information and is interconnecting different image features. In so doing, one can achieve high classification performance when the test

data set is limited in size [41] – a recognized limitation of the current study. Ongoing efforts by our group are focused on optimizing this protocol to include transfer learning and increase computing power by running the model through a remote server, as we anticipate this will significantly increase the performance of this approach.

Gestational age at delivery was an important consideration for this study, as the histological appearance of the placenta evolves across pregnancy. Across gestation the chorionic villous structures elongate and branch, increasing the maternal-fetal exchange area of the placenta. [42] With this maturation comes changes in shape and density of villous structures, as well as cellular composition of the structures seen in a histopathology specimen. Placenta specimens used in the current study included a span of gestational ages (25-40 weeks), including "immature" placentas delivered pre-term (<34 weeks). It was anticipated that the visual difference could be a confounding factor in model development, because visual differences between placentas belonging to difference classes (ex. PE vs. Control) could be confused with visual differences between placentas of different gestational ages. Therefore, gestational age at delivery was included as an extra image feature in approaches #1 and #2. Although the addition of this feature generally improved classification accuracy, it is likely due to the fact that gestational age is a good predictor of degree of placenta disease – with those cases with severe placental disease needing to be delivered earlier in pregnancy. We offer that this may not be the best way to account for this important attribute of each image. In future work it would be imperative to consider other ways to transform the image data to account for gestational age at delivery. Prior to training, features can be scaled by the gestational age rather than having it included as an additional feature. With this approach, features would be scaled by a factor that represents how far from term the pregnancy was. Alternatively, a multi-level classifier system could be used, where in the first level cases are stratified by categories of gestational age, and in the second they are classified according to the different class label schemes. As the deep learning model integrates feature extraction into the learning process, it was not

possible for us to incorporate gestational age at delivery into this model – an important consideration in the interpretation of the deep learning performance metrics. This limitation could also be tackled in the future by normalizing the features for gestational age in the pre-processing of CNN fine-tuning stages. However, to do this a large image database of placenta histopathology images from different gestational ages would be required to train each model on gestational age anatomical and histological norms.

As highlighted above, a major limitation of this study was sample size – a limitation that has hindered considerable progress in this field in general. The image dataset used in the current study is likely one of the largest highly annotated placenta histopathology image datasets specific to PE pathology currently available. However, the complexity of the human placenta, the high degree of heterogeneity of placental disease in PE [5], and the requirements for large datasets for effective ML model development [43] have likely limited the success of the current project. There are no validated guidelines for the minimum number of original images needed for ML model development, with sample sizes ranging from 7-14,000 in fields with the largest progress to date [44,45]. Having a minimum of 1000 image samples per class has been proposed as a guideline, and this value is reflected in newer articles in the domain of medical image ML [46]. According to this proposed best practice, the current study would be highly underpowered, particularly for the smaller PE subclasses such as molecular subclass 3 (N=12). In an attempt to tackle this limitation, we employed data augmentation techniques, such as patch extraction and image distortion, both widely used in the field [35]. However, patch extractions and image distortion can only increase the variability in the dataset by a finite amount. Patch extraction effectively over represents the data already present with slight variation. A better approach is to obtain more unique patient samples that would best represent the true degree of placental variability and heterogeneity present in the PE population. Increasing training sample size has been shown to increase classification accuracy on test data, as the model becomes more robust to unusual cases in the test data. Further, we must consider that within one placenta the degree of heterogeneity of placental

pathology can be quite high, indicating that we need to consider how to best optimize sampling procedures from this complex organ, as well as the methods to account for localized differences in pathology across the placenta in all our ML approaches.

From a clinical perspective, we must be cognizant of limitations of CAD-based technologies, or conversely, the benefits that come with human intuition and ability to place observed findings into a broader biological context. This is particularly true for deep learning models, such as CNNs, which lack transparency regarding how features of relevance were identified for extraction, and how they became inter-related within the model. Despite being the industry standard for medical image classification model development [18], CNNs learn features from images that cannot be clearly identified or even understood at the human level. Therefore, even if the accuracy of prediction/diagnosis is high, it may be difficult for the pathologist to explain the classification/diagnostic results to their colleagues or patients. However, this limitation is being addressed head on in a newly emerging field devoted to explainability and interpretation of the inner-workings and results of deep learning models [47]. There is no question that with the pace at which this field is advancing, the integration of deep learning CAD-tools will become the industry standard across all domains of medical imaging and will have a high degree of applicability to histopathology analysis. As such, proof-of-concept studies such as this are integral in the exploration of how this technology can be best harnessed to improve the health of different patient populations.

The current study is an encouraging first attempt at applying ML tools to model the visual appearance of the placenta in pregnancies with placenta-mediated disease. Given the moderate success achieved with these early models, and the identification of concrete next steps for model optimization, there is considerable enthusiasm that ML will be a viable approach to automate aspects of clinical placenta pathology moving forward. In so doing, the identification of distinct disease subtypes at the time of delivery may be easily achievable, clarifying underlying etiology of disease and promoting an

individualized approach to post-partum patient counselling. It would further enhance standardization in this field and improve the quality of placental diagnoses taking place in remote sites that may lack the required subspecialized training required for placenta pathology examination. The benefits made possible through the integration of this technology into the realm of perinatal pathology should serve as a strong motivation to build upon this body of work to achieve the goals of developing a large publicly available histopathology image database specific to the placenta and the further development and optimization of ML models that can be used to better understand the complexity of placenta-mediated diseases.

Competing Interests

The authors declare that they have no competing interests.

Author's Contributions

Dr. Shannon Bainbridge and Dr. David Grynspan were the principal investigators for the study and were the primary contributors to the conceptualization, funding, and interpretation and presentation of data for this manuscript. Dr. Adrian D.C. Chan and Dr. Eran Ukwatta consulted on technical aspects of ML model development and experimental design and contributed to manuscript revision. Dr. Eran Ukwatta provided sponsorship for access to Compute Canada High Performance Computing resources to be able to run the programs. Codes for data augmentation and machine learning were written by Anika Mukherjee. Sina Salsabilli applied the code developed in Salsabilli et. al. (2019) and extracted clinically relevant features from segmented placenta villi. Anika Mukherjee extracted textural features from the same samples for comparison with clinically relevant features. This manuscript was prepared by Anika Mukherjee and Dr. Shannon Bainbridge and was reviewed by all co-authors.

Acknowledgements

The following funds were used to support the authors: Faculty of Health Sciences, University of Ottawa (A.M., S.B.), Canadian Foundation for Innovation Leaders Opportunity Fund (S.B); Canadian Institute of Health Research (CIHR) (130543 CIA – S.B); CIHR (142298 MOP – S.B).

References

[1] Mol BWJ, Roberts CT, Thangaratinam S, Magee LA, de Groot CJM, Hofmeyr GJ. Pre-eclampsia. Lancet 2016;387:999–1011. https://doi.org/https://doi.org/10.1016/S0140-6736(15)00070-7.

[2] Tranquilli AL, Dekker G, Magee L, Roberts J, Sibai BM, Steyn W, et al. The classification, diagnosis and management of the hypertensive disorders of pregnancy: A revised statement from the ISSHP. Pregnancy Hypertens An Int J Women's Cardiovasc Heal 2014;4:97–104. https://doi.org/https://doi.org/10.1016/j.preghy.2014.02.001.

[3] Steegers EAP, von Dadelszen P, Duvekot JJ, Pijnenborg R. Pre-eclampsia. Lancet 2010;376:631–44. https://doi.org/https://doi.org/10.1016/S0140-6736(10)60279-6.

[4] Nair TM. Statistical and artificial neural network-based analysis to understand complexity and heterogeneity in preeclampsia. Comput Biol Chem 2018;75:222–30. https://doi.org/10.1016/j.compbiolchem.2018.05.011.

[5] Benton SJ, Leavey K, Grynspan D, Cox BJ, Bainbridge SA. The clinical heterogeneity of preeclampsia is related to both placental gene expression and placental histopathology. Am J Obstet Gynecol 2018;219:604.e1-604.e25. https://doi.org/10.1016/j.ajog.2018.09.036.

[6] Leavey Katherine J, Benton Samantha C, Grynspan David A, Kingdom John J, Bainbridge Shannon J, Cox Brian J. Unsupervised Placental Gene Expression Profiling Identifies Clinically Relevant Subclasses of Human Preeclampsia. Hypertension 2016;68:137–47. https://doi.org/10.1161/HYPERTENSIONAHA.116.07293.

[7] Staff AC, Redman CWG. The Differences Between Early- and Late-Onset Pre-eclampsia BT - Preeclampsia: Basic, Genomic, and Clinical. In: Saito S, editor., Singapore: Springer Singapore; 2018, p. 157–72. https://doi.org/10.1007/978-981-10-5891-2_10.

[8] Ismail S. Anesthetic Management of Pregnant Patients with Hypertensive Disorders BT - Obstetric Anesthesia for Co-morbid Conditions. In: Gunaydin B, Ismail S, editors., Cham: Springer International Publishing; 2018, p. 17–30. https://doi.org/10.1007/978-3-319-93163-0_2.

[9] Weiner E, Mizrachi Y, Grinstein E, Feldstein O, Rymer-Haskel N, Juravel E, et al. The role of placental histopathological lesions in predicting recurrence of preeclampsia. Prenat Diagn 2016;36:953–60. https://doi.org/10.1002/pd.4918.

[10] Stanek J. Comparison of placental pathology in preterm, late-preterm, near-term, and term births. Am J Obstet Gynecol 2014;210:234.e1-234.e6. https://doi.org/https://doi.org/10.1016/j.ajog.2013.10.015.

[11] Fuchs TJ, Buhmann JM. Computational pathology: Challenges and promises for tissue analysis. Comput Med Imaging Graph 2011;35:515–30. https://doi.org/10.1016/j.compmedimag.2011.02.006.

[12] Redline RW. Placental pathology: a systematic approach with clinical correlations. Placenta 2008;29 Suppl A:S86-91. https://doi.org/10.1016/j.placenta.2007.09.003.

[13] Gurcan MN, Boucheron LE, Can A, Madabhushi A, Rajpoot NM, Yener B. Histopathological image analysis: a review. IEEE Rev Biomed Eng 2009;2:147–71. https://doi.org/10.1109/RBME.2009.2034865.

[14] Khong TY, Mooney EE, Ariel I, Balmus NCM, Boyd TK, Brundler M-A, et al. Sampling and Definitions of Placental Lesions: Amsterdam Placental Workshop Group Consensus Statement. Arch Pathol Lab Med 2016;140:698–713. https://doi.org/10.5858/arpa.2015-0225-CC.

[15] Marques 1964- editor PM de A. Medical image analysis and informatics : computer-aided diagnosis and therapy. Boca Raton : Taylor & Francis, 2018; 2018.

[16] F.A. S, L.S. O, C. P, Spanhol FA, Oliveira LS, Petitjean C, et al. A Dataset for Breast Cancer Histopathological Image Classification. IEEE Trans Biomed Eng 2016;63:1455–62. https://doi.org/10.1109/TBME.2015.2496264.

[17] Benton SJ, Lafreniere AJ, Grynspan D, Bainbridge SA. A synoptic framework and future directions for placental pathology reporting. Placenta 2019;77:46–57. https://doi.org/https://doi.org/10.1016/j.placenta.2019.01.009.

[18] Lundervold AS, Lundervold A. An overview of deep learning in medical imaging focusing on MRI. Z Med Phys 2019;29:102–27. https://doi.org/https://doi.org/10.1016/j.zemedi.2018.11.002.

[19] Pasa F, Golkov V, Pfeiffer F, Cremers D, Pfeiffer D. Efficient Deep Network Architectures for Fast Chest X-Ray Tuberculosis Screening and Visualization. Sci Rep 2019;9:6268. https://doi.org/10.1038/s41598-019-42557-4.

[20] Hipp J, Flotte T, Monaco J, Cheng J, Madabhushi A, Yagi Y, et al. Computer aided diagnostic tools aim to empower rather than replace pathologists: Lessons learned from computational chess. J Pathol Inform 2011;2:25. https://doi.org/10.4103/2153-3539.82050.

[21] Warren Burhenne LJ, Wood SA, D'Orsi CJ, Feig SA, Kopans DB, O'Shaughnessy KF, et al. Potential contribution of computer-aided detection to the sensitivity of screening mammography. Radiology 2000;215:554–62. https://doi.org/10.1148/radiology.215.2.r00ma15554.

[22] van Ginneken B, Schaefer-Prokop CM, Prokop M. Computer-aided Diagnosis: How to Move from the Laboratory to the Clinic. Radiology 2011;261:719–32. https://doi.org/10.1148/radiol.11091710.

[23] Diiulio R. Clinical Pathology : The integration of existing pathology and information systems with new digital capabilities is just beginning to transform pathology as it did radiology 2010:16–8.

[24] Wang S, Yang DM, Rong R, Zhan X, Fujimoto J, Liu H, et al. Artificial Intelligence in Lung Cancer Pathology Image Analysis. Cancers (Basel) 2019;11. https://doi.org/10.3390/cancers11111673.

[25] Doyle S, Rodriguez C, Madabhushi A, Tomaszeweski J, Feldman M. Detecting Prostatic Adenocarcinoma From Digitized Histology Using a Multi-Scale Hierarchical Classification Approach. 2006 Int Conf IEEE Eng Med Biol Soc 2006:4759–62. https://doi.org/10.1109/IEMBS.2006.260188.

[26] Fukuma K, Prasath VBS, Kawanaka H, Aronow BJ, Takase H. A Study on Nuclei Segmentation, Feature Extraction and Disease Stage Classification for Human Brain Histopathological Images. Procedia Comput. Sci., vol. 96, 2016. https://doi.org/10.1016/j.procs.2016.08.164.

[27] Ninos K, Kostopoulos S, Kalatzis I, Sidiropoulos K, Ravazoula P, Sakellaropoulos G, et al. Microscopy image analysis of p63 immunohistochemically stained laryngeal cancer lesions for predicting patient 5-year survival. Eur Arch Oto-Rhino-Laryngology 2016;273:159–68. https://doi.org/10.1007/s00405-015-3747-x.

[28] Guenther N, Schonlau M. Support Vector Machines. Stata J 2016;16:917–37. https://doi.org/10.1177/1536867X1601600407.

[29] De Wilde 1958- P. Neural network models : theory and projects. Second edi. London ; 1997.

[30] Salsabili S, Mukherjee A, Ukwatta E, Chan ADC, Bainbridge S, Grynspan D. Automated segmentation of villi in histopathology images of placenta. Comput Biol Med 2019;113:103420. https://doi.org/10.1016/j.compbiomed.2019.103420.

[31] Finlayson GD, Schiele B, Crowley JL. Comprehensive colour image normalization BT - Computer Vision — ECCV'98. In: Burkhardt H, Neumann B, editors., Berlin, Heidelberg: Springer Berlin Heidelberg; 1998, p. 475–90.

[32] Kumar author D. Machine Learning Series: K-Means Clustering in Python. 1st editio. Technics Publications, 2019.; 2019.

[33] Bai X, Zhou F, Xue B. Image enhancement using multi scale image features extracted by top-hat transform. Opt Laser Technol 2012;44:328–36. https://doi.org/https://doi.org/10.1016/j.optlastec.2011.07.009.

[34] Lowe D. Distinctive Image Features from Scale-Invariant Keypoints. Int J Comput Vis 2004;60:91–110. https://doi.org/10.1023/B:VISI.0000029664.99615.94.

[35] Fawzi A, Samulowitz H, Turaga D, Frossard P. Adaptive data augmentation for image classification. 2016 IEEE Int. Conf. Image Process., 2016, p. 3688–92. https://doi.org/10.1109/ICIP.2016.7533048.

[36] Hussain Z, Gimenez F, Yi D, Rubin D. Differential Data Augmentation Techniques for Medical Imaging Classification Tasks. AMIA . Annu Symp Proceedings AMIA Symp 2017;2017:979.

[37] Golik P, Doetsch P, Ney H. Cross-entropy vs. squared error training: a theoretical and experimental comparison. Interspeech, vol. 13, 2013, p. 1756–60.

[38] Redline RW, Boyd T, Campbell V, Hyde S, Kaplan C, Khong TY, et al. Maternal vascular underperfusion: nosology and reproducibility of placental reaction patterns. Pediatr Dev Pathol 2004;7:237–49. https://doi.org/10.1007/s10024-003-8083-2.

[39] Krizhevsky A, Sutskever I, Hinton GE. ImageNet classification with deep convolutional neural networks. Adv. Neural Inf. Process. Syst., vol. 2, 2012, p. 1097–105.

[40] Sarkar author D. Hands-on transfer learning with Python : implement advanced deep learning and neural network models using tensorflow and keras. Birmingham ; 2018.

[41] Pan SJ, Yang Q. A Survey on Transfer Learning. IEEE Trans Knowl Data Eng 2010;22:1345–59. https://doi.org/10.1109/TKDE.2009.191.

[42] Kaufmann P, Frank H-G. Chapter 10 - Placental Development. In: Polin RA, Fox WW, Abman SHBT-F and NP (Third E, editors., W.B. Saunders; 2004, p. 85–97. https://doi.org/https://doi.org/10.1016/B978-0-7216-9654-6.50013-8.

[43] Komura D, Ishikawa S. Machine Learning Methods for Histopathological Image Analysis. Comput Struct Biotechnol J 2018;16:34–42. https://doi.org/https://doi.org/10.1016/j.csbj.2018.01.001.

[44] Xu Y, Zhu J-Y, Chang E, Tu Z. Multiple clustered instance learning for histopathology cancer image classification, segmentation and clustering. Proc. IEEE Comput. Soc. Conf. Comput. Vis. Pattern Recognit., 2012. https://doi.org/10.1109/CVPR.2012.6247772.

[45] Orlov N V, Weeraratna AT, Hewitt SM, Coletta CE, Delaney JD, Mark Eckley D, et al. Automatic detection of melanoma progression by histological analysis of secondary sites. Cytometry A 2012;81:364–73.

[46] Cireşan DC, Meier U, Schmidhuber J. Transfer learning for Latin and Chinese characters with Deep Neural Networks. 2012 Int. Jt. Conf. Neural Networks, 2012, p. 1–6. https://doi.org/10.1109/IJCNN.2012.6252544.

[47] Choo J, Liu S. Visual Analytics for Explainable Deep Learning. IEEE Comput Graph Appl 2018;38:84–92. https://doi.org/10.1109/MCG.2018.042731661.

Figures

Figure 4.1.

A. Approach #1 - Semi-Automated Supervised Machine Learning

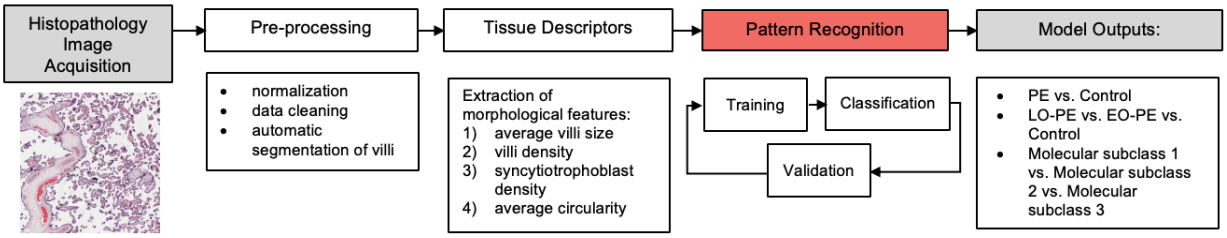

B. Approach # 2 – Automated Supervised Machine Learning

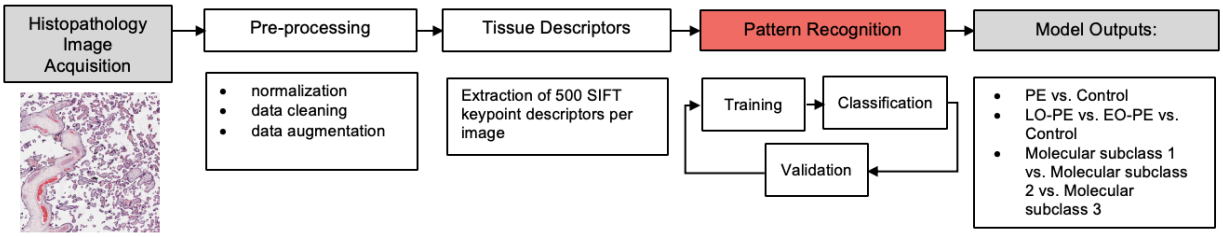

C. Approach # 3 - Supervised hierarchical feature machine learning (deep learning)

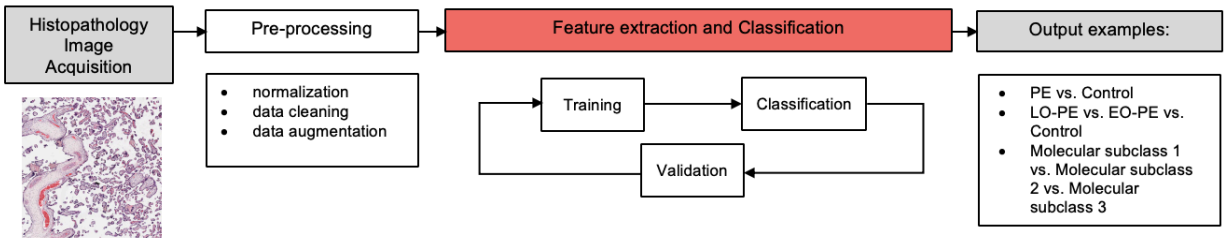

Figure 4.2.

A) Patch Extraction

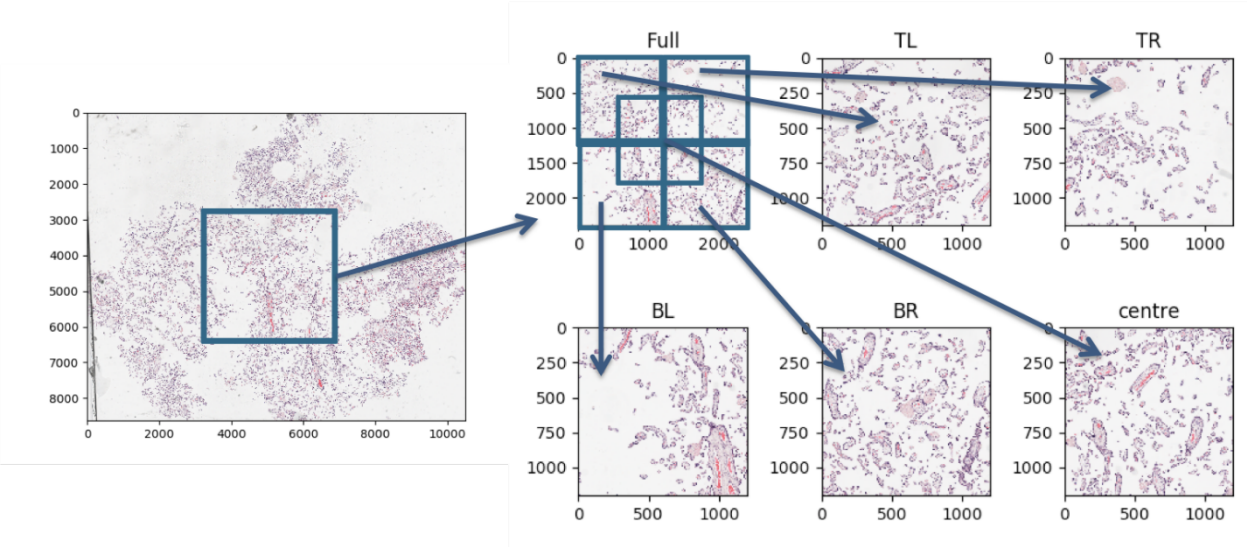

B) Image manipulations

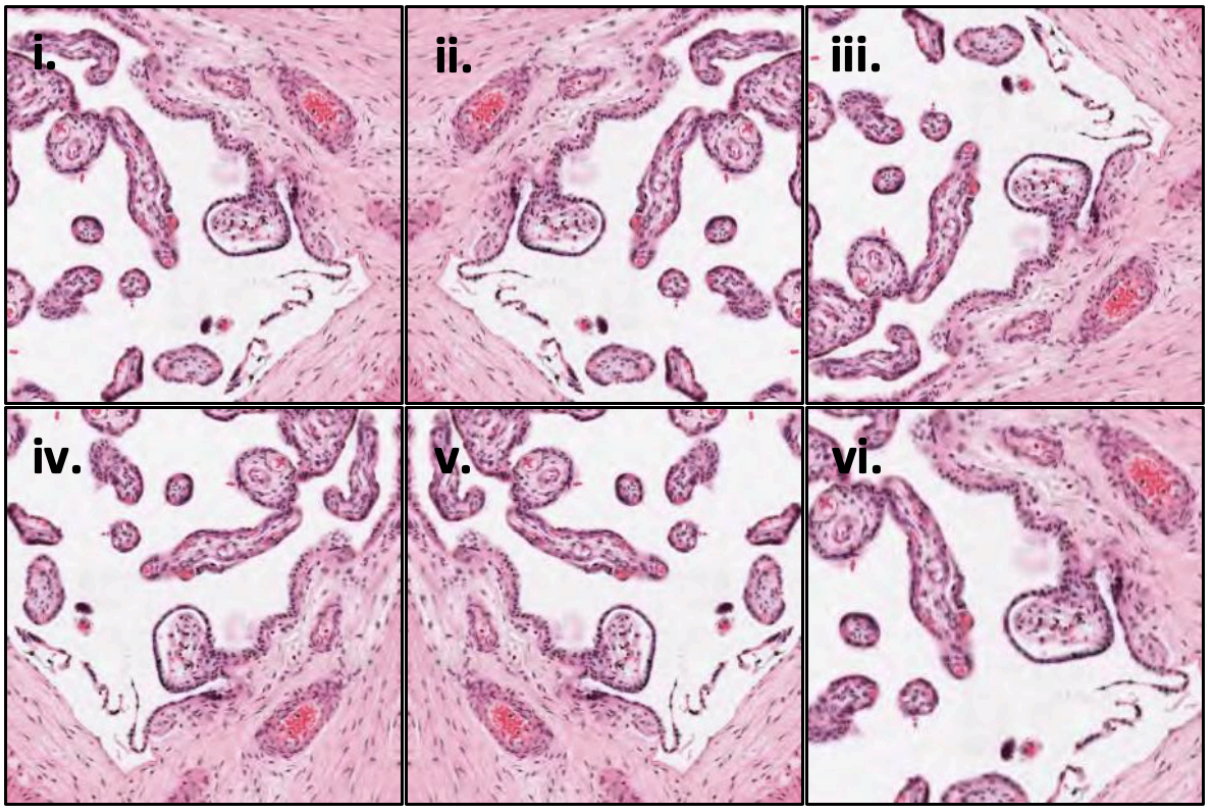

Figure 4.3.

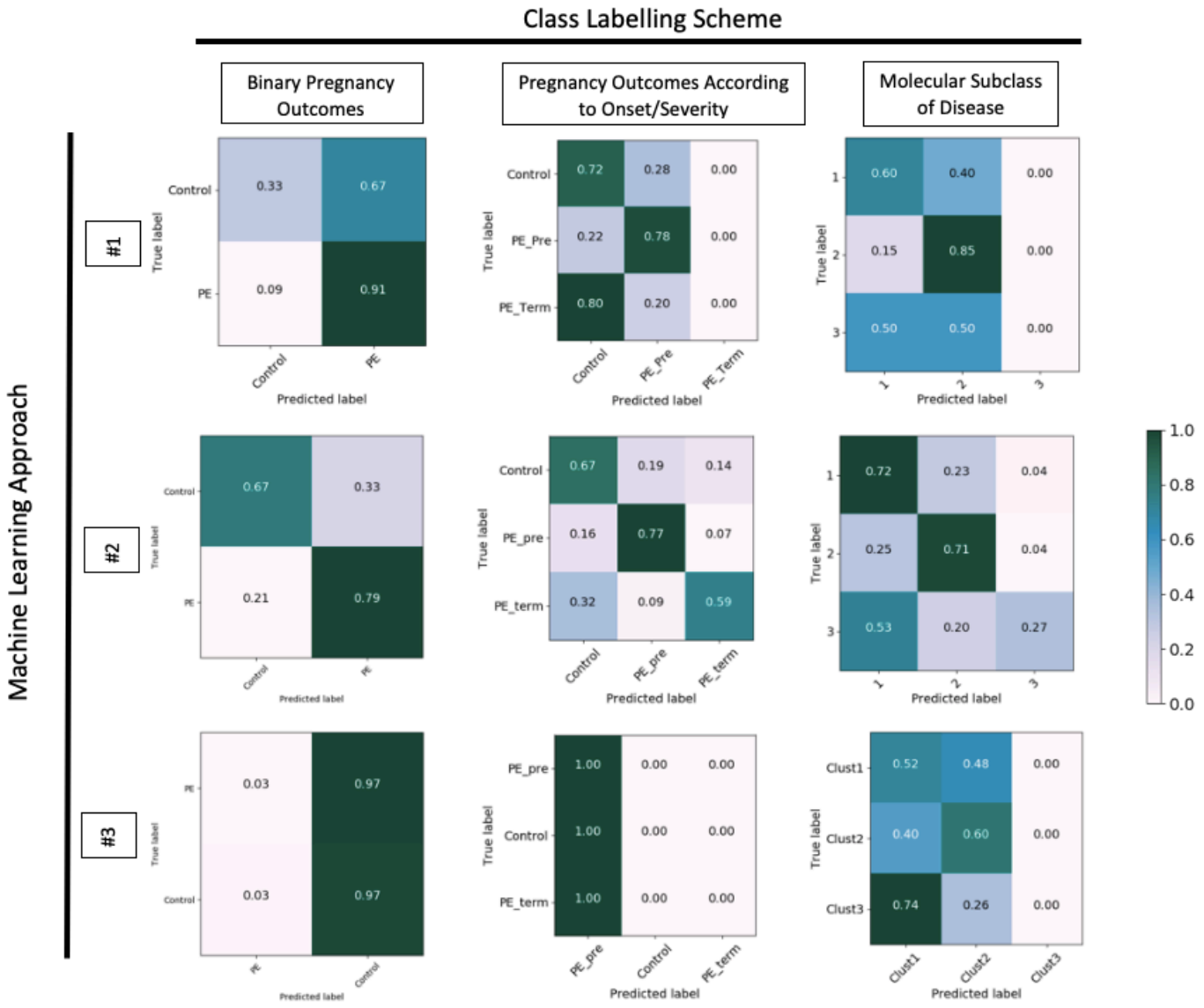
Class Labelling Scheme
Binary Pregnancy Outcomes
Pregnancy Outcomes According to Onset/Severity
Molecular Subclass of Disease
Machine Learning Approach
#1
#2
#3
True label
Predicted label
Control
PE
PE_Pre
PE_Term
PE_pre
PE_term
Clust1
Clust2
Clust3
0.33 0.67 0.09 0.91
0.72 0.28 0.00 0.22 0.78 0.00 0.80 0.20 0.00
0.60 0.40 0.00 0.15 0.85 0.00 0.50 0.50 0.00
0.67 0.33 0.21 0.79
0.67 0.19 0.14 0.16 0.77 0.07 0.32 0.09 0.59
0.72 0.23 0.04 0.25 0.71 0.04 0.53 0.20 0.27
0.03 0.97 0.03 0.97
1.00 0.00 0.00 1.00 0.00 0.00 1.00 0.00 0.00
0.52 0.48 0.00 0.40 0.60 0.00 0.74 0.26 0.00
1.0 0.8 0.6 0.4 0.2 0.0

Figure Legends

Figure 4.1. Machine learning workflow for each experimental approach tested. A) Approach #1 (semi-automated) used manual selection and extraction of histological features deemed clinically relevant to placenta mediated disease. B) Approach #2 (fully automated) used an unbiased approach to automatically extract spatial and textural visual features at 500 SIFT points across each image. C) Approach #3 (deep learning) was the most immune to feature selection bias as feature selection and extraction was inherently incorporated within the classifier, with the model selecting image features that produced optimal classification results. For all three approaches different class labels were tested, including: the binary classes of control (CT) vs. preeclamptic case (PE); the categorical classes of CT vs. early-onset/severe PE cases (EO-PE) vs. late-onset PE cases (LO-PE); and, the categorical classes of CT vs. PE subclass 1 (Maternal) vs. PE subclass 2 (Canonical) vs. PE subclass 3 (Immunological).

Figure 4.2. Data augmentation strategies. A) Patch extraction was used to increase input image dataset size in approaches #2 and #3. An initial patch was cropped at the center of each original image (Approach # 2 - 2400 x2400 pixels; Approach #3 – 300x300 pixels). In approach #2 overlapping patches cropped to 1200x1200 pixels were taken from the top right, top left, bottom right, and bottom left of the 2400x2400 pixel crop, augmenting the samples size from 148 to 740. In approach #3, a sliding window patch extraction method was applied, extracting 225 overlapping patches of 300x300 pixels across the entire image. B) Further data augmentation was applied to the dataset for Approach #3 with an image data generator to increase variability in the dataset. Sample image manipulations shown: i) original image, ii) horizontal flip, iii) vertical flip, iv) 90° rotation, iv) 90° rotation + horizontal flip, v) zoom.

Figure 4.3. Performance confusion matrices for experimental machine learning models tested. Performance confusion matrices are presented for each combination of experimental machine learning

approach (#1-3; vertical axis) and class scheme (horizontal axis) tested. Outputs are presented as a grid summarizing the distribution correctly vs. incorrectly classified images, normalized to the number of true cases per class, with degree of correct classification colour coded ranging from white (poor classification) through to green (good classification). Highest degree of model performance was seen for Approaches #1 and #2, varied according to the class labelling scheme used.

Tables

Table 4.1. Demographic characteristics of participants in study

	Control (n=69)	**Early Onset PE (N=50)**	**Late Onset PE (N=29)**
Maternal Age (Y)[a]	33(5)	32(7)	34(6)
Gestational Age at delivery (weeks)[a]	34(5)	30(2)	36(2)
Fetal Sex (F)[b]	30/69	27/50	12/29
Birth Weight (g)[a]	2297(1092)	1102(342)	2390(622)
Birthweight Percentile (<10th Percentile)[b]	13/69	22/50	13/29
Placenta Weight Percentile (<10th Percentile)[b]	19/69	42/50	14/29
Maternal Systolic Blood Pressure[a]	148(27)	169(14)	163(16)
Maternal Diastolic Blood Pressure[a]	90(17)	107(10)	102(10)
Mode of Delivery (C-section)[b]	45/69	47/50	17/29

	PE Subclass 3 (N=12)	PE Subclass 1 (N=63)	PE Subclass 2 (N=59)
Maternal Age (Y)[a]	37 (4)	33 (5)	34 (6)
Gestational Age at delivery (weeks)[a]	34 (3)	36 (4)	31 (3)
Fetal Sex (F)[b]	7/12	28/63	27/59
Birth Weight (g)[a]	1742 (865)	3635 (940)	1288 (591)
Birthweight Percentile (<10th Percentile)[b]	4/12	8/63	27/59
Placenta Weight Percentile (<10th Percentile)[b]	9/12	16/63	48/59
Maternal Systolic Blood Pressure[a]	164 (17)	153 (26)	168 (15)
Maternal Diastolic Blood Pressure[a]	100 (12)	95 (15)	107 (10)
Mode of Delivery (C-section)[b]	10/12	41/63	53/59

[a]Results presented as "mean (standard deviation)" for continuous variables

[b]Results presented as "count/clinical subset" for categorical variables

Table 4.2. Class labelling schemes used in machine learning models

Class Scheme	Class Mode	Labels
Pregnancy Outcome	Binary	PE, Control
Pregnancy Outcome with Onset Information	Categorical	PE Preterm, PE Term, Control
Molecular Clusters	Categorical	Molecular subclass 1, Molecular subclass 2, Molecular subclass 3

Table 4.3: Python libraries used for each Machine Learning Approach

Approach	Segment	Task	Python 2.7 Library	Module
#1 - Semi-Automatic	Pre-processing	Feature normalization	SciKit Learn	preprocessing.MinMaxScaler
		Dataset splitting	SciKit Learn	model_selection.train_test_split
	Classification	One vs. All Support Vector Machine for multiple classes	SciKit Learn	svm.SVC
	Evaluation	ROC curves	SciKit Learn	metrics.confusion_matrix
		Confusion Matrices	SciKit Learn	metrics.roc
#2 - Automatic	Pre-processing	Greyscale conversion	Open CV	cvtColor
		Colour normalization	Open CV	normalize
		Feature normalization	SciKit Learn	preprocessing.MinMaxScaler
		Dataset splitting	SciKit Learn	model_selection.train_test_split

	Feature Extraction	SIFT keypoint extraction	Open CV	xfeatures2d.SIFT_create and sift.detectAndCompute
	Classification	One vs. All Support Vector Machine for multiple classes	SciKit Learn	svm.SVC
	Evaluation	ROC curves	SciKit Learn	metrics.confusion_matrix
		Confusion Matrices	SciKit Learn	metrics.roc
#3 – Integrated (deep learning)	Pre-processing	RGB Patch Extraction	Open CV and OpenSlide, PIL	Read_region, crop, convert
		Minimum keypoint threshold	Open CV	cvtcolor, normalize, xfeatures2d.SIFT_create, sift.detectAndCompute
		Image Data Generator	Keras	preprocessing.image.ImageDataGenerator
		Transfer Learning	Keras	Applications.VGG19

	Feature Extraction and Classification	CNN Model	Keras	models.Sequential and models.Model
		CNN Layers	Keras	layers.Dropout, layers.Flatten, layers.Dense, and layers.GlobalAveragePooling2D
		CNN optimizer	Keras	optimizers.SGD
	Evaluation	ROC curves	SciKit Learn	metrics.confusion_matrix
		Confusion Matrices	SciKit Learn	metrics.roc

Table 4.4. CNN model architecture

Layer (type)	Output Shape	Param #
conv2d_1 (Conv2D)	(None, 62, 62, 32)	896
max_pooling2d_1 (MaxPooling2)	(None, 31, 31, 32)	0
conv2d_2 (Conv2D)	(None, 29, 29, 32)	9248
max_pooling2d_2 (MaxPooling2)	(None, 14, 14, 32)	0
flatten_1 (Flatten)	(None, 6272)	0
dense_1 (Dense)	(None, 128)	802944
dense_2 (Dense)	(None, 3)	258

Table 4.5. Summary of performance metrics for all machine learning models tested

Approach	Class Scheme	Additional Feature	Accuracy	F1 Score
#1 - Semi-Automatic	Pregnancy Outcome	N/A	0.71	0.71
	Pregnancy Outcome	Gestational Age	0.68	0.67
	Pregnancy Outcome with Onset Information	N/A	0.55	0.58
	Pregnancy Outcome with Onset Information	Gestational Age	**0.73**	0.72
	Molecular Clusters	N/A	0.58	0.55
	Molecular Clusters	Gestational Age	0.57	0.57
#2 - Automatic	Pregnancy Outcome	N/A	0.65	0.65

	Pregnancy Outcome	Gestational Age	**0.73**	0.73
	Pregnancy Outcome with Onset Information	N/A	0.62	0.62
	Pregnancy Outcome with Onset Information	Gestational Age	0.69	0.69
	Molecular Clusters	N/A	0.62	0.62
	Molecular Clusters	Gestational Age	0.68	0.68
#3 – Integrated (deep learning)	Pregnancy Outcome	N/A	**0.55**	0.48
	Pregnancy Outcome with Onset Information	N/A	0.41	0.33

	Molecular Clusters	N/A	0.51	0.35

Chapter 5

General Discussion and Conclusions

5.1 General Discussion

The overarching hypothesis of the current MSc. thesis project was that a computerized model developed with machine learning could recognize distinct morphological features in human placenta histopathology images and could be applied to automate detection of placenta-mediated diseases. Not only was this hypothesis proven with moderate success, but also several secondary research findings came from this project and new questions were opened for future investigation. To ultimately test the hypothesis in a proof-of-concept exercise, the best available machine learning methods for histopathology image analysis were applied to automate the classification of healthy and diseased placentas (Manuscript 3). However, in preparation for this experiment two crucial research aims first needed completion: 1) a systematic evaluation of the different machine learning methods and pipelines that have previously been applied to human histopathology specimens (Manuscript 1); and, 2) the development of an automated villous structure segmentation tool capable of extracting morphological features of interest from placental histopathology images (Manuscript 2). Not only were the outcomes of these foundational projects necessary to test the overarching hypothesis, but they also produced significant findings in their own respect.

In order to ensure the most applicable and effective machine learning models were tested in the context of human placenta histopathology, a systematic review of all machine learning methods developed and tested for histopathology applications was undertaken. Not surprisingly, very little work had been carried out to-date focused uniquely on the placenta [98,99]. Instead, the vast majority of the literature focused on the development and application of this technology in the context of the much broader field of onco-histopathology [56,78,80,100,101]. What was surprising, however, was the lack of consensus with regards to a “gold standard” pipeline for developing and applying machine learning models to these types of clinical samples. Certainly, this is in part the result of differences in research question and study design, however the systematic evaluation of all methods tested to date allowed for the

identification of an optimal standard workflow that could be adopted by other groups moving forward. This standard workflow will simplify study design in future research endeavours, but importantly will also allow for direct comparison of results across research groups and/or institutions. It would enable direct comparisons of similar and dissimilar morphological features seen in pathological states across different tissue beds and organs. Moreover, the highly interdisciplinary nature of these types of research endeavours, with required expertise in clinical pathology, computer programming and health system integration, makes for an intimidating and high commitment journey to embark on. Therefore, it is hoped that the streamlined workflow presented can address some of these concerns and promote advancement in this field.

An intriguing consideration when comparing different machine learning methods is the degree of user input, or human involvement required or desired. Broadly, a review of the literature reveals three main paradigms of human involvement, namely: 1) a semi-automated process with manual feature extraction prior to model development; 2) an automated feature extraction process prior to model development with minimal-to moderate human input;, and 3) feature extraction fully integrated into model development, removing human input in feature selection and extraction. Given this finding, it was desirable to investigate the utility and performance of machine learning models that employed these different user-input paradigms. In the first paradigm, previous knowledge of the pathophysiology of placenta-mediated disease could be used to inform which morphological features may be of highest relevance in the development of a classification model. While this approach most closely mimics the work carried out by a trained perinatal pathologist, it is also the method that carries with it the highest degree of bias in model development. Whereas in paradigms 2 and 3 the features selected for extraction may or may not be of known biological relevance, and user bias of which morphological features may be of highest importance is minimized. However, the user's ability to clearly delineate which features are

driving the learning model, and how they may be related to disease initiations and progression is limited, particularly in the case of paradigm 3 (deep learning).

With the fast pace advancement of machine learning model development, particularly in the realm of image analysis, there are readily available software packages that were used in the current project to generate the classification models. However, our group collectively worked to develop in house software capable of segmenting individual villous structures in a digital histopathology image of the human placenta, such that we could manually extract features deemed to be of highest relevance to the pathophysiology of PE (Manuscript 2). While the development of this software was necessary for the stated purpose of the current project, the utility of this software extends far beyond the current application. Through the application of this software program, researchers can easily extract quantitative data describing the morphological structure of the placentas in their sample set. The output metrics available can be highly informative as it relates to villous structure maturation, elongation and branching – all process of normal placental aging. As such, this program could simply be used to assess the "biological age" of a placenta in instances of both healthy and pathological pregnancies. These metrics could also be used in large population-based correlation analysis, identifying basic placental features that may be indicative of both short- and long-term health outcomes for both mothers and their babies. A 2017 publication developed a similar software that could automatically segment villi [99], however their attempt failed to address the issue of separate villi which appear connected in 2D sections and the software was not able to achieved the level of accuracy achieved with our program [88].

In the final manuscript of the thesis (Manuscript 3) a proof-of concept experiment was performed to test the hypothesis that machine learning could be used to classify histopathology images of placentas with and without placenta-mediated disease, specifically in the context of PE. The models developed and tested in this body of work demonstrated a maximal performance of 73% accuracy in the

classification of PE placentas. This maximal performance was achieved when a semi-automated machine learning model was used, with gestational age at delivery used as an additional inputted feature. While this was a promising first foray into the application of machine learning technology for this purpose, the results achieved were unexpected, particularly as it relates to the poor performance achieved using the fully integrated, deep-learning model. As highlighted in Chapter 4 (Manuscript 3), several areas of improvement and optimization steps have been identified to improve model development, which are elaborated on in section 5.3 below. It is likely that with optimization the updated models will outperform the current ones.

In summary, the primary outcomes of this research project were the development of evidence-based guidelines for best practices when applying machine learning classification models to clinical histopathology images, the development of automated software that can segment and extract biologically-relevant features from all placental villi in a digital placenta histopathology image, and piloting the application of machine learning to placenta histopathology images to distinguish morphological features that differ between healthy and diseased placentas in the context of PE.

5.2 Clinical Impacts

One of the biggest criticisms heard regarding the clinical utility of placenta pathology examinations is that the index pregnancy is over, so “what good comes from identifying underlying causes or subclasses of placenta mediated disease following delivery?” However, this criticism is short-sighted. The placenta serves as a visual diary of any aberrations in placental development and/or damage that have taken place across the pregnancy. It allows both clinicians and researchers alike to gain a better understanding of the different types of placental disease that underlie the most common obstetrical complications seen today. It is only armed with this knowledge that effective etiology-driven screening programs and therapeutic interventions can be developed and tested.

At the individual level, being given a concrete answer as to why a pregnancy has had an adverse outcome can be instrumental in the healing process [102]. Further, there is well established evidence that distinct forms of placental disease have a high degree of recurrence, and therefore the maternal care team can use these results to counsel patients in regard to risks for future pregnancies [103]. Work carried out by our group, as well as others [104–106], indicate that distinct lesions observed in the placenta at the time of delivery are highly predictive of increased lifetime risk for cardiovascular disease in the mother, further extending the possible counseling opportunities that can be provided to these women.

As we gain further insight into the developmental origins of health and disease, the evidence is becoming clear that the intrauterine environment plays a significant role in the plasticity and programming of the developing fetuses major organ systems [107,108]. In fact, several groups have identified the placenta as a "central culprit" to chronic disease in the offspring [109,110]. Therefore the findings of placenta pathology examination can not only inform clinical management and counselling of the mothers, but they can inform the neonatal health care team about the intrauterine environment the infant was exposed to, and can possibly identify future health risks for the child, opening the door to effective preventative initiatives.

The case for placenta pathology examination is clear – it has the potential to greatly improve the health and wellbeing of mothers and their children. However, as outlined throughout this thesis, there are considerable limitations to this clinical practice currently, including: lack of standardization, high degree of inter-observer and inter-institutional variability, high degree of required sub-specialty training, and pathologist burnout due to heavy workload demands. This is a clinical practice that is ripe for the introduction of computer-aided diagnosis. Collectively, this project was a first step towards exploring how machine learning models could be applied to automate some aspects of placenta histopathology examinations in the context of placenta-mediated diseases. This body of work can serve as a starting

point for this field to expand and optimize the integration of this technology for these purposes, and with more validation, can potentially develop into a commercially available tool that can be integrated into the clinical workflow of perinatal pathologists across Canada.

5.3 Limitations and Future Directions

Although the machine learning experiment was successful as a pilot project, there were several recognized limitations to the study design and obtained results which would need to be addressed and optimized for adoption into clinical practice.

The biggest limitation in this project was that the heterogeneity of PE was not fully addressed in the machine learning models, which is likely the greatest source of error in the machine learning models. In this project, the goal was to predict a clinical diagnosis (PE) from histopathology samples of placentas of the women diagnosed with the disease. While PE has been shown to be linked to placenta dysfunction, it is not always the case where there are visible pathological lesions in the placenta. Moreover, the placenta itself is a highly heterogeneous organ and one biopsy may not be indicative of the overall visual pattern across the entire organ. The model was developed with the assumption that PE can be consistently predicted solely based off placenta histopathology images – which is not the case in clinical pathology practice. The simplified model of PE produced was useful in gauging whether placenta mediated diseases can be classified with any degree of accuracy from histopathology images, but more work needs to be done to develop a more rigorous model built around the clinical spectrum of PE . Two possible future directions could address this limitation: 1) incorporating additional clinical features into the model, along with the image features, in an attempt to improve classification accuracy; and, 2) train the machine learning model to instead identify distinct types of placental lesions – using the identified lesion as the label of interest, rather than the pregnancy outcome. Our lab is currently testing the latter

approach with a machine learning model that predicts the severity of MVM on placenta images from cases of PE and IUGR.

Another considerable limitation of this project was the sample size available for training our machine learning models. For machine learning model development, a large and robust dataset is preferable to ensure the model is resilient to biological variation. While the placental histopathology image dataset used [18] is likely one of the largest image datasets with PE enrichment (N=79), it is still quite modest in size considering ideal image sample sizes for these applications have been proposed to be as high as 1000 images [111], with increased sample size consistently shown to improve classification accuracy [111,112]. A concerted effort on the part of researchers and clinicians in this field must be made to generate a publicly available image database specific to the placenta (healthy vs. diseased, different gestational ages, etc.) to help move this field forward. This initiative is ongoing within our research group. Further, the compilation of histopathology images collected from a variety of clinical/research sites could combat the issue of inter-institution differences in the visual appearance of placental histopathology specimens, resulting from differences in specimen preparation (ex. differences in washing the tissue of maternal blood, differences in staining intensity, etc.). This would ensure that any developed application could be applied successfully in pathology suites across the country and abroad.

As highlighted in Manuscript #3 (Chapter 4), the inclusion of a transfer learning phase into the deep learning CNN model would likely significantly improve its performance. Transfer learning uses a pre-established CNN model that has been partially trained on a large and robust image dataset, resulting in the model being “pre-trained” to recognize low-level image features such as edges and textures [113–116]. This partially pre-trained model is then fully trained on the dataset of interest to learn the more complex aspects of the features in the image. This would allow more of the computing resources during training be allocated toward learning actual differences across images. Transfer learning should improve

robustness to variation in image appearance in the dataset because the model would have been pre-trained on a dataset with high variance.

Ongoing research endeavours [117–120], including those conducted by our research group [18,36,121], have recently demonstrated that the clinical definition of PE, or even the binary description of early onset vs late onset, may not sufficiently describe the different types of placental disease seen across the spectrum of PE. Given that the clinical definition and understanding of this disease is still evolving, it is possible that the success of training a model to detect a "PE placenta" based on visual appearance may be limited. Instead, the application of an unsupervised, more exploratory approach, may be highly informative in the discovery of novel classes of placental disease. In the unsupervised approach no clinical labels would be used, and the goal would be to see how the images naturally cluster visually and later try and connect these visual clusters to clinical phenotypes. This approach removes the initial bias that all cases labeled "PE" are the same and instead allows investigators to assess each sample as a unique case that could be labeled based on morphological differences in the placenta histopathology specimen. Using this approach, we may better understand the distinct patterns of placental disease and determine if they correlate or predict any clinical outcomes. This is an ongoing initiative within our research group, with preliminary results included within Appendix A.

5.4 Interdisciplinary Perspective

The project presented in this thesis would not have been possible without an emphasis on the interdisciplinary nature of the research aims. The strategy for designing experiments was entirely dependent on the coming together of multiple experts from different disciplines to properly define and collectively answer the research question. Experts in the domains of obstetrics, perinatal pathology, placental biology and computer engineering worked hand in hand to identify a gap in clinical care that could be addressed, design a project that would successfully address this gap, and work together to

interpret results and provide input on how to improve the machine learning models being developed to ensure the technology was reflective of both biology and clinical findings. Without the sometimes challenging, but ultimately highly rewarding, “out-of-the-box” discussion that took place during the interdisciplinary project meetings, the development and proof-of-principal testing of this technology would not have been possible.

In this research project, the two primary domains of study – perinatal/placenta pathology and machine learning – stood to gain from the partnership. Applying novel technologies like machine learning to investigate placenta mediated diseases can accelerate progress into understanding and curing placenta mediated diseases like PE, by bringing out new ways of approaching a complex and unsolved problem. The machine learning field also benefits tremendously from the development and testing of models on digital images of a highly complicated organ of study – the placenta. Compared to solid tumors, the histological features of the human placenta are highly complex, requiring new advances in machine learning model development to properly identify and extract features of interest.

Although conducting an interdisciplinary project has been enriching to the team members and collective domains involved, this type of project is still relatively new and not without challenges. All members involved needed a minimum comfort level in each other’s domains for productive conversations about the experiments and troubleshooting to take place, meaning a steep learning curve was involved on all sides. Communication between all parties was crucial to ensure the protocols were technically sound for a machine learning experiment and that the interpretation of results was clinically meaningful. As well, the findings served to aid in the automated detection of placenta pathology lesions, as well as to test multiple different machine learning algorithms, resulting in a question of the ultimate beneficiaries of the work. Ultimately the decision was to present the work for the clinical pathology community (the guidelines for machine learning methods in histopathology) and the biomedical imaging community (the experiments in automated detection of placenta mediated disease from placenta histopathology slides).

Despite the challenges, we believe that continued focus on interdisciplinary collaboration between the healthcare fields and machine learning developers will help to advance the field in many ways and address issues such as clinical resource management/efficiency, diagnostic error and standardization of clinical decision making to name a few. Overall this was a very rewarding way of carrying out science.

5.5 Conclusion

The ultimate goal of developing a prototype automated screening tool for placenta images with machine learning was achieved, however, in the process, several crucial milestones needed to be achieved – each proving to be a significant output for this project in their own respects. First a comprehensive review of the literature was conducted to extract and synthesize the current methods being applied to similar problems in histopathology imaging. It was found that the following 5 key steps were necessary to develop a successful model: image acquisition and preparation, image preprocessing, feature extraction, pattern recognition and classification training, and model testing. Not only did the review serve its purpose of informing the experimental design for our machine learning model development, it also provided a platform to publish a set of best practice guidelines that future researchers could apply to any machine learning project on histopathology images. A secondary objective to testing machine learning on placenta histopathology images was to assess whether or not more clinically relevant features are better for model development and to do this, a reproducible method was needed to isolate individual villi from placenta images and extract relevant features. To isolate individual villi from placenta images was a project in its own right given the challenges of counting touching villi as separate entities and was a significant outcome of this work – achieving a 15.46% higher F1 score when compared with the previous standard approach. Finally, given a framework for model development from the systematic review and both clinical feature extraction and textural feature extraction methods (from previously published methods), machine learning models were developed on placenta histopathology images to distinguish controls from cases of PE or PE split by early onset cases and late

onset cases – achieving a maximum classification accuracy of 73%. The moderate success of this proof-of-concept presented opens the doors to further development in automated lesion detection and classification of placenta histopathology images and considerable insight was gained into the next steps needed to further validate such tools.

References

[1] Gude NM, Roberts CT, Kalionis B, King RG. Growth and function of the normal human placenta. Thromb Res 2004;114:397–407. https://doi.org/https://doi.org/10.1016/j.thromres.2004.06.038.

[2] Boyd JD, Hamilton WJ. The human placenta. vol. 212. Heffer; 1970.

[3] Benirschke K, Driscoll SG. The pathology of the human placenta. Placenta, Springer; 1967, p. 97–571.

[4] Avagliano L, Massa V, Bulfamante G Pietro. Histology of Human Placenta n.d.

[5] Brown H, Speechley K, Macnab J, Natale R, Campbell M. Maternal, fetal, and placental conditions associated with medically indicated late preterm and early term delivery: a retrospective study. BJOG An Int J Obstet Gynaecol 2016;123:763–70. https://doi.org/10.1111/1471-0528.13428.

[6] Hiersch L, Shinar S, Melamed N, Aviram A, Hadar E, Yogev Y, et al. Recurrent Placenta-Mediated Complications in Women With Three Consecutive Deliveries. Obstet Gynecol 2017;129:416–21. https://doi.org/10.1097/AOG.0000000000001890.

[7] Lim G, Tracey J, Boom N, Karmakar S, Wang J, Berthelot J-M, et al. CIHI survey: Hospital costs for preterm and small-for-gestational age babies in Canada. Healthc Q 2009;12:20–4.

[8] Vigil-De Gracia P. Maternal deaths due to eclampsia and HELLP syndrome. Int J Gynecol Obstet 2009;104:90–4. https://doi.org/10.1016/j.ijgo.2008.09.014.

[9] Mari G, Hanif F. Intrauterine Growth Restriction: How to Manage and When to Deliver. Clin Obstet Gynecol 2007;50:497–509. https://doi.org/10.1097/GRF.0b013e31804c96a9.

[10] Davis EF, Lazdam M, Lewandowski AJ, Worton SA, Kelly B, Kenworthy Y, et al. Cardiovascular risk factors in children and young adults born to preeclamptic pregnancies: a systematic review.(Report). Pediatrics 2012;129:e1552. https://doi.org/10.1542/peds.2011-3093.

[11] Mcdonald SD, Malinowski A, Zhou Q, Yusuf S, Devereaux PJ. Cardiovascular sequelae of preeclampsia/eclampsia: A systematic review and meta-analyses. Am Heart J 2008;156:918–30. https://doi.org/10.1016/j.ahj.2008.06.042.

[12] Smith GN, Pudwell J, Walker M, Wen S-W. Ten-Year, Thirty-Year, and Lifetime Cardiovascular Disease Risk Estimates Following a Pregnancy Complicated by Preeclampsia. J Obstet Gynaecol Canada 2012;34:830–5. https://doi.org/10.1016/S1701-2163(16)35381-6.

[13] Ahmed R, Dunford J, Mehran R, Robson S, Kunadian V. Pre-Eclampsia and Future Cardiovascular Risk Among Women. J Am Coll Cardiol 2014;63:1815–22. https://doi.org/10.1016/j.jacc.2014.02.529.

[14] Mongraw-Chaffin ML, Cirillo PM, Cohn BA. Preeclampsia and Cardiovascular Disease Death: Prospective Evidence From the Child Health and Development Studies Cohort. Hypertension 2010;56:166–71. https://doi.org/10.1161/HYPERTENSIONAHA.110.150078.

[15] Aloizos S, Seretis C, Liakos N, Aravosita P, Mystakelli C, Kanna E, et al. HELLP syndrome: Understanding and management of a pregnancy-specific disease. J Obstet Gynaecol (Lahore) 2013;33:331–7. https://doi.org/10.3109/01443615.2013.775231.

[16] Redline RW, Boyd T, Campbell V, Hyde S, Kaplan C, Khong TY, et al. Maternal vascular underperfusion: nosology and reproducibility of placental reaction patterns. Pediatr Dev Pathol 2004;7:237–49. https://doi.org/10.1007/s10024-003-8083-2.

[17] Starzyk KA, Salafia CM, Pezzullo JC, Lage JM, Parkash V, Vercruysse L, et al. Quantitative differences in arterial morphometry define the placental bed in preeclampsia. Hum Pathol 1997;28:353–8. https://doi.org/10.1016/s0046-8177(97)90135-0.

[18] Leavey Katherine J, Benton Samantha C, Grynspan David A, Kingdom John J, Bainbridge Shannon J, Cox Brian J. Unsupervised Placental Gene Expression Profiling Identifies Clinically Relevant Subclasses of Human Preeclampsia. Hypertension 2016;68:137–47. https://doi.org/10.1161/HYPERTENSIONAHA.116.07293.

[19] Babic I, Ferraro ZM, Garbedian K, Oulette A, Ball CG, Moretti F, et al. Intraplacental villous artery resistance indices and identification of placenta-mediated diseases. J Perinatol 2015;35:793–8. https://doi.org/10.1038/jp.2015.85.

[20] Goldman-Wohl D, Yagel S. Regulation of trophoblast invasion: from normal implantation to pre-eclampsia. Mol Cell Endocrinol 2002;187:233–8. https://doi.org/10.1016/s0303-7207(01)00687-6.

[21] Rampersad R, Nelson DM. Trophoblast biology, responses to hypoxia and placental dysfunction in preeclampsia. Front Biosci 2007;12:2447–56. https://doi.org/10.2741/2246.

[22] Redman CWG, Sargent IL. Circulating microparticles in normal pregnancy and pre-eclampsia. Placenta 2008;29 Suppl A:S73–7. https://doi.org/10.1016/j.placenta.2007.11.016.

[23] Sargent IL, Germain SJ, Sacks GP, Kumar S, Redman CWG. Trophoblast deportation and the maternal inflammatory response in pre-eclampsia. J Reprod Immunol 2003;59:153–60. https://doi.org/10.1016/s0165-0378(03)00044-5.

[24] Walsh SW. What causes endothelial cell activation in preeclamptic women? Am J Pathol 2006;169:1104–6. https://doi.org/10.2353/ajpath.2006.060713.

[25] Maynard SE, Min J-Y, Merchan J, Lim K-H, Li J, Mondal S, et al. Excess placental soluble fms-like tyrosine kinase 1 (sFlt1) may contribute to endothelial dysfunction, hypertension, and proteinuria in preeclampsia. J Clin Invest 2003;111:649–58. https://doi.org/10.1172/JCI17189.

[26] Brewster JA, Orsi NM, Gopichandran N, McShane P, Ekbote U V, Walker JJ. Gestational effects on host inflammatory response in normal and pre-eclamptic pregnancies. Eur J Obstet Gynecol Reprod Biol 2008;140:21–6. https://doi.org/10.1016/j.ejogrb.2007.12.020.

[27] Roberts JM, Hubel CA. The two stage model of preeclampsia: variations on the theme. Placenta 2009;30 Suppl A:S32–7. https://doi.org/10.1016/j.placenta.2008.11.009.

[28] Vinnars M-T, Wijnaendts LCD, Westgren M, Bolte AC, Papadogiannakis N, Nasiell J. Severe preeclampsia with and without HELLP differ with regard to placental pathology. Hypertens (Dallas, Tex 1979) 2008;51:1295–9. https://doi.org/10.1161/HYPERTENSIONAHA.107.104844.

[29] Huppertz B. Placental Origins of Preeclampsia: Challenging the Current Hypothesis. Hypertension 2008;51:970–5. https://doi.org/10.1161/HYPERTENSIONAHA.107.107607.

[30] Huppertz B. Placental pathology in pregnancy complications. Thromb Res 2011;127:S96–9.

https://doi.org/10.1016/S0049-3848(11)70026-3.

[31] Valensise Herbert P, Vasapollo Barbara P, Gagliardi Giulia P, Novelli Gian P. Early and Late Preeclampsia: Two Different Maternal Hemodynamic States in the Latent Phase of the Disease. Hypertension 2008;52:873–80. https://doi.org/10.1161/HYPERTENSIONAHA.108.117358.

[32] Gillon TER, Pels A, von Dadelszen P, MacDonell K, Magee LA. Hypertensive Disorders of Pregnancy: A Systematic Review of International Clinical Practice Guidelines. PLoS One 2014;9:e113715.

[33] Raymond D, Peterson E. A critical review of early-onset and late-onset preeclampsia. Obstet Gynecol Surv 2011;66:497–506. https://doi.org/10.1097/OGX.0b013e3182331028.

[34] Mackay AP, Berg CJ, Atrash HK. Pregnancy-related mortality from preeclampsia and eclampsia. Obstet Gynecol 2001;97:533–8. https://doi.org/10.1016/S0029-7844(00)01223-0.

[35] Long PA, Abell DA, Beischer NA. FETAL GROWTH RETARDATION AND PRE-ECLAMPSIA. BJOG An Int J Obstet Gynaecol 1980;87:13–8. https://doi.org/10.1111/j.1471-0528.1980.tb04419.x.

[36] Benton SJ, Leavey K, Grynspan D, Cox BJ, Bainbridge SA. The clinical heterogeneity of preeclampsia is related to both placental gene expression and placental histopathology. Am J Obstet Gynecol 2018;219:604.e1-604.e25. https://doi.org/10.1016/j.ajog.2018.09.036.

[37] Langston C, Kaplan C, Macpherson T, Manci E. Practice guideline for examination of the placenta. Arch Pathol Lab Med 1997;121:449–76.

[38] Khong editor TY, Mooney editor EE, Nikkels editor PGJ, Morgan editor TK, Gordijn editor SJ. Pathology of the placenta : a practical guide. Cham : Springer, 2019; 2019.

[39] Redline RW. Placental pathology: a systematic approach with clinical correlations. Placenta 2008;29 Suppl A:S86-91. https://doi.org/10.1016/j.placenta.2007.09.003.

[40] Slaoui M, Fiette L. Histopathology Procedures: From Tissue Sampling to Histopathological Evaluation. Methods Mol Biol 2011;691:69–82. https://doi.org/10.1007/978-1-60761-849-2_4.

[41] Alturkistani HA, Tashkandi FM, Mohammedsaleh ZM. Histological Stains: A Literature Review and Case Study. Glob J Health Sci 2015;8:72–9. https://doi.org/10.5539/gjhs.v8n3p72.

[42] Benton SJ, Lafreniere AJ, Grynspan D, Bainbridge SA. A synoptic framework and future directions for placental pathology reporting. Placenta 2019;77:46–57. https://doi.org/https://doi.org/10.1016/j.placenta.2019.01.009.

[43] Redline RW. Classification of placental lesions. Am J Obstet Gynecol 2015;213:S21–8. https://doi.org/https://doi.org/10.1016/j.ajog.2015.05.056.

[44] Stark MW, Clark L, Craver RD. Histologic Differences in Placentas of Preeclamptic/Eclamptic Gestations by Birthweight, Placental Weight, and Time of Onset. Pediatr Dev Pathol 2014;17:181–9. https://doi.org/10.2350/13-09-1378-OA.1.

[45] Ernst LM. Maternal vascular malperfusion of the placental bed. APMIS 2018;126:551–60. https://doi.org/10.1111/apm.12833.

[46] Kovo M, Schreiber L, Bar J. Placental vascular pathology as a mechanism of disease in pregnancy complications. Thromb Res 2013;131:S18–21. https://doi.org/https://doi.org/10.1016/S0049-

3848(13)70013-6.

[47] LITTLE WA. Placental infarction. Obstet Gynecol 1960;15:109–30.

[48] Fitzgerald B, Kingdom J, Keating S. Distal villous hypoplasia. Diagnostic Histopathol 2012;18:195–200.

[49] Mukherjee A, Chan ADC, Keating S, Redline RW, Fritsch MK, Machin GA, et al. The placental distal villous hypoplasia pattern: Interobserver agreement and automated fractal dimension as an objective metric. Pediatr Dev Pathol 2016;19. https://doi.org/10.2350/15-03-1619-OA.1.

[50] Jones CJ, Fox H. Syncytial knots and intervillous bridges in the human placenta: an ultrastructural study. J Anat 1977;124:275–86.

[51] Roberts DJ, Oliva E. Clinical significance of placental examination in perinatal medicine. J Matern Neonatal Med 2006;19:255–64. https://doi.org/10.1080/14767050600676349.

[52] Derricott H, Jones RL, Heazell AEP. Investigating the association of villitis of unknown etiology with stillbirth and fetal growth restriction – A systematic review. Placenta 2013;34:856–62. https://doi.org/https://doi.org/10.1016/j.placenta.2013.07.003.

[53] Kim J, Romero R, Kim MR, Kim YM, Friel L, Espinoza J, et al. Involvement of Hofbauer cells and maternal T cells in villitis of unknown aetiology. Histopathology 2008;52:457–64.

[54] Uxa R, Baczyk D, Kingdom JCP, Viero S, Casper R, Keating S. Genetic polymorphisms in the fibrinolytic system of placentas with massive perivillous fibrin deposition. Placenta 2010;31:499–505.

[55] Longtine MS, Nelson DM. Placental dysfunction and fetal programming: the importance of placental size, shape, histopathology, and molecular composition. Semin Reprod Med 2011;29:187–96. https://doi.org/10.1055/s-0031-1275515.

[56] Belle A, Kon MA, Najarian K. Biomedical Informatics for Computer-Aided Decision Support Systems: A Survey. Sci World J 2013;2013:1–8. https://doi.org/10.1155/2013/769639.

[57] Kamel HM. Trends and Challenges in Pathology Practice: Choices and necessities. Sultan Qaboos Univ Med J 2011;11:38–44.

[58] Rabe K, Snir OL, Bossuyt V, Harigopal M, Celli R, Reisenbichler ES. Interobserver variability in breast carcinoma grading results in prognostic stage differences. Hum Pathol 2019. https://doi.org/https://doi.org/10.1016/j.humpath.2019.09.006.

[59] Khong TY, Mooney EE, Ariel I, Balmus NCM, Boyd TK, Brundler M-A, et al. Sampling and Definitions of Placental Lesions: Amsterdam Placental Workshop Group Consensus Statement. Arch Pathol Lab Med 2016;140:698–713. https://doi.org/10.5858/arpa.2015-0225-CC.

[60] Soares MJ, Iqbal K, Kozai K. Hypoxia and Placental Development. Birth Defects Res 2017;109:1309–29. https://doi.org/10.1002/bdr2.1135.

[61] Duttaroy AK. Early nutrition and lifestyle factors : effects on first trimester placenta . Switzerland: Springer; 2016.

[62] Wang S, Yang DM, Rong R, Zhan X, Fujimoto J, Liu H, et al. Artificial Intelligence in Lung Cancer Pathology Image Analysis. Cancers (Basel) 2019;11. https://doi.org/10.3390/cancers11111673.

[63] Jimenez-del-Toro O, Otálora S, Andersson M, Eurén K, Hedlund M, Rousson M, et al. Chapter 10 - Analysis of Histopathology Images: From Traditional Machine Learning to Deep Learning. In: Depeursinge A, S. Al-Kadi O, Mitchell JRBT-BTA, editors., Academic Press; 2017, p. 281–314. https://doi.org/https://doi.org/10.1016/B978-0-12-812133-7.00010-7.

[64] Massad LS, Jeronimo J, Schiffman M, Group for the NI of HS for C and CP (NIH/ASCCP) R. Interobserver Agreement in the Assessment of Components of Colposcopic Grading. Obstet Gynecol 2008;111.

[65] Allison KH, Reisch LM, Carney PA, Weaver DL, Schnitt SJ, O'Malley FP, et al. Understanding diagnostic variability in breast pathology: lessons learned from an expert consensus review panel. Histopathology 2014;65:240–51. https://doi.org/10.1111/his.12387.

[66] Diiulio R. Clinical Pathology : The integration of existing pathology and information systems with new digital capabilities is just beginning to transform pathology as it did radiology 2010:16–8.

[67] van Ginneken B, Schaefer-Prokop CM, Prokop M. Computer-aided Diagnosis: How to Move from the Laboratory to the Clinic. Radiology 2011;261:719–32. https://doi.org/10.1148/radiol.11091710.

[68] Langley P. Machine Learning as an Experimental Science.(Author abstract)(Editorial). Mach Learn 1988;3:5. https://doi.org/10.1007/BF00115008.

[69] Baldi P. Bioinformatics : the machine learning approach. Cambridge, Mass.: Cambridge, Mass. : MIT Press, c1998.; 1998.

[70] Gutierrez author D. Machine Learning and Data Science: An Introduction to Statistical Learning Methods with R. 1st editio. Technics Publications, 2015.; 2015.

[71] Boulesteix A-L, Schmid M. Machine learning versus statistical modeling. Biometrical J 2014;56:588–93. https://doi.org/10.1002/bimj.201300226.

[72] Chaovalit P, Zhou L. Movie Review Mining: a Comparison between Supervised and Unsupervised Classification Approaches. Proc. 38th Annu. Hawaii Int. Conf. Syst. Sci., 2005, p. 112c-112c. https://doi.org/10.1109/HICSS.2005.445.

[73] Love BC. Comparing supervised and unsupervised category learning. Psychon Bull Rev 2002;9:829–35.

[74] Kotsiantis SB, Zaharakis I, Pintelas P. Supervised machine learning: A review of classification techniques. Emerg Artif Intell Appl Comput Eng 2007;160:3–24.

[75] Längkvist M, Karlsson L, Loutfi A. A review of unsupervised feature learning and deep learning for time-series modeling. Pattern Recognit Lett 2014;42:11–24.

[76] Chowriappa P, Dua S, Todorov Y. Introduction to Machine Learning in Healthcare Informatics BT - Machine Learning in Healthcare Informatics. In: Dua S, Acharya UR, Dua P, editors., Berlin, Heidelberg: Springer Berlin Heidelberg; 2014, p. 1–23. https://doi.org/10.1007/978-3-642-40017-9_1.

[77] Chen M, Hao Y, Hwang K, Wang L, Wang L. Disease Prediction by Machine Learning Over Big Data From Healthcare Communities. IEEE Access 2017;5:8869–79. https://doi.org/10.1109/ACCESS.2017.2694446.

[78] Hipp J, Flotte T, Monaco J, Cheng J, Madabhushi A, Yagi Y, et al. Computer aided diagnostic tools aim to empower rather than replace pathologists: Lessons learned from computational chess. J Pathol Inform 2011;2:25. https://doi.org/10.4103/2153-3539.82050.

[79] Deo RC. Machine learning in medicine. Circulation 2015;132:1920–30.

[80] Bhargava R, Madabhushi A. Emerging Themes in Image Informatics and Molecular Analysis for Digital Pathology. Annu Rev Biomed Eng 2016;18:387–412. https://doi.org/10.1146/annurev-bioeng-112415-114722.

[81] Wang F, Preininger A. AI in Health: State of the Art, Challenges, and Future Directions. Yearb Med Inf 2019;28:16–26. https://doi.org/10.1055/s-0039-1677908.

[82] Donsa K, Spat S, Beck P, Pieber TR, Holzinger A. Towards Personalization of Diabetes Therapy Using Computerized Decision Support and Machine Learning: Some Open Problems and Challenges BT - Smart Health: Open Problems and Future Challenges. In: Holzinger A, Röcker C, Ziefle M, editors., Cham: Springer International Publishing; 2015, p. 237–60. https://doi.org/10.1007/978-3-319-16226-3_10.

[83] El Emam K. Risk-based de-identification of health data. IEEE Secur Priv 2010;8:64–7.

[84] Rodgers SE, Demmler JC, Dsilva R, Lyons RA. Protecting health data privacy while using residence-based environment and demographic data. Heal Place 2012;18:209–17. https://doi.org/10.1016/j.healthplace.2011.09.006.

[85] Development. O for EC and. Health Data Governance: Privacy, Monitoring and Research . Paris: OECD Publishing; 2015. https://doi.org/10.1787/9789264244566-en.

[86] Dankar FK, El Emam K. The application of differential privacy to health data. Proc. 2012 Jt. EDBT/ICDT Work., ACM; 2012, p. 158–66.

[87] Yue X, Wang H, Jin D, Li M, Jiang W. Healthcare data gateways: found healthcare intelligence on blockchain with novel privacy risk control. J Med Syst 2016;40:218.

[88] Salsabili S, Mukherjee A, Ukwatta E, Chan ADC, Bainbridge S, Grynspan D. Automated segmentation of villi in histopathology images of placenta. Comput Biol Med 2019;113:103420. https://doi.org/10.1016/j.compbiomed.2019.103420.

[89] Zhang P. Decidual Vasculopathy in Preeclampsia and Spiral Artery Remodeling Revisited: Shallow Invasion versus Failure of Involution. AJP Rep 2018;8:e241–6. https://doi.org/10.1055/s-0038-1675348.

[90] Vahanian SA, Vintzileos AM. Placental implantation abnormalities: a modern approach. Curr Opin Obstet Gynecol 2016;28:477–84. https://doi.org/10.1097/GCO.0000000000000319.

[91] Racicot K, Cardenas I, Wünsche V, Aldo P, Guller S, Means RE, et al. Viral infection of the pregnant cervix predisposes to ascending bacterial infection. J Immunol 2013;191:934–41. https://doi.org/10.4049/jimmunol.1300661.

[92] Burton GJ, Baergen RN. Villous Maldevelopment. 6th ed. 2012. Berlin, Heidelberg: Springer Berlin Heidelberg; 2012. https://doi.org/10.1007/978-3-642-23941-0_15.

[93] Heider A. Fetal Vascular Malperfusion. Arch Pathol Lab Med 2017;141:1484–9. https://doi.org/10.5858/arpa.2017-0212-RA.

[94] Dommisse J, Tiltman AJ. Placental bed biopsies in placental abruption. Br J Obstet Gynaecol 1992;99:651–4. https://doi.org/10.1111/j.1471-0528.1992.tb13848.x.

[95] Kaufmann P, Huppertz B, Frank HG. The fibrinoids of the human placenta: origin, composition and functional relevance. Ann Anat 1996;178:485–501. https://doi.org/10.1016/S0940-9602(96)80102-6.

[96] Morgen EK, Fitzgerald B, Keating S. Intervillous Thrombosis BT - Pathology of the Placenta: A Practical Guide. In: Khong TY, Mooney EE, Nikkels PGJ, Morgan TK, Gordijn SJ, editors., Cham: Springer International Publishing; 2019, p. 67–76. https://doi.org/10.1007/978-3-319-97214-5_7.

[97] Kim CJ, Romero R, Chaemsaithong P, Kim J-S. Chronic inflammation of the placenta: definition, classification, pathogenesis, and clinical significance. Am J Obstet Gynecol 2015;213:S53–69. https://doi.org/https://doi.org/10.1016/j.ajog.2015.08.041.

[98] X. P, L. L, H. Y, Z. L, J. Y, L. Z, et al. Accurate segmentation of nuclei in pathological images via sparse reconstruction and deep convolutional networks. vol. 229. H. Yang, School of Automation, Beijing University of Posts and Telecommunications, Beijing, China. E-Mail: Yhh@bupt.Edu.Cn: Elsevier B.V.; 2017. https://doi.org/10.1016/j.neucom.2016.08.103.

[99] Kidron D, Vainer I, Fisher Y, Sharony R. Automated image analysis of placental villi and syncytial knots in histological sections. Placenta 2017;53:113–8. https://doi.org/10.1016/j.placenta.2017.04.004.

[100] Shamir L, Delaney JD, Orlov N, Eckley DM, Goldberg IG. Pattern recognition software and techniques for biological image analysis. PLoS Comput Biol 2010;6:e1000974. https://doi.org/10.1371/journal.pcbi.1000974.

[101] Lisboa PJ, Taktak AFG. The use of artificial neural networks in decision support in cancer: A systematic review. Neural Networks 2006;19:408–15. https://doi.org/10.1016/j.neunet.2005.10.007.

[102] Guidelines for health care professionals supporting families experiencing a perinatal loss. Paediatr Child Health 2001;6:469–90.

[103] Weiner E, Rymer-Haskel N, Grinstein E, Feldstein O, Mizrachi Y, Schreiber L, et al. 571: Can placental vascular lesions predict reccurence of preeclampsia? Am J Obstet Gynecol 2016;214:S307–8. https://doi.org/https://doi.org/10.1016/j.ajog.2015.10.616.

[104] Thornburg KL, O'Tierney PF, Louey S. Review: The Placenta is a Programming Agent for Cardiovascular Disease.(Report). Placenta 2010;31:S54–9.

[105] Romagnuolo I, Sticchi E, Attanasio M, Grifoni E, Cioni G, Cellai AP, et al. Searching for a common mechanism for placenta-mediated pregnancy complications and cardiovascular disease: role of lipoprotein(a). Fertil Steril 2016;105:1287-1293.e3. https://doi.org/10.1016/j.fertnstert.2016.01.014.

[106] Siddiqui N, Hladunewich M. Understanding the Link Between the Placenta and Future Cardiovascular Disease. Trends Cardiovasc Med 2011;21:188–93. https://doi.org/10.1016/j.tcm.2012.05.008.

[107] Intrauterine Growth and Development 2012:1–18. https://doi.org/10.1002/9781118477076.ch1.

[108] Lee YQ, Collins CE, Gordon A, Rae KM, Pringle KG. The Relationship between Maternal Nutrition during Pregnancy and Offspring Kidney Structure and Function in Humans: A Systematic Review. Nutrients 2018;10. https://doi.org/10.3390/nu10020241.

[109] Burton GJ, Fowden AL, Thornburg KL. Placental Origins of Chronic Disease. Physiol Rev 2016;96:1509–65. https://doi.org/10.1152/physrev.00029.2015.

[110] Thornburg KL, Marshall N. The placenta is the center of the chronic disease universe. Am J Obstet Gynecol 2015;213:S14–20. https://doi.org/10.1016/j.ajog.2015.08.030.

[111] Cui Z, Gong G. The effect of machine learning regression algorithms and sample size on individualized behavioral prediction with functional connectivity features. Neuroimage 2018;178:622–37. https://doi.org/10.1016/j.neuroimage.2018.06.001.

[112] Vapnik V. The nature of statistical learning theory. Springer science & business media; 2013.

[113] Pan SJ, Yang Q. A Survey on Transfer Learning. IEEE Trans Knowl Data Eng 2010;22:1345–59. https://doi.org/10.1109/TKDE.2009.191.

[114] Sarkar author D. Hands-on transfer learning with Python : implement advanced deep learning and neural network models using tensorflow and keras. Birmingham ; 2018.

[115] Perlich C, Dalessandro B, Raeder T, Stitelman O, Provost F. Machine learning for targeted display advertising: transfer learning in action. Mach Learn 2014;95:103–27. https://doi.org/10.1007/s10994-013-5375-2.

[116] Fernandes J. Transfer Learning for Images Using PyTorch: Essential Training 2019.

[117] Nair TM. Statistical and artificial neural network-based analysis to understand complexity and heterogeneity in preeclampsia. Comput Biol Chem 2018;75:222–30. https://doi.org/10.1016/j.compbiolchem.2018.05.011.

[118] von Dadelszen P, Magee LA, Roberts JM. Subclassification of Preeclampsia. Hypertens Pregnancy 2003;22:143–8. https://doi.org/10.1081/PRG-120021060.

[119] Ogge G, Chaiworapongsa T, Romero R, Hussein Y, Kusanovic JP, Yeo L, et al. Placental lesions associated with maternal underperfusion are more frequent in early-onset than in late-onset preeclampsia. J Perinat Med 2011;39:641–52. https://doi.org/10.1515/JPM.2011.098.

[120] Egbor M, Ansari T, Morris N, Green CJ, Sibbons PD. Maternal medicine: Morphometric placental villous and vascular abnormalities in early-and late-onset pre-eclampsia with and without fetal growth restriction. BJOG An Int J Obstet Gynaecol 2006;113:580–9.

[121] Leavey K, Wilson SL, Bainbridge SA, Robinson WP, Cox BJ. Epigenetic regulation of placental gene expression in transcriptional subtypes of preeclampsia. Clin Epigenetics 2018;10:28. https://doi.org/10.1186/s13148-018-0463-6.

Appendices

Appendix A. Preliminary Results from Unsupervised Machine Learning Experiments

A.1. Two distinct visual clusters found in the dataset of placenta histopathology images. **A.** The median 500 SIFT descriptors for each image was clustered with a K-means clustering algorithm. Clusters are plotted along the top 3 principal components with visual cluster 1 represented in orange and visual cluster 2 represented in blue. **B.** Images found to be in visual cluster 1 are presented with an orange border, and visual cluster 2 is presented with a blue border. **C.** A silhouette analysis was performed, and 2 clusters was found to be the optimal distribution of the data.

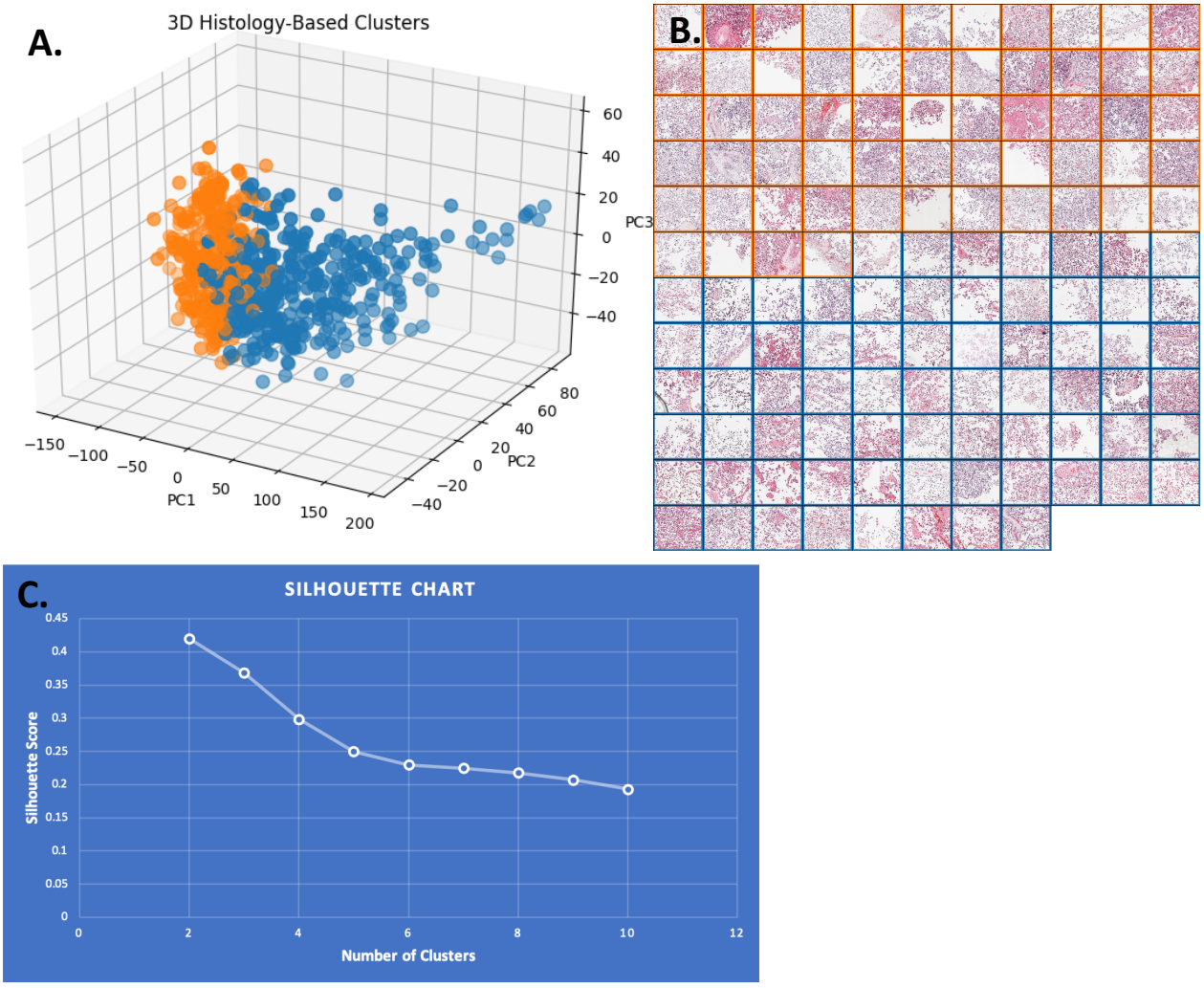

A.2. Clinical outcome overlay on histology-based clusters distribution

- Cases of PE (purple) and controls (yellow) plotted on top 3 principal components with strong representation of PE in histology cluster 2.

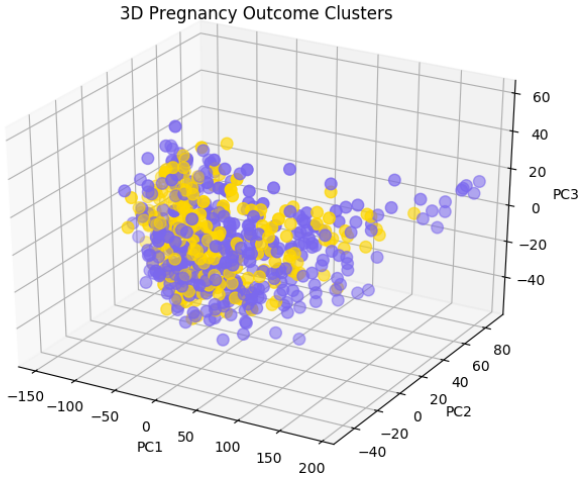

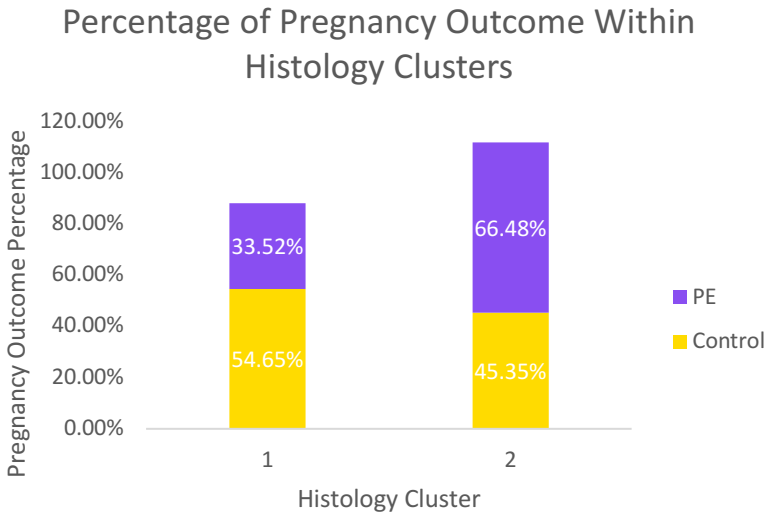

- Cases of early onset PE (turquoise), late onset PE (coral), and controls (yellow) plotted on top 3 principal components with strong representation of early onset PE in histology cluster 2.

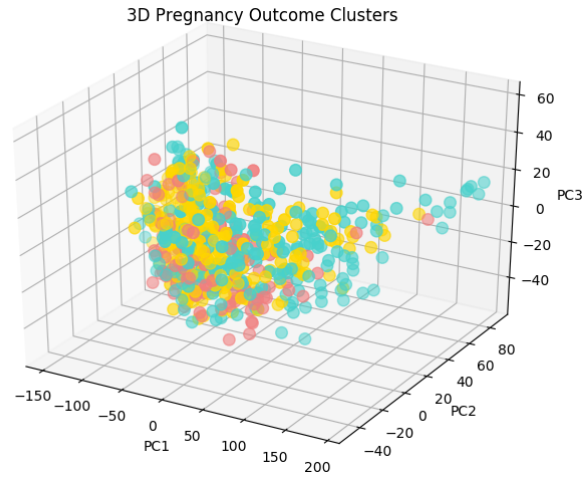

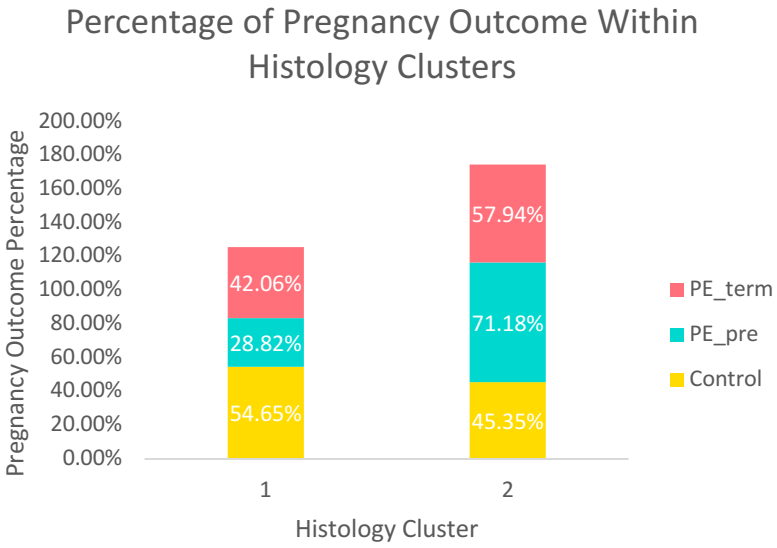

A.3. Maternal vascular malperfusion severity overlay on histology-based clusters distribution

- Severity of MVM plotted on top 3 principal components with an enrichment of higher severity (scores of 3-5 and 6-8) in histology cluster 2.

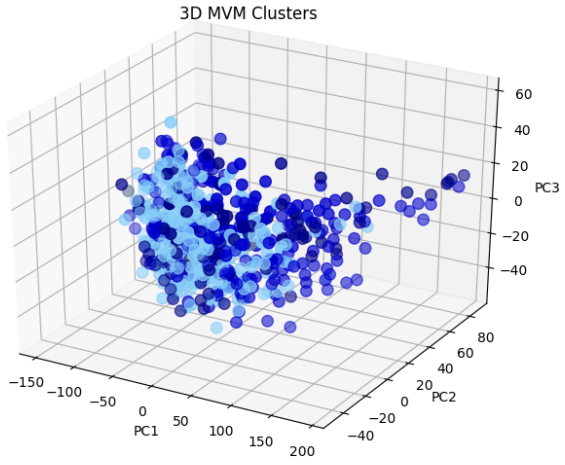

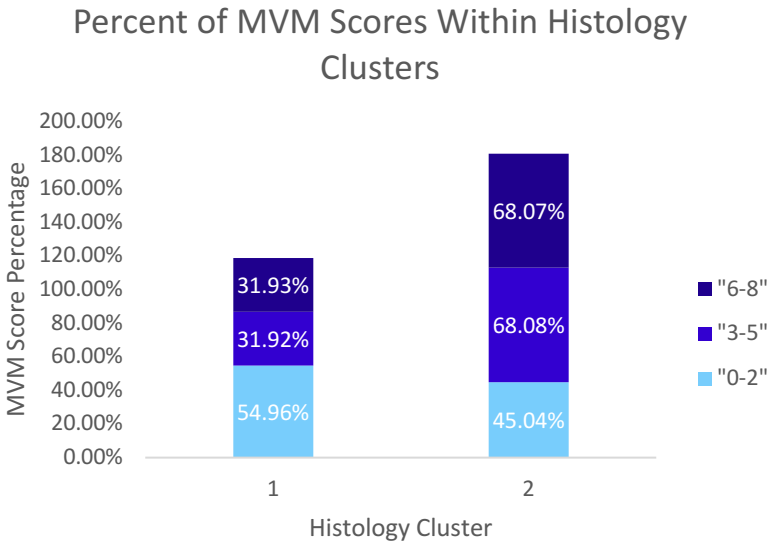

Appendix B. Research Ethics Certificates

B.1. Letter of Administrative Approval from the University of Ottawa Office of Research Ethics and Integrity

24/08/2018

Université d'Ottawa
Bureau d'éthique et d'intégrité de la recherche

University of Ottawa
Office of Research Ethics and Integrity

Lettre d'approbation administrative I Letter of administrative approval

Numéro de dossier / Ethics File Number	H-08-18-1023
Titre du projet / Project Title	Identification of Molecular Subclasses of Preeclampsia
Type de projet / Project Type	Recherche de professeur / Professor's research project
CÉR primaire / Primary REB	Réseau de science de la santé d'Ottawa (RSSO) / Ottawa Health Science Network (OHSN)
Statut du projet / Project Status	Approuvé / Approved
Date d'approbation (jj/mm/aaaa) / Approval Date (dd/mm/yyyy)	24/08/2018
Date d'expiration (jj/mm/aaaa) / Expiry Date (dd/mm/yyyy)	18/10/2018

Équipe de recherche / Research Team

Chercheur / Researcher	Affiliation	Role
Shannon BAINBRIDGE-WHITESIDE	École interdisciplinaire des sciences de la santé / Interdisciplinary School of Health Sciences	Chercheur Principal / Principal Investigator
Samantha BENTON	Département de médecine cellulaire et moléculaire / Department of Cellular and Molecular Medicine	Co-chercheur / Co-investigator
Jeremiah GAUDET		Assistant de recherche / Research Assistant
Pascale ROBINEAU-CHARETTE	Département de médecine cellulaire et moléculaire / Department of Cellular and Molecular Medicine	Étudiant-chercheur / Student-researcher
Anika MUKHERJEE	École interdisciplinaire des sciences de la santé / Interdisciplinary School of Health Sciences	Étudiant-chercheur / Student-researcher

Conditions spéciales ou commentaires / Special conditions or comments:

550, rue Cumberland, pièce 154 Ottawa (Ontario) K1N 6N5 Canada
550 Cumberland Street, Room 154 Ottawa, Ontario K1N 6N5 Canada

613-562-5387 • 613-562-5338 • ethique@uOttawa.ca / ethics@uOttawa.ca
www.recherche.uottawa.ca/deontologie I www.recherche.uottawa.ca/ethics

B.2. Certificate of Ethics Approval (Renewal) from the University of Ottawa Office of Research Ethics and Integrity

15/04/2019

Université d'Ottawa
Bureau d'éthique et d'intégrité de la recherche

University of Ottawa
Office of Research Ethics and Integrity

CERTIFICAT D'APPROBATION ÉTHIQUE I CERTIFICATE OF ETHICS APPROVAL

Numéro du dossier / Ethics File Number	H-08-18-1023
Titre du projet / Project Title	Identification of Molecular Subclasses of Preeclampsia
Type de projet / Project Type	Recherche de professeur / Professor's research project
Statut du projet / Project Status	Renouvelé / Renewed
Date d'approbation (jj/mm/aaaa) / Approval Date (dd/mm/yyyy)	15/04/2019
Date d'expiration (jj/mm/aaaa) / Expiry Date (dd/mm/yyyy)	18/10/2019

Équipe de recherche / Research Team

Chercheur / Researcher	Affiliation	Role
Shannon BAINBRIDGE-WHITESIDE	École interdisciplinaire des sciences de la santé / Interdisciplinary School of Health Sciences	Chercheur Principal / Principal Investigator
Samantha BENTON	Département de médecine cellulaire et moléculaire / Department of Cellular and Molecular Medicine	Co-chercheur / Co-investigator
Jeremiah GAUDET		Assistant de recherche / Research Assistant
Pascale ROBINEAU-CHARETTE	Département de médecine cellulaire et moléculaire / Department of Cellular and Molecular Medicine	Étudiant-chercheur / Student-researcher
Anika MUKHERJEE	École interdisciplinaire des sciences de la santé / Interdisciplinary School of Health Sciences	Étudiant-chercheur / Student-researcher

Conditions spéciales ou commentaires / Special conditions or comments

550, rue Cumberland, pièce 154 Ottawa (Ontario) K1N 6N5 Canada
550 Cumberland Street, Room 154 Ottawa, Ontario K1N 6N5 Canada

613-562-5387 • 613-562-5338 • ethique@uOttawa.ca / ethics@uOttawa.ca
www.recherche.uottawa.ca/deontologie I www.recherche.uottawa.ca/ethics

B.3. Certificate of Completion of TCPS 2: CORE Course

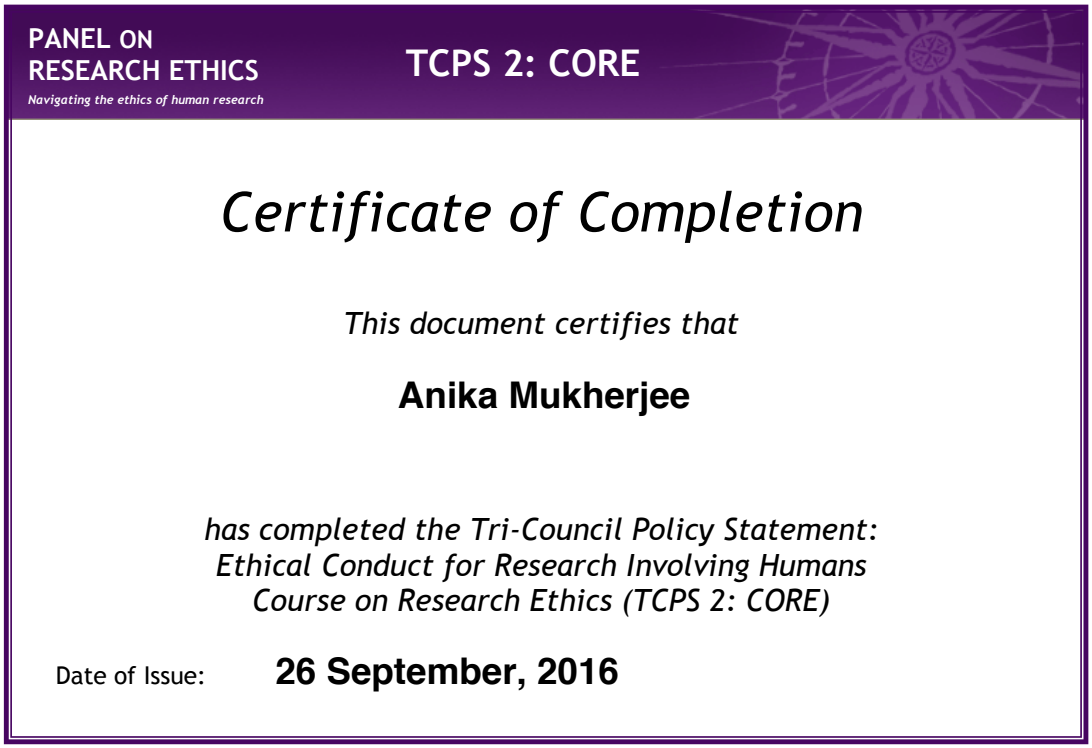

PANEL ON RESEARCH ETHICS
Navigating the ethics of human research

TCPS 2: CORE

Certificate of Completion

This document certifies that

Anika Mukherjee

has completed the Tri-Council Policy Statement:
Ethical Conduct for Research Involving Humans
Course on Research Ethics (TCPS 2: CORE)

Date of Issue: **26 September, 2016**

Appendix C. Scholarly Achievements

C.1. Scholarships

1. University of Ottawa Graduate Admission Scholarship (September 2016 – August 2018)

C.2. Publications

1. Salsabili, S., Mukherjee, A., Ukwatta, E., Chan, A. D. C., Bainbridge, S., & Grynspan, D. (2019). Automated segmentation of villi in histopathology images of placenta. *Computers in Biology and Medicine*, *113*, 103420. doi: 10.1016/j.compbiomed.2019.103420
2. Mukherjee, A., Chan, A. D., Keating, S., Redline, R. W., Fritsch, M. K., Machin, G. A., Cornejo-Palma, D., de Nanassy, J., El-Demellawy, D., von Dadelszen, P., Benton, SJ, Grynspan, D. (2016). The Placental Distal Villous Hypoplasia Pattern: Interobserver Agreement and Automated Fractal Dimension as an Objective Metric. *Pediatric and Developmental Pathology*, *19*(1), 31–36. doi: 10.2350/15-03-1619-oa.1

C.3. Published Abstracts

1. Mukherjee A, Salsabili S, Chan ADC, Leckie M, Grynspan D, Bainbridge S. (2020). Modelling Placenta Mediated Diseases with Supervised Machine Learning. *Reproductive Sciences* 27(1):171A.
2. Mukherjee A, Grynspan D, Bainbridge S. (2019). Clustering Preeclampsia Histopathology Images with K-means Clustering for Pattern Recognition and Therapeutic Target Discovery. *Reproductive Sciences* 26(Supp 1):177A.
3. Mukherjee A, Salsabili S, Chan ADC, Ukwatta E, Leckie M, Grynspan D, Bainbridge S. (2018). Automating Segmentation of Placenta Tissue Images for Computer Aided Diagnosis and Creating Objective Measures for Microscopic Components. *Reproductive Sciences* 25(Supp. 1):244A.

C.4. Workshops

1. Health Sciences Startup Bootcamp 2019. University of Ottawa. February 2019.
2. Quantitative 3D Microscopic Analysis of Isolated Human Peripheral Placental Villous Trees: Theory and Practice. Ludwig-Maximilians-Universitat Munchen. February 2018.

C.5. Presentation

1. Modelling Placenta Mediated Diseases with Machine Learning. Poster presentation at the Society of Reproductive Investigation 67th Annual Meeting, 2020.
2. Clustering Preeclampsia Histopathology Images with K-Means Clustering for Pattern Recognition and Therapeutic Target Discovery. Poster presentation at the Society of Reproductive Investigation 65th Annual Meeting, 2019.
3. Automating Segmentation of Placenta Tissue Images for Computer Aided Diagnosis and Creating Objective Measures for Microscopic Components. Poster presentation at the Society of Reproductive Investigation 66th Annual Meeting, 2018.
4. Women in Data Science Ottawa Conference 2018 – Panel Discussion. March 2018.
5. Pint of Science – Our Body. Co-presenter of presentation titled “The Placenta – The Most Important Organ You Have Ever Owned” with Dr. Shannon Bainbridge. May 2018.

Appendix D. Permissions for Publication

D.1. Permission to include *Automated Segmentation of Villi in Histopathology Images of Placenta* in a thesis

Title: Automated segmentation of villi in histopathology images of placenta

Author: S. Salsabili,A. Mukherjee,E. Ukwatta,A.D.C. Chan,S. Bainbridge,D. Grynspan

Publication: Computers in Biology and Medicine

Publisher: Elsevier

Date: October 2019

LOGIN

If you're a copyright.com user, you can login to RightsLink using your copyright.com credentials.

Already **a RightsLink user** or want to learn more?

Please note that, as the author of this Elsevier article, you retain the right to include it in a thesis or dissertation, provided it is not published commercially. Permission is not required, but please ensure that you reference the journal as the original source. For more information on this and on your other retained rights, please visit: https://www.elsevier.com/about/our-business/policies/copyright#Author-rights

BACK CLOSE WINDOW